ALGERIAN REPUBLIC DEMOCRATIC AND POPULAR
MINISTRY OF THE SUPERIOR EDUCATION
AND OF THE SCIENTIFIC RESEARCH

UNIVERSITY OF MENTOURI CONSTANTINE
FACULTY OF EXACT SCIENCES
DEPARTMENT OF PHYSICS

Order number:…………………
Serial number:…………………

THESIS
Submitted for the degree of

DOCTORATE IN SCIENCES

Option: ENERGY

Theme

NUMERICAL STUDY OF TRANSIENT LAMINAR MIXED CONVECTION IN
VERTICAL THICK CYLINDRICAL DUCT

By

Abdeslam OMARA
Examined on: 07 April 2007

Jury :

President	: M. KAJA	**Professor**	**Univ of Mentouri Constantine**
Supervisor	: S. ABBOUDI	**M. of Conferences**	**UTBM-Belfort France**
Co-Supervisor	: M. BOUMAZA	**Professor**	**Univ of Mentouri Constantine**
Members	: Z. NEMMOUCHI	**Professor**	**Univ of Mentouri Constantine**
	: M. SI-AMEUR	**Professor**	**Univ of Hadj-Lakhdar Batna**
	: C. BOUGRIOU	**M. of Conferences**	**Univ of Hadj-Lakhdar Batna**

Chapter 1

Literature Review

1.1 Theoretical analysis

Laminar mixed convection in tubes finds itself in many industrial applications such as cooling corps in nuclear reactors [1], solar water heating systems [2], heat exchangers [3] and closed-loops thermosyphon [4]. These numerous domains of applications justify the production of an abundant bibliography in the past decades. On the other hand, the understanding of the inherent physical phenomena to the interaction of the free and forced convection constitutes in itself a very important objective.

For the two kinds of mixed convection in ducts (upward mixed convection and downward mixed convection), one finds few works treating the transient downward or upward mixed convection in vertical duct with or without the effect of axial wall and fluid conductions, while in the steady state, these two kinds of mixed convection have received a rather particular attention from researchers in the past decades.

To the departure, the researchers used simplified models like those based on the equations of the boundary layer approximations but, these last years, the spectacular development of the computers and the techniques of numerical analysis have permitted the modelling of the mixed convection phenomena from the Navier-Stockes equations.

Between 1901 and 1903, Gauthier-Villars published in Paris, Joseph Boussinesq's treaty entitled: "Analytic theory of the Heat" in which one recovers the following fragment: "… it was necessary to observe again that, in most movements provoked by the heat on our

heavy fluids, the volumes or the densities are conserved to very little near, although the corresponding variation of the weight of the unit volume is justly the reason of the phenomena that it is about analysing. There results from that the possibility to disregard the variations of the density, where they are not multiplied by the gravity g, while keeping, in the calculations, their product by this one ".

This drives to the more used hypothesis in the natural or mixed convection that is called "the Boussinesq approximation". It means that the density ρ is supposed constant except in the gravitation term of the equation of quantity of movement.

The experimental studies imply costs of very important realization. For this reason we find a few experimental works in the literature that concern the mixed convection. Besides, the chosen geometry doesn't facilitate us the task. Two techniques have been used until now in the experimental studies: the first one is quantitative while the second is qualitative. The first consists in taking measures of temperature or velocity on several sections along an opaque tube, while the second consists in visualizing the flowing fluid in a transparent tube.

Among the first experimental studies concerning the assisted or opposed mixed convection in a vertical tube one recovers the one of **Hanratty et al** [5] in 1958. The authors show experimentally and numerically that the non-isotherm flow becomes unstable, even for a weak Reynolds number. The thermal boundary condition (positive or negative wall heat flux) has been realized by the way of a plastic cutaway fixed in a concentric manner around the tube in which circulates hot or cold water. Two cases have been analyzed:

(1) the heated upward flow (or the cooled downward flow) that corresponds to the assisted mixed convection, and

(2) the cooled upward flow (or the heated downward flow) that coincides with the opposed mixed convection.

In the first case they observed that the fluid in the center of the tube is decelerated, while the one close to the pipe wall is accelerated, so that a recirculation zone of parabolic shape appears. They also observed that if the temperature in the envelope decreases or the debit in the tube increases, the summit of the parabola goes up. In the second case they observed the inverse phenomenon. Otherwise, for a value of Reynolds equal to 50, and a

temperature difference between the zone where the fluid is heated or cooled by the cutaway and the inlet of the tube of 10 the turbulent régime gets settled.

In 1972, **Zeldin** and **Schmidt** [6] have studied the effect of the gravitation force on the hydrodynamic and thermal characteristics of the flow in a vertical tube. The used fluid is air. The temperature of the pipe wall is assumed constant and the velocity at the inlet of the tube is either constant or parabolic. The system is composed of two concentric tubes in which the one that is inside serves to take the measures and the annular space ensure to maintain the temperature of the interior wall tube constant while making circulate water. The authors found that the heat transfer has been improved by the action of the gravity when the ratio $Gr/Re < 0$, and that the Nusselt number varies linearly with Gr/Re when $-50 \leq Gr/Re \leq 0$.

Mori and **Ohbuchi** [7] have realized an experimental study of a downward water flow in a uniformly heated tube. They found that for weak heat flux values, the heat transfer is decreased by the effect of the natural convection compared to the case of the forced convection.

Bernier and **Baliga** [8] finalized a technique of visualization in a uniformly heated vertical tube through the intermediary of a very thin and semitransparent gold leaf. The experiences have been done for several representative cases of assisted mixed convection. They have observed, for each case, a recirculation cell in the centre of the tube. The apparition of these cells are due to the fact that the fluid close to the pipe wall is hot therefore its density decreases in relation to the one that is far from the pipe wall. This difference of density added to the force of gravity lead to the acceleration of the fluid adjacent to the pipe wall and at the same time, to keep the conservation of the mass, the fluid at the centre decelerates.

The numerical studies of steady combined forced and free convection in vertical parallel plate or pipe, without the effect of wall conduction, have been performed by numerous researchers, which refer to different kinds of boundary conditions [9-17].

Carlos and **Guidice** [18] presented a numerical analysis of the effect of the entrance region on mixed convection in horizontal concentric cylinders.

Fusegi [19] investigated the combined effect of the oscillatory through-flow and the buoyancy on the heat characteristics of a laminar flow in a periodically grooved channel.

Cheng and **Weng** [20] numerically studied the mixed convection flow and heat transfer processes in the developing region of a vertical rectangular duct with one heating wall.

Morton and **Leung** [21] investigated numerically and experimentally the mixed convection in vertical circular duct subjected to constant temperature condition. In the downward mixed convection, a recirculation cell has been observed experimentally in the vicinity of the wall. They have shown that the upstream extent of the observed recirculation cell is more important than the one computed numerically. **Morton** and **Leung** have attributed this effect to the axial conduction of heat in the pipe wall.

Chan and **Leung** [22] shows that in the case of the opposed mixed convection, the correlation between the Nusselt number and the ratio Gr/Re^2 is:

$Nu = 8.16 * (Gr/Re^2)^{-0.15}$ if $0.5 \, \mathbf{p} \, Gr/Re^2 \, \mathbf{p} \, 2.77$

$Nu = 8.54 * (Gr/Re^2)^{-0.38}$ if $0.008 \, \mathbf{p} \, Gr/Re^2 \, \mathbf{p} \, 0.35$

Wang et **al** [23] have presented a numerical analysis of upward and downward mixed convections in vertical and horizontal circular ducts with reversed flow. Their results indicate that the velocity profile distortions increase with (Gr/Re) but decrease considerably when Pe increases for a constant value of (Gr/Re). They have also shown that for high values of Gr/Re, the recirculation zone appears at the center of the tube for the heating case and near the pipe wall for the cooling case.

Chow et **al** [24] have analysed the effect of the natural convection and the fluid axial conduction on the fully developed laminar flow in a vertical channel subjected to constant wall temperature. The temperature profile at the inlet of the channel is assumed constant. They treated two cases: heating and cooling. Their results indicate that in the heating case, the heat flux and the Nusselt number increase with the Grashof number. On the contrary, in the cooling case these last two magnitudes decrease with the increase of Grashof number.

Barletta et **al** [25] have studied the non-axisymmetric forced and free convection in vertical circular duct subjected to:
   (1) Periodic sinusoidal temperature change at the wall, or
   (2) Convection from Ambient.
For these two cases they find a critical value of Gr/Re, corresponding to the apparition of the recirculation zones that depends on the angular frequency q for the first case:

$(Gr/Re)_{critical} = 32(q+1)$, and the number of Biot for the second case:

$$(Gr/Re)_{critical} = \frac{16p}{Bi}\left[\sum_{n=1}^{\infty}\frac{(-1)^{n+1}}{n(2n-1)(2n-1+Bi)}\right]^{-1}$$

Joye [26] performs a comparison of heat transfer in a vertical tube between the assisted-buoyancy and the opposed-buoyancy cases. He shows that in the case of the opposed-buoyancy, there is an increase of the heat transfer compared to the case of the assisted-buoyancy.

Zghal et **al** [27] studied numerically laminar upward mixed convection flows in a vertical tube with a uniformly heated zone preceded and followed by adiabatic zones for a wide range of heating lengths, Reynolds and Richardson numbers. According to the combination of these parameters, the results show the existence of five regime of flow: developing with or without flow reversal, developing followed by a fully developed region both without flow reversal, and developing with flow reversal followed by a fully developed region with or without flow reversal. The conditions leading to the flow reversal as well as significant upstream diffusion of heat and momentum have been mapped on the Peclet-Richardson plan for different lengths of the heated zone.

More lately, **Behzadmher** et **al** [28] examined a similar problem of laminar and turbulent mixed convection, while using the turbulent model k-ε for the turbulent regime. The upward flow of air in a vertical heated tube has been analysed for two values of Reynolds number (*Re=1000, 1500*) and for several values of the Grashof number (*Gr£10^8*). A correlation for the Nusselt number, valid in laminar and in turbulent regime, has been elaborated for *Gr£ 5.10^7* and *1000£ Re £1500*:

$$Nu_M = 4.36\left(1+\frac{Gr^{0.468}}{750+0.24\,Re}\right)$$

Hadjadj and **El Kyal** [29] studied numerically the effect of two sinusoidal protuberances on natural convection in a vertical concentric annulus. They found that the presence of protuberances, lead to an increase in the heat transfer rate in the location of the obstruction along the wall.

El-Shaarawi and **Negm** [30] have studied numerically the coupling between the wall conduction and the laminar natural convection in open-ended vertical concentric annuli.

The effect of the wall-to-fluid thermal conductivity ratio has been investigated and found to have prominent effects on the steady heat transfer parameters.

Busedra and **Soliman** [31] have considered the geometry of semicircular duct and solved the problem of laminar fully developed mixed convection under buoyancy-assisted and opposed conditions. Their results are presented with a detailed assessment of the effects of inclination, Reynolds number, Grashof number and the thermal boundary conditions.

Other works about this subject in the steady state regime can be consulted in the references [32-39].

The effect of axial wall conduction on the steady combined forced and free convection in vertical pipes or parallel plates has been studied by numerous researchers.

Bernier and **Baliga** [40] have presented the steady state results of a numerical investigation of conjugate conduction and laminar mixed convection in vertical cylindrical pipe for upward flow and uniform wall heat flux. The Prandtl number was fixed at *5*, the Grashof number, based on heat flux, was set at *5000*. In their study, two values *1* and *10* of the Reynolds number are used. The results are presented for four different values of solid-to-fluid thermal conductivity ratio *K* (*0.5*, *5*, *50* and *500*) and three different values of wall thickness-to-pipe diameter ratio *D* (*0.01*, *0.05* and *0.25*). For Re equal to 1, they found that the effects of axial conduction in the pipe wall are quite pronounced when *K* and/or *D* are high. Furthermore, they found that the upstream axial conduction distorted the parabolic velocity profile in the upstream adiabatic section to the point that the centreline velocity was negative at the entrance of the heated section, which established a zone of recirculation.

A similar survey is achieved by, **Heggs** et **al** [41] for opposed mixed convection. In their study, some parameters have been fixed such: *Re=50, Gr=-10000, Pr=7*. The ratio (R_e/R_i) between the external (R_e) and internal (R_i) radius of the tube vary between *1.1* and *1.4*. The results are presented for three different values of solid-to-fluid thermal conductivity ratio *K* (*0.5*, *5* and *500*). The authors observe that the effect of axial wall conduction on the mixed convection increases with the increase of the values of these last ratios.

The effect of wall axial conduction on downward flow with opposed mixed convection in vertical circular duct have also been examined numerically by, **LaPlante** and

Bernier [42]. The results are presented for (*Pr=5*), for a Reynolds number equal to *1* and *10*, and for two values of the Richardson number (*Ri=5000* and *50*). Their study demonstrates that, under buoyancy effect, and for high values of the solid-to-fluid thermal conductivity ratio and high pipe thickness-to-diameter ratio, some heat flux quantities, are redistributed in the upstream adiabatic section situated forward of the beginning of the recirculation cell. They also show that in some cases the heating effects are felt until 25 diameters upstream of the heated section.

Nasredine et **al** [43] have studied the effect of the axial wall conduction on the upward mixed convection.

Ouzzane and **Galanis** [44] have analyzed numerically the effects of the axial wall conduction and the non-uniform heat flux condition on the upward mixed convection in an inclined circular duct. They found that the calculated results for local parameters (circumferential distribution of the interfacial temperature or axial velocity profile) and for average variables (circumferentially average values of the Nusselt number and of the interfacial shear stress) are quite different, especially for high values of Grashof number. As a consequence, they found that for $Gr=10^6$, *Re=500* and *Pr=7*, the asymptotic average Nusselt number for a uniform heat flux applied over the entire outer tube surface is *16.47*. The corresponding values for the case of a heat flux applied on the fluid-solid interface is *26.14* for a uniform heat flux over the entire circumference, and *29.71* for a heat flux applied only on the top half of the interface.

Burch et **al** [45] performed a pioneering study of wall conduction effect on steady natural convection between vertical parallel plates.

Similar studies were also performed by, **Kim** et **al** [46] and **Anand** et **al** [47]. Their results show that the influence of wall conduction on the heat transfer and flow behaviors are significant, particularly for the system with higher Grashof number, larger wall-to-fluid conductivity ratio or thicker wall.

In the transient regime, **Mai** et **al** [48-49] have studied the problem of upward vertical pipe flow with step change in the inlet temperature and velocity. Their results show a dissymmetry of the velocity and temperature profiles between the positive and negative step changes.

Nguyen et **al** [50] have studied the problem of 3D transient laminar mixed convection flow in vertical tube with negligible thickness under buoyancy effect and time

dependant wall heat flux condition. Their results have shown that the flow seems to remain stable and unique for $Gr=5.10^5$ and 10^6, respectively for opposed and assisted-buoyancy cases. Beyond this critical Grashof numbers, an extremely slow and rather difficult and tedious convergence behaviours have been experienced, which are believed to be due to a possible flow transition.

Barletta and **Rossi di Shio** [51] have studied the fully developed laminar mixed convection in vertical circular duct subjected to a periodic sinusoidal temperature change at the wall. Their results show that there exists resonance frequency such that the velocity, the friction coefficient and the heat flux reach a maximum.

The unsteady mixed convection heat transfer in a vertical channel was presented by, **Lin** et **al** [52] and **Yan** [53]. Their results show that the wall heat capacity can have a profound influence on the unsteady mixed convection flow and thermal characteristics. The axial conduction in the fluid and in the pipe wall remains untreated in [52, 53] and hence its effect is not known.

Lee and **Yan** [54] have presented a numerical analysis for unsteady mixed convection heat transfer in a parallel-plate channel or a circular pipe experiencing a sudden change in ambient temperature with high Péclet number and a relatively thick pipe. So the axial conduction in both the flow and the pipe wall is negligibly small. Their results show that the ignorance of wall effect causes a substantial error, especially in the early transient period.

Bae et **al** [55] numerically investigated the enhancement of mixed convection heat in a multi-block heater arrangement in a channel. For the studied specific case they demonstrate the possibility of resonant heat transfer augmentation by thermal modulation. The resonance frequency depends on the heater block geometry and the spacing between neighbouring blocks.

Cheng et **al** [56] conduct their numerical study on the criterion of apparition of the recirculation zones in the case of assisted mixed convection between vertical parallel plates. Special attention is devoted to the following sets of thermal boundary conditions imposed on the two opposed duct walls:

- Uniform heat flux Q_1 at $Y=1$ -Uniform heat flux Q_2 at $Y=0$ with $Q_1> Q_2$ or $Q_1= Q_2$.
- Uniform heat flux Q_1 at $Y=1$ -Uniform temperature T_2 at $Y=0$.
- Uniform temperature T_1 at $Y=1$ -Uniform temperature T_2 at $Y=0$ with $T_1> T_2$.

In the first situation, two cases have been examined: symmetrical heating $r_H = Q_2/Q_1 = 1$ and asymmetrical heating $r_H = Q_2/Q_1 < 1$. For the symmetrical heating case, the condition for the onset of the flow reversal is $Gr/\text{Re} < 3{,}2.10^{-4}$, while of the case where $r_H < 1$, the recirculation zones appear for large values of the ratio Gr/Re. Besides, the authors presented a diagram with the recirculation zones in the r_H and Re/Gr coordinates in which one observes that for $r_H > 0.053$, the velocity profile include two points of inflection and for $0 < r_H < 0.053$, it includes one of it only.

In the second situation $Q_1 - T_2$, the conditions for the onset of the flow reversal have been defined as follows:

$$\left[\frac{dU}{dY}\bigg|_{Y=0} \right] \left[\frac{dU}{dY}\bigg|_{Y=1} \right] \geq 0.$$ What is equivalent to $\dfrac{Q_1 + 3}{3} \leq \dfrac{dP}{dX} \leq \dfrac{Q_1 + 2}{2}$.

In the third situation $T_1 - T_2$, the conditions for the onset of the flow reversal have been defined as follows: $\dfrac{2r_T + 1}{3} \leq \dfrac{dP}{dX} \leq \dfrac{r_T + 1}{2}$ where $r_T = \dfrac{T_2 - T_0}{T_1 - T_0}$.

In the same geometry, **Hamadah** and **Wirtz** [57] have conducted a similar analysis for a downward opposed mixed convection flow and for the same boundary conditions. They define the criterion for the onset of the reversal flow, respectively for the second and the third case, as follows:

$$\left(\frac{Gr}{Re} \right)_{REV} = \frac{288}{1 - r_T}, \quad \left(\frac{Gr}{Re} \right)_{REV} = 576.$$

For the first case, they found that criterion for the onset of the reversal flow depends on the values of the ratio $r_H = Q_1/Q_2$.

In the study of unsteady forced convection channel flow, **Abboudi** et **al** [58], **Bilir** and **Ateş** [59] and **Faghri** and **Sparrow** [60] found that both heat conduction in the wall and wall heat capacity play an important role in the case of transient conjugated heat transfer.

As can be shown from the previous literature review the effect of wall conduction on the characteristics of purely free or mixed convection channel flows at the steady state have received more attention, contrary to the case of transient mixed convection channel flows.

1.2 Summarized of the literature review

The first numerical studies on the mixed convection stayed limited to the fully developed flows. The arrival of the computers made possible the resolution of the simultaneous development of the thermal and hydrodynamical boundary layers.

Several cases of mixed convection have been solved numerically with parabolic algorithms by using the boundary layer approximations. However, when the axial conduction becomes important or when the flow is reversed, an elliptic algorithm is required to solve the problem of mixed convection. In the case where no instability appears in the flow, the existing results are in agreement on the fact that the mixed convection increases the heat transfer for assisted mixed convection (upward with heating or downward with cooling), while for opposed mixed convection (downward with heating or upward with cooling) the heat transfer is reduced.

Several experimental studies show that the apparition of instabilities in the flow coincides with the apparition of an inflection point in the axial velocity profile and can really occur for Reynolds numbers below 2300, especially for a downward flow. However, for low Reynolds numbers and for a relatively short heating section, stable and symmetric recirculation cells have been observed experimentally for laminar flow.

Although it is generally accepted that, for the forced convection flows the axial conduction becomes only important when the Péclet number is lower than 100. For the mixed convection case, no similar rule has been established.

1.3 Conclusion

Through this literature review it can be concluded that the most part of works treated this problem in the steady state, while in the transient state the available few works neglect the coupling between the pipe wall and the fluid flow. The lack of information on transient conjugated laminar mixed convection motivates the present work, which represents an extension of the steady state cases studied before by different authors and the continuation of our investigations [61-63, 74].

1.4 Objective

The main objective of the present work is to analyze numerically the effects of wall and fluid axial conduction, physical and geometrical properties and heat capacity in the

pipe wall on the transient downward mixed convection in a circular duct experiencing a sudden change of the applied heat flux on the outside surface of a central zone preceded and followed by adiabatic zones.

Chapter 2

Mathematical modelling

2. 1 Introduction

As it has been mentioned in the previous chapter, the present study treats the transient mixed convection problem. One studies the conjugated heat transfer in a vertical duct submitted to a uniform heat flux and in which one recovers a downward transient mixed convection flow.

2. 2 Problem formulation and boundary conditions

The problem consists of a simultaneously developing conjugated downward flow inside a vertical tube with a uniformly heated section preceded and followed by adiabatic sections. A schematic drawing of the problem under consideration is presented in Figure 3.1a. One will first of all note that the origin of the system of axes is situated at the entry of the heated section *(x=0)* on the symmetry axis of the tube *(h=0)*. Upstream and downstream adiabatic sections have been added to the heated section in order to permit the study of: (1) axial diffusion of quantity of movement and (2) axial fluid and wall heat conduction. The governing equations are: the mass conservation equation, the Navier-Stockes equations and the equation of energy in the fluid and in the pipe wall. In view of the tubular geometry of the domain, these equations will be written in cylindrical coordinates. Besides, being given the bi-directional nature of the problem, the elliptic equations should be solved.

2.2.1 Hypothesis

Several hypotheses have been restraint on the above-mentioned system of equations. On the one hand, these hypotheses permit to avoid a heaviness of the problem, and on the other hand, they simplify the application of the boundary conditions while, keeping a good physical representation of the problem. These hypotheses are:

1. The flow and heat transfer are axisymmetric and two-dimensional (none azimuthal variation).

2. The thermal radiation is negligible.

3. The flow is assumed to be incompressible, laminar and transient.

4. The viscous dissipation and the pressure force work are negligible.

5. The physical properties of the fluid $(C_p,\ m,\ k_f,\ r$ and $b)$ and of the wall $(C_p,\ k_p$ and $r)$ are constant and estimated at the fluid temperature at the entry of the tube. However, the density varies linearly with the temperature in the term representing the body forces in the momentum equation according to the axis Z (Boussinesq approximation). Thus, r is replaced by the expression $r_0\{1 - b(T - T_0)\}$.

6. The fluid is Newtonien.

7. The fluid enters in the upstream section with a uniform temperature and a fully developed velocity profile.

8. The upstream and downstream sections, including the extremities of the tube, are perfectly isolated.

9. Initially $(t = 0)$, the whole systems, including the flowing fluid and the duct wall are at the same uniform temperature T_0. The velocity of the flowing fluid is assumed parabolic and the applied heat flux at the outer surface of the central section Q is zero. At $t > 0$, the heat flux applied at the outer surface of the central section is suddenly raised to a new value $Q > 0$ and maintained at this level thereafter.

10. At the exit of the duct, the adiabatic downstream section is considered long enough to permit an axial invariance of the velocity components and of the axial diffusive thermal flux, and a preponderance of the convective contribution over to the diffusive one.

The hypotheses 1) and 2) merit some reflections. As it has been mentioned in chapter 1, the opposed mixed convection flows tend to become asymmetric under some conditions. Thus, for a relatively high values of the ratio Gr/Re^2 or Gr/Re, the main flow arranges

itself uncertainly on one hand of the tube, whereas if the ratio Gr/Re^2 or Gr/Re is raised enough, one observes a recirculation cell on the other side. It seems that the apparition of this asymmetry is joined to the length of the heated section. Thus, **Senécal** [65] have observed experimentally this asymmetry for a ratio $L_h/D = 54$ and for Gr/Re^2 ratios of the order of those used in the present study. On the other hand, the experimental studies of **Morton** et **al** [21] show a nearly perfect symmetry of the flow for $L_h/D = 0.85$. The ratio L_h/D used in the present study is of *10*. This value is located between the geometry of **Senécal** and the one of **Morton** et **al**. For such ratio, one can affirm with certainty that the flow will stay symmetrical.

As for the hypothesis of a negligible thermal radiance, it carries to controversy when one uses a gas as fluid coolant. The presented farther results are for *Pr=5*, representing a fluid whose properties are typically similar to those of water. For this case, the coefficients of extinction are relatively high for the wavelengths corresponding to the infrared radiance (**Siegel** and **Howel** [66]). Consequently, the liquid being in contact with the wall immediately absorbs the thermal radiation given out by the wall.

2.2.2 Governing equations

With reference to the nomenclature presented in Fig. 1a, the governing equations and boundary conditions for the transient conjugated heat conduction and laminar mixed convection are presented as follows:

Conservation of mass:

$$\frac{1}{r}\frac{\partial(\,rv\,)}{\partial r} + \frac{\partial u}{\partial z} = 0 \tag{2.1}$$

Conservation of momentum:

$$r_0(\frac{\partial v}{\partial t} + v\frac{\partial v}{\partial r} + u\frac{\partial v}{\partial z}) = -\frac{\partial p}{\partial r} + \frac{m}{r}\frac{\partial}{\partial r}\left(r\frac{\partial v}{\partial r}\right) - \frac{m\,v}{r^2} + m\frac{\partial^2 v}{\partial z^2} \tag{2.2}$$

$$r_0(\frac{\partial u}{\partial t} + v\frac{\partial u}{\partial r} + u\frac{\partial u}{\partial z}) = \rho g - \beta\rho_0 g(T - T_0) - \frac{\partial p}{\partial z} + \frac{m}{r}\frac{\partial}{\partial r}\left(r\frac{\partial u}{\partial r}\right) + m\frac{\partial^2 u}{\partial z^2} \tag{2.3}$$

Conservation of energy in the fluid:

$$r_0 C_p \left(\frac{\partial T}{\partial t} + v \frac{\partial T}{\partial r} + u \frac{\partial T}{\partial z} \right) = \frac{k_f}{r} \frac{\partial}{\partial r} \left(r \frac{\partial T}{\partial r} \right) + k_f \frac{\partial^2 T}{\partial z^2} \qquad (2.4)$$

Conservation of energy in the pipe wall:

$$r_p C_p \left(\frac{\partial T}{\partial t} \right) = \frac{k_p}{r} \frac{\partial}{\partial r} \left(r \frac{\partial T}{\partial r} \right) + k_p \frac{\partial^2 T}{\partial z^2} \qquad (2.5)$$

2.2.3 Initial and boundary conditions

2.2.3.1 Initial conditions

$t = 0:$ $\qquad\qquad u(r) = 2V \left(1 - (r/R_i)^2 \right) \qquad v = 0 \qquad T = 0 \qquad\qquad (2.6)$

2.2.3.2 Boundary conditions

$t \, \mathbf{f} \, 0:$

- Inlet of the duct: $x = -L_u$

$0 \leq r < R_i \qquad\qquad u(r) = 2V \left(1 - (r/R_i)^2 \right) \qquad v = 0 \qquad T = T_0 \qquad (2.7a)$

$R_i \leq r \leq R_i + R_e \quad u = 0 \qquad v = 0 \qquad \frac{\partial T}{\partial z} = 0 \qquad\qquad\qquad (2.7b)$

- Upstream and downstream sections: $-L_u < z < 0 \ \text{and} \ L_h < z < L_h + L_d$

$r = 0 \qquad\qquad\qquad \frac{\partial u}{\partial r} = 0 \quad v = 0 \quad \frac{\partial T_f}{\partial r} = 0 \qquad\qquad\qquad (2.8a)$

$r = R_i \qquad\qquad\qquad u = 0 \qquad v = 0 \qquad\qquad\qquad\qquad\qquad (2.8b)$

$r = R_i + R_e \qquad\qquad \frac{\partial T_w}{\partial r} = 0 \qquad\qquad\qquad\qquad\qquad\qquad (2.8c)$

-Heated section: $0 \leq z \leq L_h$

$r = 0 \qquad\qquad\qquad \frac{\partial u}{\partial r} = 0 \quad v = 0 \quad \frac{\partial T_f}{\partial r} = 0 \qquad\qquad\qquad (2.9a)$

$r = R_i \qquad\qquad\qquad u^* = 0 \quad v^* = 0 \qquad\qquad\qquad\qquad\qquad (2.9b)$

19

$$r = R_i + R_e \qquad l_w \frac{\partial T_w}{\partial r} = Q \tag{2.9c}$$

- Outlet of the duct: $z = L_h^* + L_d^*$

$$0 \le r < R_i \qquad \frac{\partial u}{\partial z} = 0 \quad \frac{\partial v}{\partial z} = 0 \quad \frac{\partial T_f}{\partial z} = 0 \tag{2.10a}$$

$$R_i \le r \le R_i + R_e \quad u = 0 \qquad v = 0 \qquad \frac{\partial T_w}{\partial z} = 0 \tag{2.10b}$$

2.2.4 **Adimensionalization**

The governing equations as well as the boundary conditions presented in the previous section were nondimensionalized using the following dimensionless variables:

$$u^* = \frac{u}{V} \qquad v^* = \frac{v}{V} \qquad h = \frac{r}{D} \qquad x = \frac{z}{D} \tag{2.11a}$$

$$L_u^* = \frac{L_u}{D} \qquad L_h^* = \frac{L_h}{D} \qquad L_d^* = \frac{L_d}{D} \tag{2.11b}$$

$$q = \frac{T - T_0}{QD / k_f} \qquad P = \frac{p - r_0 gz}{r_0 V^2} \qquad (D = 2R_i) \tag{2.11c}$$

Where V is the average axial velocity at the entrance of the duct.

2.2.5 **Dimensionless governing equations**

Conservation of mass:

$$\frac{1}{h} \frac{\partial (hv^*)}{\partial h} + \frac{\partial u^*}{\partial x} = 0 \tag{2.12}$$

Conservation of momentum:

$$\frac{\partial v^*}{\partial t} + v^* \frac{\partial v^*}{\partial h} + u^* \frac{\partial v^*}{\partial x} = -\frac{\partial P}{\partial h} + \frac{1}{Re} \left[\frac{1}{h} \frac{\partial}{\partial h} \left(h \frac{\partial v^*}{\partial h} \right) - \frac{v^*}{h^2} + \frac{\partial^2 v^*}{\partial x^2} \right] \tag{2.13}$$

$$\frac{\partial u^*}{\partial t} + v^* \frac{\partial u^*}{\partial h} + u^* \frac{\partial u^*}{\partial x} = -\frac{Gr}{Re^2} q - \frac{\partial P}{\partial x} + \frac{1}{Re} \left[\frac{1}{h} \frac{\partial}{\partial h} \left(h \frac{\partial u^*}{\partial h} \right) + \frac{\partial^2 u^*}{\partial x^2} \right] \tag{2.14}$$

Conservation of energy in the fluid:

$$\frac{\partial q}{\partial t} + v^* \frac{\partial q}{\partial h} + u^* \frac{\partial q}{\partial x} = \frac{1}{Pe} \left[\frac{1}{h} \frac{\partial}{\partial h} \left(h \frac{\partial q}{\partial h} \right) + \frac{\partial^2 q}{\partial x^2} \right] \tag{2.15}$$

Conservation of energy in the pipe wall:

$$\frac{\partial q}{\partial t} = \frac{A}{Pe}\left[\frac{1}{h}\frac{\partial}{\partial h}\left(h\frac{\partial q}{\partial h}\right) + \frac{\partial^2 q}{\partial x^2}\right] \tag{2.16}$$

2.2.6 Dimensionless initial and boundary conditions

2.2.6.1 Initial conditions:

$$t = 0 \qquad\qquad u^*(h) = 2\left[1 - (2h)^2\right]; \; v^* = 0; \; q = 0 \tag{2.17}$$

2.2.6. 2 Boundary conditions:

- Inlet of the duct: $x = -L^*$

$$0 \le h < \frac{1}{2} \qquad\qquad u^*(h) = 2\left[1 - (2h)^2\right]; \; v^* = 0; \; q = 0 \tag{2.18a}$$

$$\frac{1}{2} \le h \le \frac{1}{2} + \Delta \qquad u^* = 0; \; v^* = 0; \; \frac{\partial q_w}{\partial x} = 0 \tag{2.18b}$$

- Upstream $-L_u^* < x < 0$, and downstream sections $L_h^* < x < L_h^* + L_d^*$

$$h = 0 \qquad\qquad \frac{\partial u^*}{\partial h} = 0; \; v^* = 0; \; \frac{\partial q_f}{\partial h} = 0 \tag{2.19a}$$

$$h = \frac{1}{2} \qquad\qquad u^* = 0; \; v^* = 0 \tag{2.19b}$$

$$h = \frac{1}{2} + D \qquad\qquad \frac{\partial q}{\partial h} = 0 \tag{2.19c}$$

- Heated section: $0 \le x \le L_h^*$:

$$h = 0 \qquad\qquad \frac{\partial u^*}{\partial h} = 0; \; v^* = 0; \; \frac{\partial q_f}{\partial h} = 0 \tag{2.20a}$$

$$h = \frac{1}{2} \qquad\qquad u^* = 0; \; v^* = 0 \tag{2.20b}$$

$$h = \frac{1}{2} + D \qquad\qquad \frac{\partial q_w}{\partial h} = 1 \tag{2.20c}$$

- Outlet of the duct: $x = L_h^* + L_d^*$

$$0 \le h < \frac{1}{2} \qquad\qquad \frac{\partial u^*}{\partial x} = 0, \; \frac{\partial v^*}{\partial x} = 0, \; \frac{\partial q_f}{\partial x} = 0 \tag{2.21a}$$

$$\frac{1}{2} \leq h \leq \frac{1}{2} + \Delta \qquad u^* = 0 \, ; \;\; v^* = 0 \, ; \;\; \frac{\partial q_w}{\partial x} = 0 \qquad\qquad\qquad (2.21b)$$

Based on this nondimensionalization, the parameters governing the transient conjugated mixed convection are:

$$Re = \frac{VD}{n} \qquad\qquad \text{(Reynolds number)}$$

$$Gr_Q = \frac{gbQD^4}{n^2 k_f} \qquad \text{(Grashof number based on the heat flux)}$$

$$Pe = Re.Pr = \frac{r_0 VDC_p}{k_f} \text{(Péclet number)}$$

$$K = \frac{k_w}{k_f} \qquad\qquad \text{(wall-to-fluid conductivity ratio)}$$

$$\Delta = \frac{R_e - R_i}{D} = \frac{d}{D} \qquad\quad \text{(pipe thickness to diameter ratio)}$$

$$A = \frac{a_w}{a_f} \qquad\qquad \text{(wall-to-fluid diffusivity ratio)}$$

Chapter 3

Numerical resolution

3.1 Introduction

In this chapter we present the methodology of resolution of the dimensionless system of equations presented in the chapter 2 and the grid points distributions in both axial and radial directions.

Considering the transient and the non-linear character of this system of equations as well as the high coupling between the gravity and the advection terms, the solution of the prescribed system of equations is exclusively numerical.

In addition to the finite volumes method adopted in the setting of this work, the finite differences and the finite elements methods are frequently used in the numerical simulations of fluid mechanic and heat transfer problems. In each of these numerical methods, one proceeds by the substitution of the differential equations of motion by a system of algebraic equations. These algebraic equations describe the same modeling physical phenomena by the original differential equations but at certain discrete number of points named nodes.

The finite volumes method, developed at the origin by **Patankar** and **Spalding** [67], has experienced an important success during the years 1980 due to many advantages that it offers, such as:

- The differences equations have a conservative property. This means that the extension of the conservation principle, written under a discretized form for a typical finite volume, is verified for the whole numerical domain.

- Its ability, its numerical robustness and its formalism very close to the physical reality (rate of heat flux and quantity of movement).

As introduced by **Patankar** [64], the finite volumes method consists in dividing the domain of computation in a finite number of volumes where each volume surrounds a node. The terms of the modeling differential equations are integrated on every control volume by using a suitable approximation scheme. The algebraic equations produced with this manner express the conservation principle for a finite control volume in the same way that the differential equations express it for an infinitesimal control volume.

3.2 Discretization of the physical domain

This section presents the discretization of the solution domain comprised between $0 \leq h \leq 0.5 + \Delta$ and $-L_u^* \leq x \leq L_h^* + L_d^*$. This domain is two-dimensional according to h and x, what presupposes that the angular component of the control volume is equal to one radian. The schematic of the system, including the coordinates and the representation of the grid distribution in the duct is sketched, respectively in Figures 3.1a and 3.1b.

The grid points were arranged according to the Type-B practice of **Patankar** [64], with control volume faces placed at the wall-fluid interface ($h = 0.5$) and at the discontinuities in the thermal boundary conditions ($x = 0$ and $x = L_h^*$).

The problem of interest was solved as if it were a fluid flow problem throughout the entire calculation domain ($0 \leq h \leq 0.5 + \Delta$). In the solid region ($0.5 < h \leq 0.5 + \Delta$), following the recommendation of **Patankar** [64], the viscosity was set to a very large value, resulting in zero velocities in that region.

To obtain enhanced accuracy, grids were chosen to be non-uniform both in the axial and radial directions (based one a geometric series progression) to account to uneven variations of velocity and temperature at the wall-fluid interface, at the inlet of the duct and at the interfaces between the heated section and its downstream and upstream sections. In the pipe wall, the grid distributions according to the radial direction are chosen uniform.

(a)   (b)
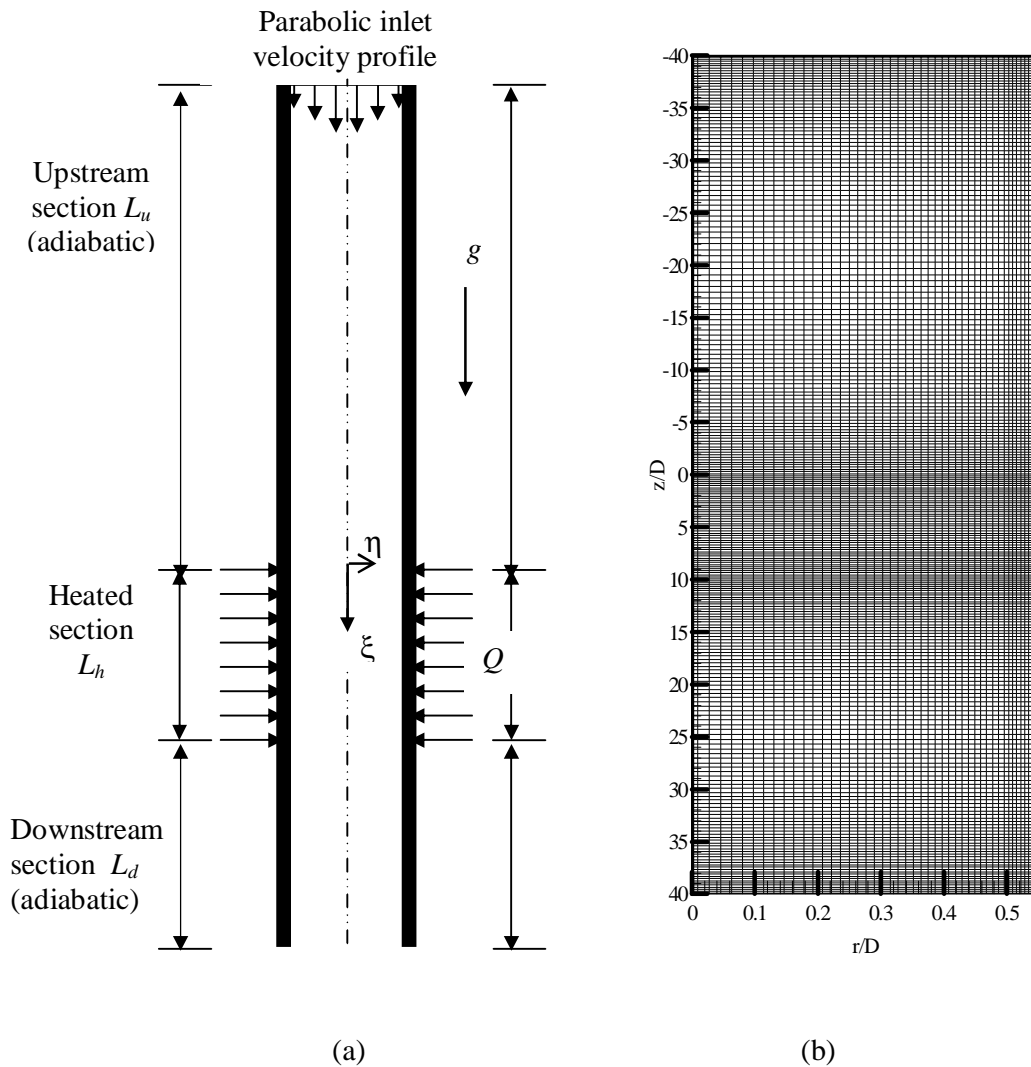
Figure 3.1: (a) Schematic diagram of the flow and the geometrical configuration

(b) Representation of the grid distribution in the fluid and in the pipe wall

The Figure 3.2 illustrates the main control volume ($\Delta V = h_P.\Delta h.\Delta x$) in which the geometric center is associated to the node P. This control volume is delimited by the faces *n*, *s*, *e* and *w*, corresponding respectively to the common sides of the control volumes belonging to the neighboring nodes N, S, E and W. In this numerical method, the scalar magnitudes (pressure and temperature) are calculated at the node P, while the vectorial magnitudes (velocities) are calculated at the points that lie on the faces of the control volume. Thus, the axial and radial velocities, are respectively calculated at the faces which are normal to x and h directions, as can be shown in Figure 3.2.

It is noticed that, with respect to the main grid points, the axial velocity locations are staggered only in the x-direction. In other words, the location of the axial velocity lies on the x-direction link joining two adjacent main grid points. Similarly, the radial velocity locations are staggered only in the h-direction.

An important advantage of the staggered grid is that the pressure difference between two adjacent grid points becomes the natural driving force for the velocity component located between these grid points, contrary to the case of the non-staggered grid points.
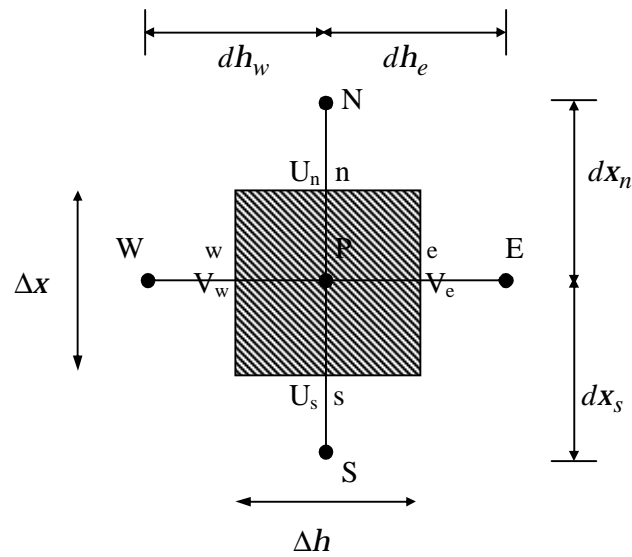
Fig. 3.2 Typical control volume

3.2.1 Radial grid-point distributions

The grid distributions according to the radial direction are shown in Figure 3.3. The i points are centered in the $\Delta h(i)$, who are the measurements of the finite volumes according to h direction.
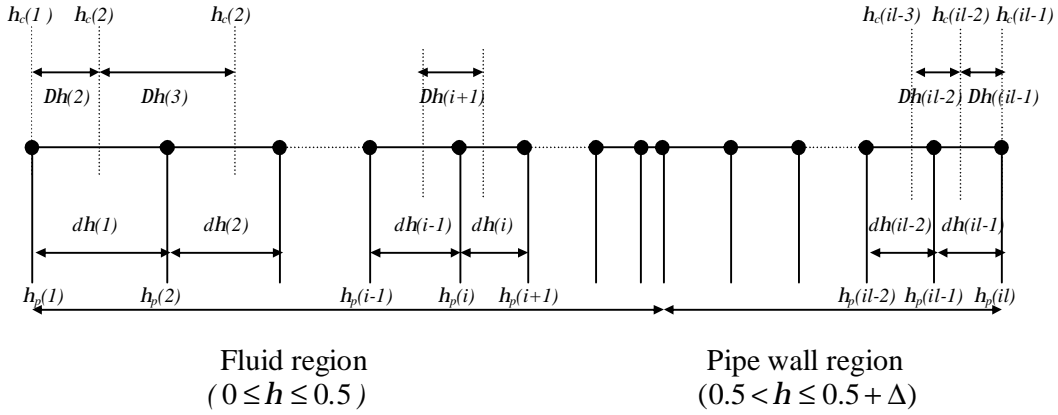
Figure 3.3: Radial distributions of the grid-point $(0 \leq h \leq 0.5 + \Delta)$

3.2.2 Axial grid-point distributions

The grid distributions according to the axial direction are shown in Figure 3.4a-b, respectively for the upstream and the heated sections (Figure 4a), and for the downstream section (Figure 3.4b). For each figure, the j points are centered in the $\Delta x(j)$, who are the measurements of the finite volumes according to x direction.
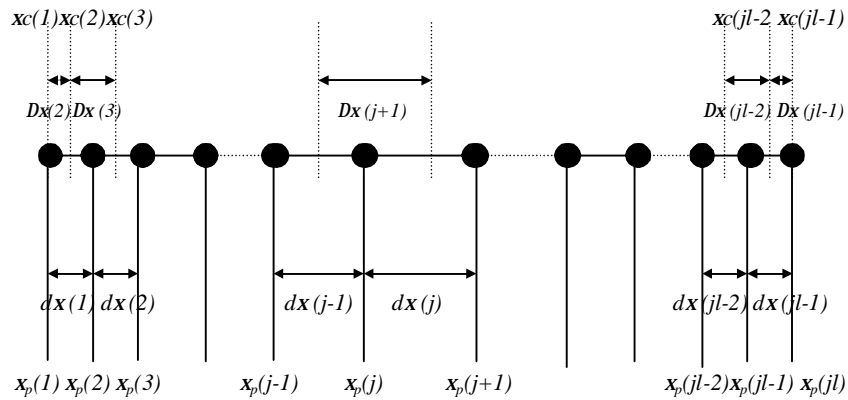
Figure 3.4a: Axial distributions of the grid-point in the upstream $(0 \leq x < L_u)$ and heated $(L_u \leq x \leq L_u + L_h)$ sections.
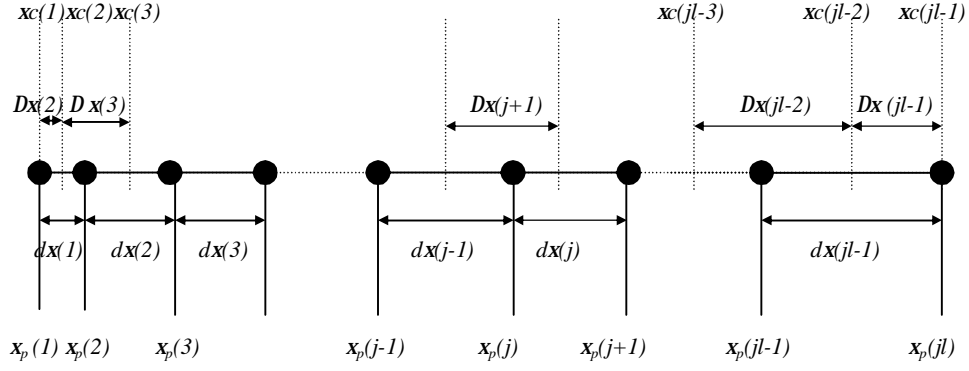
Figure 3.4b: Axial distribution of the grid-point in the downstream section

$$(L_u + L_h < x \leq L_u + L_h + L_d)$$

3.3 Conservative form of the conservation equations

The dimensionless system of equations (2-12)-(2-16), described in chapter 2, can be written in dimensionless local and conservative form, as follows:

$$\frac{\partial f}{\partial t} + e \frac{1}{h} \frac{\partial}{\partial h}(h\, V^* f) + e \frac{\partial}{\partial x}(U^* f) = \Gamma_f \left[\frac{1}{h} \frac{\partial}{\partial h}\left(h \frac{\partial f}{\partial h}\right) + \frac{\partial}{\partial x}\left(\frac{\partial f}{\partial x}\right) \right] + S_f \qquad (3.1)$$

where f, G_f, e and S_f, for each equation, are given as follow:

Governing equations	f	Γ_f	e	S_f
Mass	*1*	*0*	*1*	*0*
Axial momentum equation	u^*	*1 / Re*	*1*	$-(Gr/\mathrm{Re}^2)q - \partial P/\partial x$
Radial momentum equation	v^*	*1 / Re*	*1*	$-\partial P/\partial h - v^*/(h^2\, Re)$
Energy equation in the fluid	q	*1 / Pe*	*1*	*0*
Energy equation in the pipe wall	q	*A / Pe*	10^{30}	*0*

Table 3.1 Expressions of the variables f, coefficients of diffusion Γ_f, e and the source terms S_f used in the conservative equations.

3.4 Spatial and temporal discretization schemes

3.4.1 Discretization scheme of the transient terms

Within the interval time Δt, the integration of the transient terms, over the typical control volume (Figure 2) is obtained according to a progressive differences scheme of the first order. For example, when the variable $f = q$ the integration of the transient term (integration over the non-staggered control volume Figure 2) is calculated as follows:

$$\int\int_{w\,s}^{e\,n} (\int_{t}^{t+\Delta t} \frac{\partial f}{\partial t})h\partial h.\partial x.\partial t = \left[f_P^{t+\Delta t} - f_P^t \right] h_P.\Delta h_P.\Delta x_P \tag{3.2}$$

Where $\Delta h_P = h_e - h_w$, $\Delta x_P = x_n - x_s$ and f_P^t represents the dependent variable at the instant t that precedes the instant $t + \Delta t$ for which the variable $f_P^{t+\Delta t}$ is unknown. One admits that f at the point P $(= f_P^t)$ is the representation of f for the whole typical control volume at the instant t.

For each variable f (q, u^* and v^*), the other terms of the discretization equation are evaluated at the instant $t + \Delta t$, what corresponds to the implicit scheme. Indeed, because of the non-linearity of the Navier-Stockes equations, the used scheme is in fact semi implicit.

3.4.2 Discretization schemes of the spatial terms

For the spatial discretization, one uses the centered differences scheme of the second order, known by the appellation CDS (formulation with two points). Thus, the value of the variable f on a common face of two finite adjacent volumes is the half of the nodal values. Also, the spatial derivative of the variable f on a common face is the difference of the nodal variable values upstream and downstream of the interface divided by the distance between the two corresponding nodal, as can be shown in the examples below (Eqs.3.3 and 3.4) and Figures 3.5a-b.

$$f_n = \frac{f_P + f_N}{2} \qquad f_s = \frac{f_P + f_S}{2} \qquad \frac{\partial f}{\partial x}\bigg|_n = \frac{f_N - f_P}{dx_n} \qquad \frac{\partial f}{\partial x}\bigg|_s = \frac{f_P - f_S}{dx_s} \tag{3.3}$$

$$f_e = \frac{f_P + f_E}{2} \qquad f_w = \frac{f_P + f_W}{2} \qquad \frac{\partial f}{\partial h}\bigg|_e = \frac{f_E - f_P}{dh_e} \qquad \frac{\partial f}{\partial h}\bigg|_w = \frac{f_P - f_W}{\partial h_w} \tag{3.4}$$
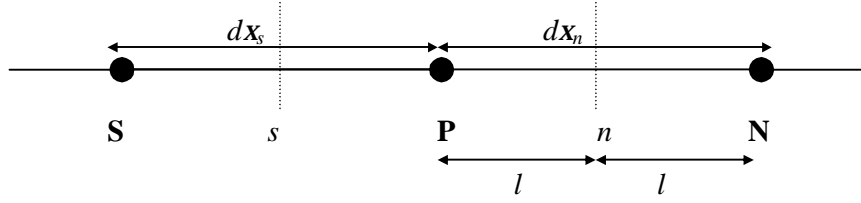
Figure 3.5a: Typical grid points for the calculation of f at the interface (s or n)
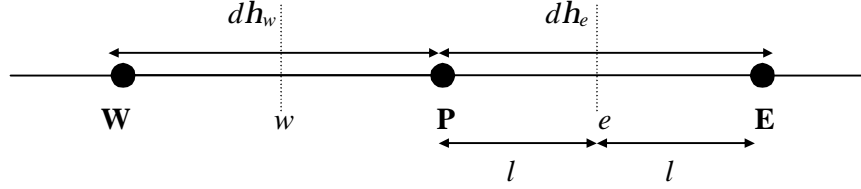
Figure 3.5b: Typical grid points for the calculation of f at the interface (w or e)

What follows is a demonstration of the precision of the scheme CDS. Referring to the Figures 3.5a and 3.5b, and while using the development in Taylor series of the function f, one shows that:

$$f_P = f_n - l \frac{\partial f}{\partial x}\bigg|_n + \frac{l^2}{2} \frac{\partial^2 f}{\partial x^2}\bigg|_n - \frac{l^3}{6} \frac{\partial^3 f}{\partial x^3}\bigg|_n + \dots\dots \tag{3.5}$$

$$f_N = f_n + l \frac{\partial f}{\partial x}\bigg|_n + \frac{l^2}{2} \frac{\partial^2 f}{\partial x^2}\bigg|_n + \frac{l^3}{6} \frac{\partial^3 f}{\partial x^3}\bigg|_n + \dots\dots \tag{3.6}$$

If we subtract Eq. (3. 6) from Eq. (3. 5), we have:

$$f_N - f_P = 2.l \frac{\partial f}{\partial x}\bigg|_n + \frac{l^3}{3} \frac{\partial^3 f}{\partial x^3}\bigg|_n \tag{3.7}$$

By substitution of the value of $l = dx_n / 2$, one obtains:

$$\frac{\partial f}{\partial x}\bigg|_n = \frac{f_N - f_P}{\partial x_n} - \frac{1}{24} \frac{\partial^3 f}{\partial x^3}\bigg|_n \Delta x^2 \tag{3.8}$$

From equation (3. 8), it is clear that the truncate error is of order of Δx^2.

Similar expressions can be obtained by the same development for the others derivative of f at the interfaces s, e, w. For example, the derivative of f at the interface e is given by the following expression:

$$\frac{\partial f}{\partial h}\bigg|_e = \frac{f_E - f_P}{\partial h_e} - \frac{1}{24}\frac{\partial^3 f}{\partial h^3}\bigg|_n \Delta h^2 \tag{3.9}$$

3.5 Discretization of the conservative equations

3.5.1 Discretization of the conservative equation of energy

The terms of the equation of conservation of energy are integrated over the typical control volume $(\Delta V_{Typique} = h_P \Delta h.\Delta x)$(Figure 2), between the instants t and $t + \Delta t$.

$$\int\limits_t^{t+\Delta t}\int\limits_{sw}^{ne}\frac{\partial q}{\partial t}hdh.dx.dt + e\int\limits_t^{t+\Delta t}\int\limits_{sw}^{ne}\frac{1}{h}\frac{\partial}{\partial h}(hu^*q)hdh.dx.dt + e\int\limits_t^{t+\Delta t}\int\limits_{sw}^{ne}\frac{\partial}{\partial x}(v^*q)hdh.dx.dt$$

$$= \Gamma_q\int\limits_t^{t+\Delta t}\int\limits_{sw}^{ne}\left[\frac{1}{h}\frac{\partial}{\partial h}\left(h\frac{\partial q}{\partial h}\right) + \frac{\partial}{\partial x}\left(\frac{\partial q}{\partial x}\right)\right]hdh.dx.dt \tag{3.10}$$

An appropriate rearrangement of the resulting terms from this integral gives the following general discretized form:

$$a_P^{t+\Delta t}q_P^{t+\Delta t} = a_N^{t+\Delta t}q_N^{t+\Delta t} + a_S^{t+\Delta t}q_S^{t+\Delta t} + a_E^{t+\Delta t}q_E^{t+\Delta t} + a_W^{t+\Delta t}q_W^{t+\Delta t} + b_q^t \tag{3.10a}$$

With:

$$a_P^{t+\Delta t} = a_N^{t+\Delta t} + a_S^{t+\Delta t} + a_E^{t+\Delta t} + a_W^{t+\Delta t} + a_P^t = \sum_{nb=N,S,E,W}a_{nb}^{t+\Delta t} + a_P^t \tag{3.10b}$$

Where the coefficients a_P, a_E, a_W, a_N, a_S are evaluated according to the hybrid scheme of **Patankar** [64]. This scheme is based on the absolute value of the local Péclet number associated to the controle volume. The local Péclet number *(Pe)* is defined as the ratio of the convection to the diffusion magnitudes *(Pe = F/D)*. The hybrid differentiation consists in using the following combination for the calculation of the above coefficients:

$$a_E = max\left[-F_e,\ D_e - \frac{F_e}{2},\ 0\right]\qquad a_W = max\left[-F_w,\ D_w - \frac{F_w}{2},\ 0\right] \tag{3.11}$$

$$a_N = max\left[-F_n,\ D_n - \frac{F_n}{2},\ 0\right]\qquad a_S = max\left[-F_s,\ D_s - \frac{F_s}{2},\ 0\right] \tag{3.12}$$

The significance of the hybrid scheme can be understood by observing that (1) it is identical with central-difference scheme for the Péclet number range $-2 \le Pe \le 2$, and (2) outside this range it reduces to the upwind scheme in which the diffusion has been set equal to zero. It should be noted that the hybrid scheme is in fact a less expensive

approximation in time of calculation of the exponential scheme [64], developed to assure an exact solution to a one-dimensional problem of convection/diffusion in the steady state. Some superior order schemes are recognized generally more precise, but more expensive and less robust [68-71].

It should also be noted that this formulation is valid for any arbitrary location of the interfaces between the grid points and is not limited to midway interfaces.

Furthermore, to handle the abrupt change of the conductivity at the wall-fluid interface, and consequently to obtain, a good representation for the interfacial heat flux, the conductivity at the wall-fluid interface is obtained by way of the harmonic mean of k_w and k_f [64].

3.5.2 Discretization of the conservative momentum equations

3.5.2.1 Axial direction

The terms of the conservation equation of the axial momentum are integrated on the staggered control volume $(\Delta V_{Su} = h_{Pu}.\Delta h.dx)$ in the axial direction, Figure 3. 6, between the instants t and $t + \Delta t$ (the superscript * of the axial velocity has been voluntarily omitted).
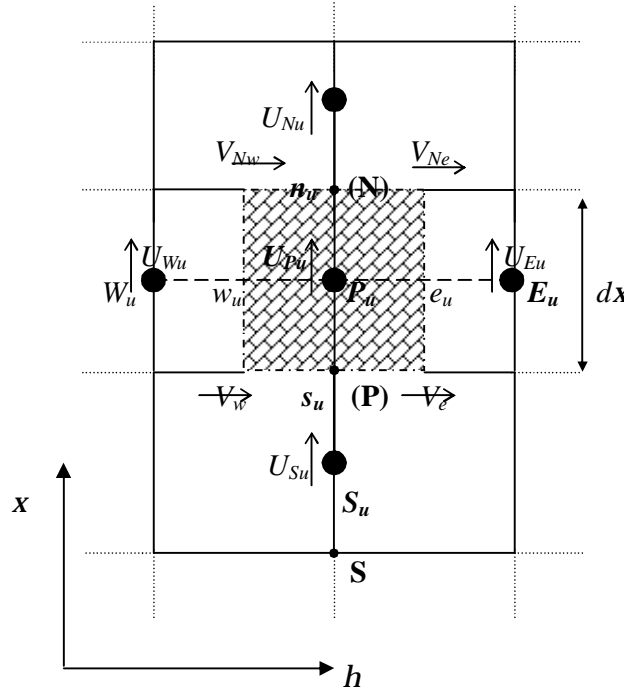
Figure 3.6: Staggered internal control volume for the axial velocity

$$\int_{t}^{t+\Delta t}\int_{su}^{nu}\int_{wu}^{eu} \frac{\partial u}{\partial t}hdh.dx.dt + e\int_{t}^{t+\Delta t}\int_{su}^{nu}\int_{wu}^{eu}\frac{1}{h}\frac{\partial}{\partial h}(hu\ u\ )hdh.dx.dt + e\int_{t}^{t+\Delta t}\int_{su}^{nu}\int_{wu}^{eu}\frac{\partial}{\partial x}(v\ u\ )hdh.dx.dt$$

$$= -(Gr/Re^2)\int_{t}^{t+\Delta t}\int_{su}^{nu}\int_{wu}^{eu}qhdh.dx.dt - \int_{t}^{t+\Delta t}\int_{su}^{nu}\int_{wu}^{eu}(\partial P/\partial x)hdh.dx.dt +$$

$$\Gamma_u\int_{t}^{t+\Delta t}\int_{su}^{nu}\int_{wu}^{eu}\left[\frac{1}{h}\frac{\partial}{\partial h}\left(h\frac{\partial u}{\partial h}\right)+\frac{\partial}{\partial x}\left(\frac{\partial u}{\partial x}\right)\right]hdh.dx.dt \tag{3.13}$$

An appropriate rearrangement of the resulting terms from this integral gives the following general discretized form:

$$a_{Pu}^{t+\Delta t} u_{Pu}^{t+\Delta t} = a_{Nu}^{t+\Delta t} u_{Nu}^{t+\Delta t} + a_{Su}^{t+\Delta t} u_{Su}^{t+\Delta t} + a_{Eu}^{t+\Delta t} u_{Eu}^{t+\Delta t} + a_{Wu}^{t+\Delta t} u_{Wu}^{t+\Delta t} + b_u^t -$$

$$(Gr/\mathrm{Re}^2).q_P^t.\Delta V_{Su} - (P_N^t - P_P^t).\Delta V_{Su} \tag{3.13a}$$

With:

$$a_{Pu}^{t+Dt} = a_{Nu}^{t+Dt} + a_{Su}^{t+Dt} + a_{Eu}^{t+Dt} + a_{Wu}^{t+Dt} + a_{Pu}^t = \sum_{nb\,=\,Nu,\,Su,\,Eu,\,Wu} a_{nb}^{t+Dt} + a_{Pu}^t \tag{3.13b}$$

Where $(P_N^t - P_P^t).\Delta V_{Su}$ is the appropriate pressure force in the axial direction.

3.5.2.2 Radial direction

The terms of the conservation equation of the radial momentum are integrated over the staggered control volume $(\Delta V_{Sv} = h_{Pv}.dh.\Delta x)$, Figure 3.7, between the instants t and $t + \Delta t$ (the superscript * of the radial velocity has been voluntarily omitted)
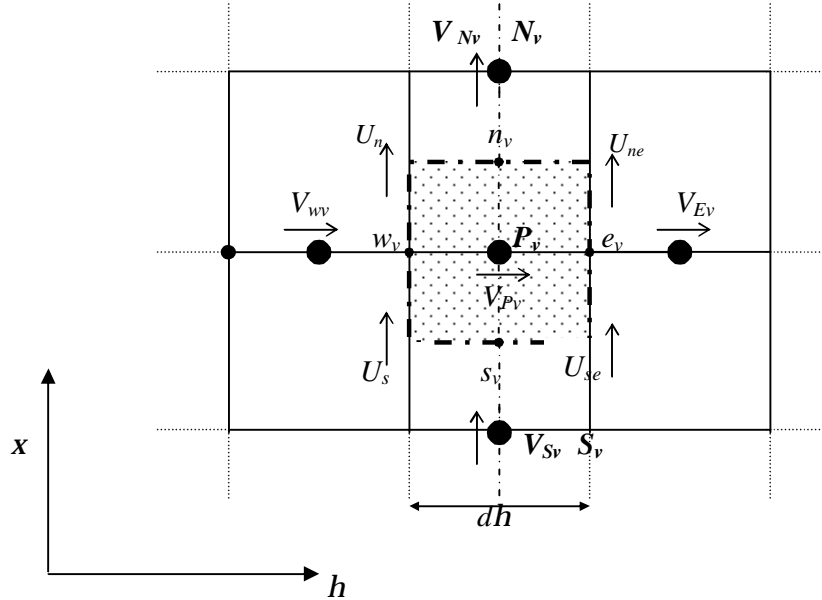
Figure 3.7: Staggered internal control volume for the radial velocity.

$$\int_t^{t+\Delta t}\int_{sv}^{nv}\int_{wv}^{ev} \frac{\partial v}{\partial t} h dh.dx.dt + e \int_t^{t+\Delta t}\int_{sv}^{nv}\int_{wv}^{ev} \frac{1}{h}\frac{\partial}{\partial h}(h\ u\ v\ )h dh.dx.dt + e \int_t^{t+\Delta t}\int_{sv}^{nv}\int_{wv}^{ev} \frac{\partial}{\partial x}(v\ v\ )h dh.dx.dt$$

$$= -\int_t^{t+\Delta t}\int_{sv}^{nv}\int_{wv}^{ev}\left(\frac{v}{h^2\,Re}\right)h dh.dx.dt - \int_t^{t+\Delta t}\int_{sv}^{nv}\int_{wv}^{ev}(\partial P/\partial h)h dh.dx.dt +$$

$$\Gamma_v \int\limits_{t}^{t+\Delta t} \int\limits_{sv}^{nv} \int\limits_{wv}^{ev} \left[\frac{1}{h}\frac{\partial}{\partial h}\left(h\frac{\partial v}{\partial h} \right) + \frac{\partial}{\partial x}\left(\frac{\partial v}{\partial x} \right) \right] h dh.dx.dt \qquad (3.14)$$

An appropriate rearrangement of the resulting terms from this integral gives the following general discretized form:

$$a_{Pv}^{t+\Delta t} v_{Pv}^{t+\Delta t} = a_{Nv}^{t+\Delta t} v_{Nv}^{t+\Delta t} + a_{Sv}^{t+\Delta t} v_{Sv}^{t+\Delta t} + a_{Ev}^{t+\Delta t} v_{Ev}^{t+\Delta t} + a_{Wv}^{t+\Delta t} v_{Wv}^{t+\Delta t} + b_v^t - (P_E^t - P_P^t).\Delta V_{Sv}$$

$$(3.14a)$$

With:

$$a_{Pv}^{t+Dt} = a_{Nv}^{t+Dt} + a_{Sv}^{t+Dt} + a_{Ev}^{t+Dt} + a_{Wv}^{t+Dt} + a_{Pv}^{t} = \sum_{nb = Nv, Sv, Ev, Wv} a_{nb}^{t+Dt} + a_{Pv}^{t} \qquad (3.14b)$$

Where $(P_E^t - P_P^t).\Delta V_{Sv}$ is the appropriate pressure force in the radial direction.

Let's note, that the coefficients a_{Pu}, a_{Eu}, a_{Wu}, a_{Nu}, a_{Su}, and a_{Pv}, a_{Ev}, a_{Wv}, a_{Nv}, a_{Sv}, respectively for the axial and the radial momentum equations are obtained by the same manner as those of the energy equation.

The viscosity at the wall-fluid interface is obtained by way of the harmonic mean of the fluid and solid viscosities. In the fluid, the real viscosity is used. In the wall region, a very big value (10^{30}) of viscosity is used, resulting in zero velocities in that region.

3.6 Equation of pressure

3.6.1 Pressure and velocities corrections

The coupling of the discretized equations of conservation is at the origin of the complexity of their resolution. In addition to the velocities and the temperature appearing in the momentum and the energy equations, one finds the unknown pressure field that intervenes in the momentum equations. This paragraph presents the development of the equations that leads to the discretized equation of pressure. The used development is based on the SIMPLE algorithm developed by **Patankar** [64]. The pressure field is unknown; an initial field is necessary to start the iterative process of solution. This p^* field, when applied to the equations (3.13a) and (3.14a) leads to values of u^* and v^* that don't satisfy exactly the conservation equation of mass. One considers that the exact pressure is given by:

$$p=p*+p\mathcal{C} \tag{3.15}$$

Where $p\mathcal{C}$ is the pressure correction.

In the same way, the exact velocities are:

$$u=u*+u\mathcal{C} \tag{3.16}$$

and

$$v=v*+v \tag{3.17}$$

Where $u\mathcal{C}$ and $v\mathcal{C}$ are the corresponding velocity corrections.

By substitution of the values of u, v and p by $u*$, $v*$ and $p*$ in the equation (3. 13a) and (3. 14a), one obtains:

$$a_{Pu}^{t+\Delta t}u{_{Pu}^{*t+\Delta t}} = \sum_{nb=Nu,Su,Eu,Wu} a_{nb}^{t+\Delta t}u{_{nb}^{*t+\Delta t}}+b_u^t+(P_P^{*t}-P_N^{*t}).\Delta V_{Su} \tag{3.18}$$

and

$$a_{Pv}^{t+\Delta t}v{_{Pv}^{*t+\Delta t}} = \sum_{nb=Nv,Sv,Ev,Wv} a_{nb}^{t+\Delta t}v{_{nb}^{*t+\Delta t}}+b_v^t+(P_P^{*t}-P_E^{*t}).\Delta V_{Sv} \tag{3.19}$$

If we subtract Eq. (3.18) from Eq. (3.13a) and Eq. (3.19) from Eq. (3.14a), we have:

$$a_{Pu}^{t+\Delta t}u{_{Pu}^{\prime t+\Delta t}} = \sum_{nb=Nu,Su,Eu,Wu} a_{nb}^{t+\Delta t}u{_{nb}^{\prime t+\Delta t}}+(P_P^{\prime t}-P_N^{\prime t}).\Delta V_{Su} \tag{3.20}$$

and

$$a_{Pu}^{t+\Delta t}v{_{Pv}^{\prime t+\Delta t}} = \sum_{nb=Nv,Sv,Ev,Wv} a_{nb}^{t+\Delta t}v{_{nb}^{\prime t+\Delta t}}+(P_P^{\prime t}-P_E^{\prime t}).\Delta V_{Sv} \tag{3. 21}$$

By disregarding the terms, $\sum a_{nb}^{t+\Delta t}u{_{nb}^{\prime t+\Delta t}}$ and $\sum a_{nb}^{t+\Delta t}v{_{nb}^{\prime t+\Delta t}}$ of the right member of equations (3. 20) and (3. 21), one obtains:

$$a_{Pu}^{t+\Delta t}u{_{Pu}^{\prime t+\Delta t}} = (P_P^{\prime t}-P_N^{\prime t}).\Delta V_{Su} \tag{3.22}$$

$$a_{Pv}^{t+\Delta t}v{_{Pv}^{\prime t+\Delta t}} = (P_P^{\prime t}-P_E^{\prime t}).\Delta V_{Sv} \tag{3.23}$$

or

$$u{_{Pu}^{\prime t+\Delta t}} = d_{Pu}.(P_P^{\prime t}-P_N^{\prime t}) \tag{3.24}$$

$$v{_{Pv}^{\prime t+\Delta t}} = d_{Pv}.(P_P^{\prime t}-P_E^{\prime t}) \tag{3.25}$$

where:

$$d_{Pu} = \frac{\Delta V_{Su}}{a_{Pu}^{t+\Delta t}} \tag{3.26}$$

and

$$d_{Pv} = \frac{\Delta V_{Sv}}{a_{Pv}^{t+\Delta t}} \tag{3.27}$$

An extensive discussion of these actions can be found in [64]. Equations (3.24) and (3.25) would be called the velocity-correction formulas, who can be also written as:

$$u_{Pu}^{t+\Delta t} = u_{Pu}^{*t+\Delta t} + d_{Pu}.(P_P^{'t} - P_N^{'t}) \tag{3.28}$$

$$v_{Pu}^{t+\Delta t} = v_{Pu}^{*t+\Delta t} + d_{Pv}.(P_P^{'t} - P_N^{t'}) \tag{3.29}$$

This shows how the started velocities $u_{Pu}^{*t+\Delta t}$ and v_{Pv}^{*t+Dt} are to be corrected in response to the pressure corrections to produce, respectively $u_{Pu}^{t+\Delta t}$ and v_{Pv}^{t+Dt}.

3.6.2 Pressure-correction equation

The continuity equation is:

$$\frac{1}{h}\frac{\partial(hv)}{\partial h} + \frac{\partial u}{\partial x} = 0 \tag{3.30}$$

We shall integrate this equation over the typical control volume, shown previously in Figure 3.2, as follows:

$$\int_t^{t+\Delta t}\int_s^n\int_w^e \frac{1}{h}\frac{\partial(hv)}{\partial h}hdh.dx.dt + \int_t^{t+\Delta t}\int_s^n\int_w^e \frac{\partial u}{\partial x}hdh.dx.dt = 0 \tag{3.30a}$$

With an appropriate rearrangement of the resulting terms from this integral, the integrated form of this equation becomes:

$$(h_e v_e^{t+\Delta t} - h_w v_w^{t+\Delta t})\Delta x.\Delta t + 0.5(u_n^{t+\Delta t} - u_s^{t+\Delta t}).(h_e^2 - h_w^2).\Delta t = 0 \tag{3.30b}$$

If now we substitute for the two velocity components the expressions given by the velocity-correction formulas, such as Eqs. (3.28)- (3.29), we obtain, after an appropriate arrangement, the following discretization equation for the pressure $p\phi$

$$a_P^{t+\Delta t}p_P^{'t+\Delta t} = a_N^{t+\Delta t}p_N^{'t+\Delta t} + a_S^{t+\Delta t}p_S^{'t+\Delta t} + a_E^{t+\Delta t}p_E^{'t+\Delta t} + a_W^{t+\Delta t}p_W^{'t+\Delta t} + b^{t+\Delta t} \tag{3.31}$$

where

$$a_N^{t+\Delta t} = d_n . h_P \Delta h_P \Delta t \tag{3.31a}$$

$$a_S^{t+\Delta t} = d_s . h_P \Delta h_P \Delta t \tag{3.31b}$$

$$a_E^{t+\Delta t} = d_e . \Delta x . \Delta t \tag{3.31c}$$

$$a_W^{t+\Delta t} = d_w . \Delta x . \Delta t \tag{3.30d}$$

$$a_P^{t+\Delta t} = a_N^{t+\Delta t} + a_S^{t+\Delta t} + a_E^{t+\Delta t} + a_W^{t+\Delta t} \tag{3.31e}$$

$$b^{t+\Delta t} = (h_w u_w^* - h_e u_e^*) \Delta x \Delta t + (u_s^* - u_n^*) h_P \Delta h_P \Delta t \tag{3.31f}$$

Let's note that if $b^{t+\Delta t}$ is zero; it means that the started velocities satisfy the continuity equation, and no pressure correction is needed. The term $b^{t+\Delta t}$ thus represents a "mass source", which the pressure corrections must annihilate.

The discretized equations for *T, u, v* and *p* (3.10, 3.13a, 3.14a and 3.31) represent a general formulation. This generality in the establishment of these equations will permit us to use the same resolver for *T, u, v* and *p* for every global iteration of the solution process.

3.7 Boundary conditions: discretized equations for *T, u, v* and *p*

The following paragraphs describe in the order the application of the boundary conditions for the discretized equations for *T, u, v* and *p*. For all cases, the boundary conditions will be expressed under the same form than the one of the general equation.

3.7.1 Discretized equations for *T*

- On the axis of the cylinder ($h = 0$), what corresponds to ($i=1, 1 \leq j \leq JL$), we have:

$\frac{\partial \theta}{\partial \eta} = 0$. The discretized form of this equation is: $\frac{\theta(2, j) - \theta(1, j)}{D\eta(1)} = 0$, or $\theta(2, j) = \theta(1, j)$, what

corresponds to $a_P^{t+\Delta t} = a_E^{t+\Delta t} = 1$, $a_W^{t+\Delta t} = a_N^{t+\Delta t} = a_S^{t+\Delta t} = b^{t+\Delta t} = 0$.

- For the control volumes adjacent to the outer surface of the pipe wall of the heated section, the heat flux is introduced in the term *b* by the discretization of the boundary

condition $K \frac{\partial \theta}{\partial \eta}\big|_{h=0.5+\Delta} = 1$, it results $a_P^{t+\Delta t} = a_W^{t+\Delta t} = 1$, $a_E^{t+\Delta t} = a_N^{t+\Delta t} = a_S^{t+\Delta t} = 0$,

$$b^{t+Dt} = \frac{1}{K} Dh(_{NT-1}).$$

- For the control volumes adjacent to the pipe wall of the adiabatic sections and those adjacent to the exit of the tube, we have respectively:

$$a_P^{t+\Delta t} = a_W^{t+\Delta t} = 1, \; a_E^{t+\Delta t} = a_N^{t+\Delta t} = a_S^{t+\Delta t} = b^{t+\Delta t} = 0.$$

and

$$a_P^{t+\Delta t} = a_S^{t+\Delta t} = 1, \; a_E^{t+\Delta t} = a_W^{t+\Delta t} = a_N^{t+\Delta t} = b^{t+\Delta t} = 0.$$

- At the entry of the tube, in the fluid, the treatment is trivial because the temperature is known. In the solid, the treatment is similar to the one of the adiabatic sections.

3.7.2 Discretized equations for *u*

In the case of the discretized equation of axial momentum and for the control volumes adjacent to the pipe wall, an equation similar to the equation (3.13a) is applied with $u_{Eu}^{t+\Delta t} = 0$. For the control volumes adjacent to the line of symmetry, the same equation is applied but this time while, ignoring the condition to the node Wu ($u_{Wu}^{t+\Delta t} = 0$). In this case, at every time steps (i.e. at the end of every global iteration), $u_{Wu}^{t+\Delta t}$ is set equal to $u_{Pu}^{t+\Delta t}$.

At the inlet of the duct (Figure 3.8), the equation (3.13a) is applied. In this case, $u_{Su}^{t+\Delta t}$ corresponds to the inlet velocity, supposed known.

At the exit of the tube (Figure 3.9), the same equation is also applied but this time while ignoring the conditions to the node N_u ($u_{Nu}^{t+\Delta t} = 0$) and at every time steps (i.e. at the end of every global iteration), $u_{Nu}^{t+\Delta t}$ is set equal to $u_{Pu}^{t+\Delta t}$.
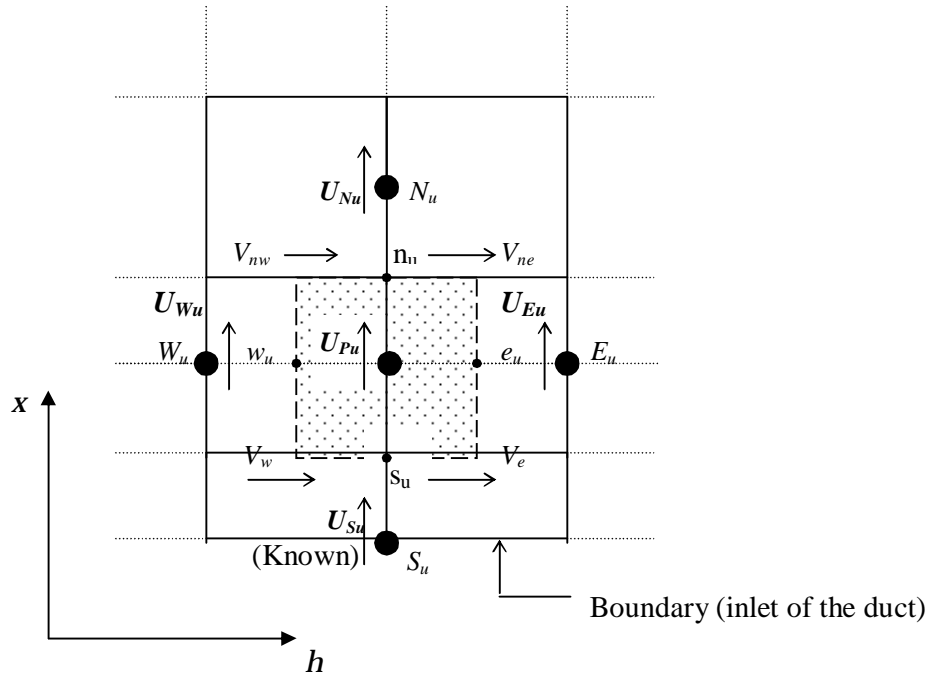
Figure 3.8 Staggered control volume at the inlet of the duct for the axial velocity
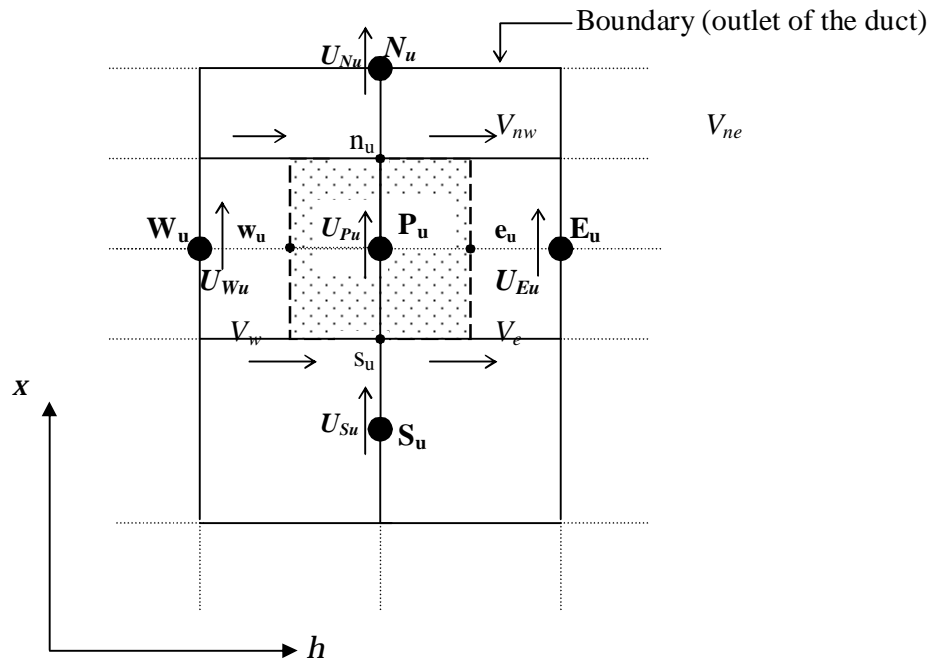
Figure 3.9: Staggered control volume at the outlet of the duct for the axial velocity

3.7.3 Discretized equations for *v*

The same principle is applied for the equation of radial momentum. At the line of symmetry *(h=0)*, (Figure 3.10), the same equation is applied with $v_{Wv}^{t+\Delta t} = 0$. At the outside surface of the duct *(h=0.5+D)* (Figure 3.11), the equation (3.14a) is applied with $v_{Ev}^{t+\Delta t} = 0$. At the entry and the exit of the duct, the same equation is applied while putting $v_{Sv}^{t+\Delta t} = 0$ at the entry and while omitting $v_{Nv}^{t+\Delta t} = 0$ at the exit.
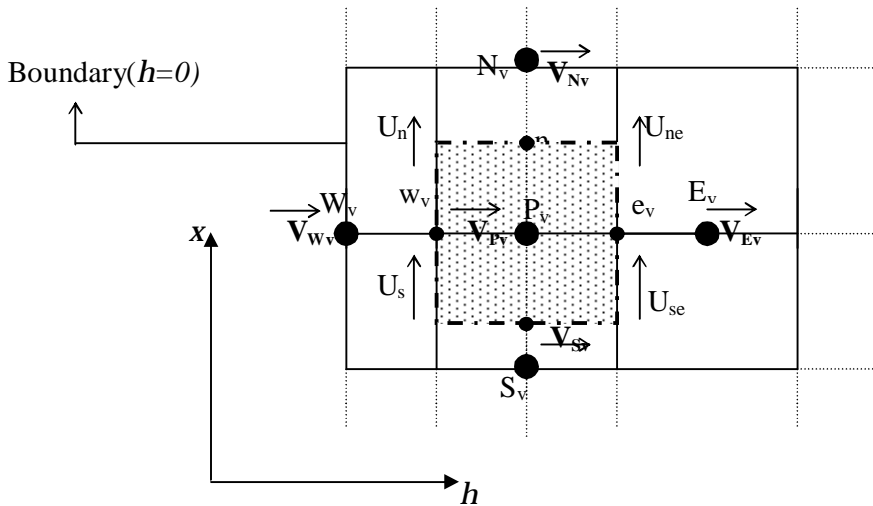
Figure 3.10: Staggered control volume at the symmetry line *(h=0)* for the radial velocity
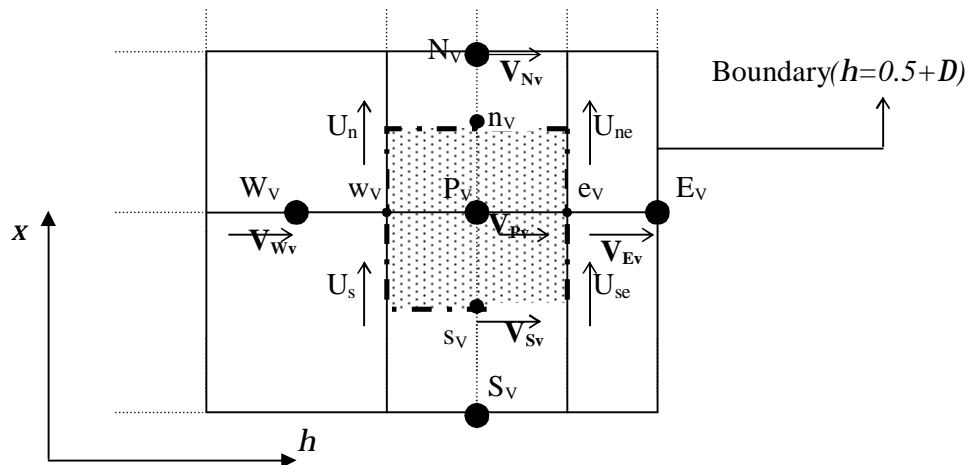
Figure 3.11: Staggered control volume at the outside surface of the tube *(h=0.5+D)* for the radial velocity

3.7.4 Discretized equations for *p*

Finally, the boundary conditions for the discretized equation of pressure are established, as follows. The equation (3. 31) is applied by considering: $a_E^{t+\Delta t} = 0$ for the control volumes situated in the fluid along the wall-fluid interface *(h=0.5)*; $a_W^{t+\Delta t} = 0$ at the line of symmetry *(h=0)*; $a_N^{t+\Delta t} = 0$ at the exit of the tube and $a_S^{t+\Delta t} = 0$ at the inlet of the duct. In the solid region, a zero value is assigned to the pressure. The calculated pressure at every point in the fluid is normalized by subtracting form it the value of the pressure of the control volume situated at the entry and adjacent to the line of symmetry.

3. 8 Method of solution

Due to the fact that the basic equations are non-linear and highly coupled, an iterative algorithm based on the SIMPLE method [50] is used to solve these equations. The establishment of the iterative solution is as follows:

1. Start with a guessed pressure fields p^* at the time τ

2. Change the time $\tau=\tau+\Delta\tau$

3. Solve the momentum equations, such as (3.18)- (3.19), to obtain u^* and v^*.

4. Solve the p' equation (3.31)

5. Calculate p from equation (3.15) by adding p' to p^*.

6. Calculate u and v from their starred values using the velocity-correction formulas (3.28)- (3.29).

7. Solve the discretized equation for the equation of energy (3-10a) and deduct the temperature *q*.

8. Treat the corrected pressure p as a new guessed pressure p^*, return to step 2, and repeat the whole procedure until the steady state regime is obtained.

3.9 Underrelaxation and convergence

3.9.1 Underrelaxation

In the iterative solution of the algebraic equations or in the overall iterative scheme used for handling non-linearity, it is often desirable to slow down the changes, from iteration to iteration, in the values of the dependant variable. This process is called *under-relaxation*. Underrelaxation is a very useful device for nonlinear problems. It is often employed to avoid divergence in the iterative solution of strongly nonlinear equations.

In the purpose of introducing the under-relaxation, we shall work with the general discretization equation of the form

$$a_P^{t+\Delta t} f_P^{t+\Delta t} = \sum a_P^{t+\Delta t} f_P^{t+\Delta t} + b^{t+\Delta t} \tag{3.32}$$

Further, f_P^t will be taken as the value of f_P from the previous iteration. Equation (3.32) can be written as:

$$f_P^{t+\Delta t} = \frac{\sum a_P^{t+\Delta t} f_P^{t+\Delta t} + b^{t+\Delta t}}{a_P^{t+\Delta t}} \tag{3.32a}$$

If we add f_P^t to the right-hand side and subtract it, we have

$$f_P^{t+\Delta t} = f_P^t + \left(\frac{\sum a_P^{t+\Delta t} f_P^{t+\Delta t} + b^{t+\Delta t}}{a_P^{t+\Delta t}} - f_P^t \right) \tag{3.32b}$$

Where the contents of the parentheses represent the change in f_P produced by the current iteration. This change can be modified by the introduction of a relaxation factor α, so that

$$f_P^{t+\Delta t} = f_P^t + a \left(\frac{\sum a_P^{t+\Delta t} f_P^{t+\Delta t} + b^{t+\Delta t}}{a_P^{t+\Delta t}} - f_P^t \right) \tag{3.32c}$$

$$\frac{a_P^{t+\Delta t}}{a} f_P^{t+\Delta t} = \sum a_P^{t+\Delta t} f_P^{t+\Delta t} + b^{t+\Delta t} + (1-a) \frac{a_P^{t+\Delta t}}{a} f_P^t \tag{3.32d}$$

There are no general rules for choosing the best value of a. The optimum value depends upon a number of factors, such as the nature of problem, the number of grid

points, the grid spacing, and the iterative procedure used. In this work, the values of the used relaxation factors are:

Axial velocity: $\alpha_u = 0.5$

Radial velocity: $\alpha_v = 0.5$

Pressure: $\alpha_p = 0.8$

These values of the relaxation factors have been found to be satisfactory in a large number of fluid-flow computations **Patankar** [64].

3.9.2 Convergence

The marching in the time is assured by an external loop in which the dependent variables at the instant $t + \Delta t$ are affected in those at the instants t. In this work, we are fixed two criteria of convergence of the numerical code, as follows:

1. Convergence was considered as being achieved when $\left| (f_{i,j}^{k+1} - f_{i,j}^{k}) / f_{i,j}^{k} \right| < 10^{-4}$ where $f_{i,j}^{k}$ is u^* or q at every (x_j, h_i) location of the discretized domain at the iteration k.

2. One verifies, graphically, in some points of the domain that there are not anymore temporal variations of all variables associated to these points.

Chapter 4

Numerical results and analyses

4.1 Introduction

This chapter is devoted to the results of the numerical simulation of the transient conjugated mixed convection in a vertical thick tube. The considered geometry as well as the boundary conditions and the grid-point distributions have been presented in Figures 3.1a and 3.1b. The dimensionless thickness of the pipe wall is equal to D. A uniform heat flux, Q is applied at the external surface of the tube on the central section. This section is located between two adiabatic sections that permit the study of the diffusion in the fluid and in the pipe wall. The fluid flow is laminar, transient and axisymmetric. Besides, the fluid penetrates to the top of the tube (inlet) and falls down toward the bottom (exit); therefore one is in presence of opposed mixed convection flow case.

Natural convection flow, resulting from the variation of the fluid density inside the tube, is then superposed to the forced convection flow of Poiseuille type. So, a decrease of the fluid density in the neighbouring region of the heated pipe wall provokes a corresponding deceleration of the fluid in that region. One even attends, for a sufficiently elevated heat flux (or equivalently elevated Gr) to the reversing of the flow close to the pipe wall, and consequently to the apparition of a recirculation cell. In some cases, the wall thermal conduction generates an important redistribution of the applied heat flux, what generates an elongation of this cell upstream of the heated section. The cell acts like an insulator in the upstream section and the interfacial heat flux propagates itself upstream of this cell before being transmitted to the fluid.

4.2 Preliminary considerations

4. 2.1 Selection of the dimensionless parameters

The foregoing analysis indicates that the heat transfer characteristics in the flow and in the pipe wall depend on five dimensionless groups, namely: the Prandtl number *Pr,* the Richardson number Gr/Re^2 (or *Gr* and *Re),* the wall-to-fluid conductivity ratio *K*, dimensionless wall thickness *D*, and the wall-to-fluid diffusivity ratio *A*.

One recovers the first two parameters in all mixed convection problems. The second two other parameters are specific to the calculations of the steady or transient conjugated heat transfer, while the last parameter is specific to the transient conjugated heat transfer problems. In addition to the already mentioned parameters, the solution of this problem requires the specification of the length of each of the three sections of the domain: *(L_i /D),* where *i=u, h, d.*

In the transient state regime, a parametric study of all these individual parameters would have required an enormous set of results and this was not the main goal of this work. In order to present a reasonable quantity of solutions and to concentrate on the understanding of the transient conjugate mixed convection heat transfer characteristics, all numerical runs were performed for *Pr=5*, what represents a fluid whose properties are similar to those of the water. The Grashof number has been fixed at 5.10^3 and 5.10^5. Three velocities of the flow have been kept, leading to three values of the Reynolds number *1, 10* and *100*, qualified of low and high *Re*. The corresponding Gr/Re^2 ratios are *5000* and *50*. In summary, three cases of mixed convection are examined:

Low *Re*   High *Re*

$Gr_q=5000$ $Gr_q=5000, 500000$

Re=1   *Re=10, 100*

$Gr/Re^2=5000$ $Gr/Re^2=50$

Pe=5   *Pe=5*

The dimensionless heated length, $L_h^* = 10$. This length is judged adequate because it permits to study the development of the flow while, keeping the length of the calculation domain to an acceptable level.

The first and the third portion of the duct namely respectively: the upstream and the downstream sections are insulated. Their values were sufficiently long for all cases considered in this work to study:

----

(1) The diffusion of heat by axial conduction,

(2) To ensure that the inlet conditions remain no affected by mixed convection in the upstream section,

(3) To ensure that the outlet boundary conditions in the fluid region were appropriate, as can be seen, respectively in Figure 4.1, Figure 4.4, Figure 4.6 and Figure 4.12b for the hydrodynamic field, and in Figures 4.2a-b for the thermal field. In these figures, one can note that the corresponding hydrodynamical and thermal fields at the outlet of the duct are fully developed.

Parameter *K* is chosen to have the value 10, 50, *100* or *500*, and *A* is assigned to have the values 0.01, 0.03 or 4. Parameter *D* is chosen to have the values *0.01, 0.05, 0.15* or *0.25*. A typical case for *Gr/Re²=5000*, *K=50*, *D=0.05* and *A=4* is discussed in detail.

These values of the stated parameters were selected as appropriate for problems of engineering interest and from the range that all the presumed effects of the defined problem, i.e. two dimensional wall and axial fluid conduction are in a significant level [36, 40, 42, 59].
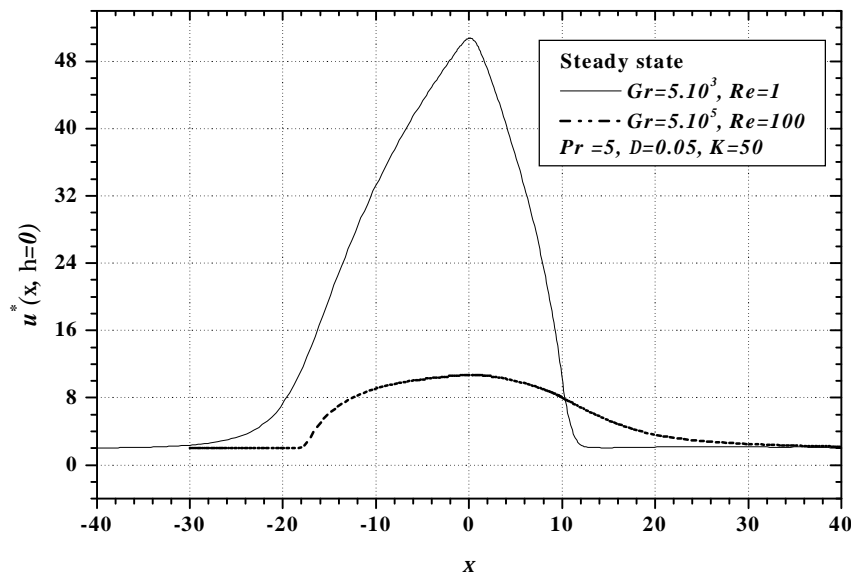
Figure 4.1 Evolution of the centreline axial velocity at the steady state
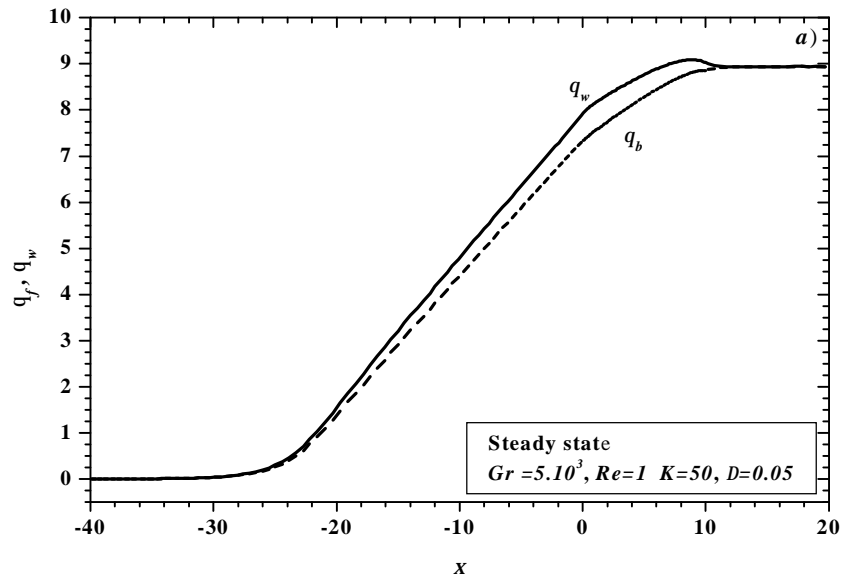
Figure 4.2a Axial evolution of bulk fluid and wall temperatures
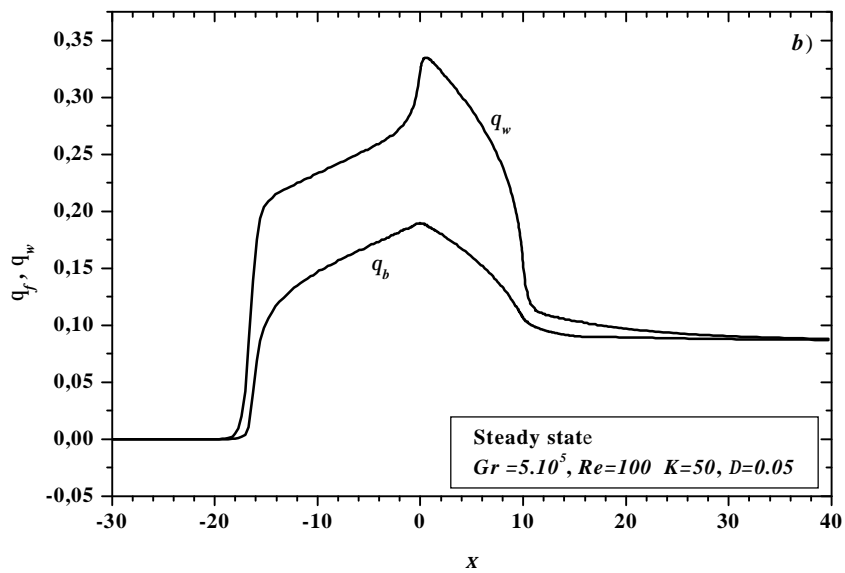
Figure 4.2b Axial evolution of bulk fluid and wall temperatures

4.2.2 Grid independency

Numerical experiments were made to ensure that the numerical results are grid independent for *Re=100*, *Gr=5.10⁵*, *D=0.05* and *K=50*. This case has been retained because of the importance of the two modes of convection and the extent of the heat flux redistribution in the upstream section.

While beginning with an enough coarse grids and while refining it, the obtained results have been compared until the refinement doesn't have a noticeable effect anymore on the solution. One estimates whereas that, solution is grid independent.

Some exploratory simulations demonstrated that, ten (10) nodes in the pipe wall are sufficient to get the grid independency. Therefore, this number has been adopted in the pipe wall. It is why, in what follows, one only preoccupies of the grid effect in the radial direction in the fluid.

The grid independency has been verified with the help of four criteria:
-The profile of dimensionless axial velocity, *u/V*
-The axial distributions of q_w and q_b
-The axial redistributions of the friction coefficient ratio *(f .Re)/(f .Re)₀*
-The normalized interfacial heat flux Q_{wi}.

Among these criteria, the axial distribution of the friction coefficient ratio and of the normalized interfacial heat flux proved to be the more severe criteria. For this reason, only these results are presented.

For different grid arrangements in the axial direction, namely: *A(30,16,30), B(60,30,60), C(90,60,90), D(150,90,120)* and *E(180,90,120)* we present in Figures 4.3a-c, the axial distribution of the interfacial heat flux at several instants of the transient period including the steady state, and in Figure 4.4, the axial distribution of the friction coefficient at the steady state.

For each cases *A, B, C, D* and *E*, the first, the second and the third value refer respectively, to the upstream section, the heated and the downstream sections. For these grid arrangements, the number of nodes in the radial direction is *30* and *10*, respectively in the fluid and in the pipe wall.

One concludes that the increase of the nodes improve the accuracy of the interfacial heat flux and the friction coefficient ratio, in particular, in the upstream section. In these figures,

it is obvious that the grid arrangement corresponding to the case *D* is sufficiently accurate to describe the heat transfer in the duct.

It may be observed that Q_{wi} presents large extreme values in the upstream section. This behaviour will be explained in the following paragraphs.

The effect of the number of nodes in the radial direction is presented at the steady state in Figures 4.5 and 4.6, respectively for the interfacial heat flux and for the friction coefficient ratio. It may be observed that the curve corresponding to the case *C1* is sufficiently accurate.

Consequently and based on these numerical experiments, all numerical runs were performed with the case *D (150, 90, 120)* in the axial direction, and with the case *C1(40, 10),* in the radial direction.
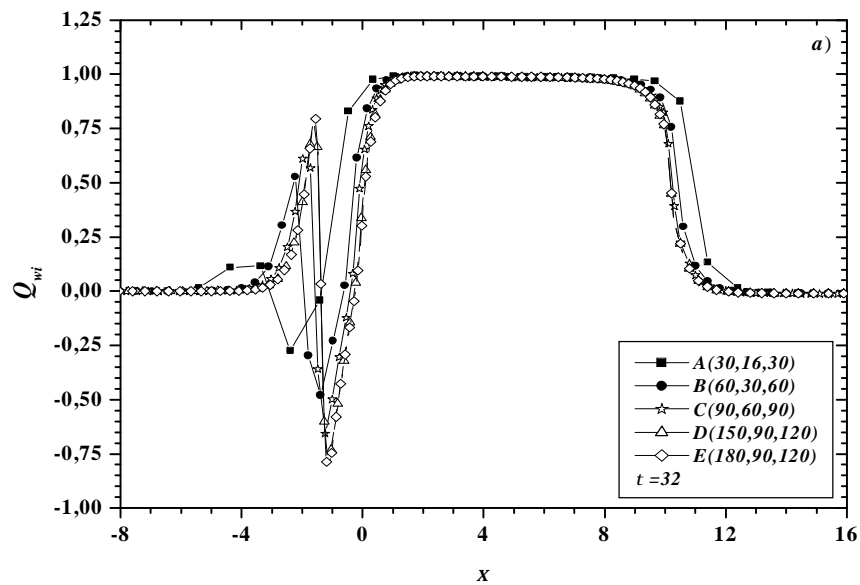
Figure 4.3a Influence of the grid distribution in the axial direction on the interfacial heat flux

Chapter 4   *Numerical results*
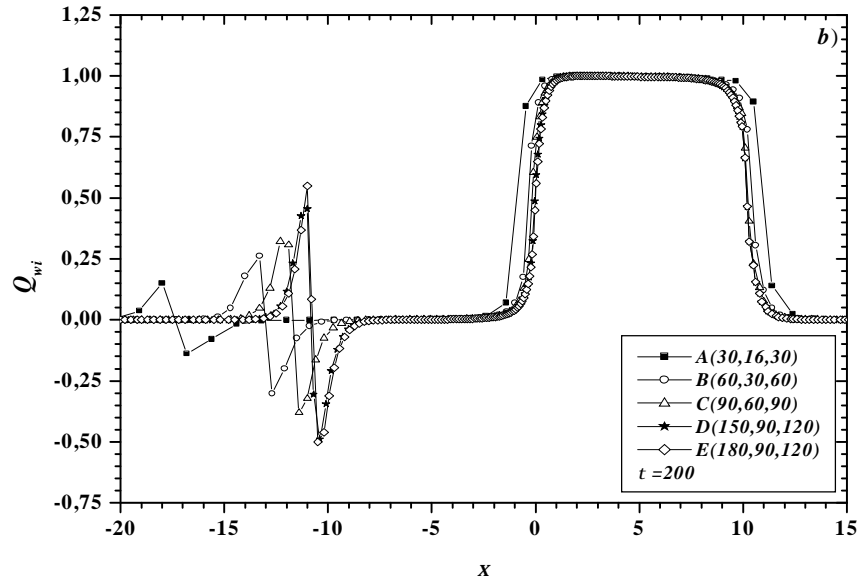
Figure 4.3b Influence of the grid distribution in the axial direction on the interfacial heat flux
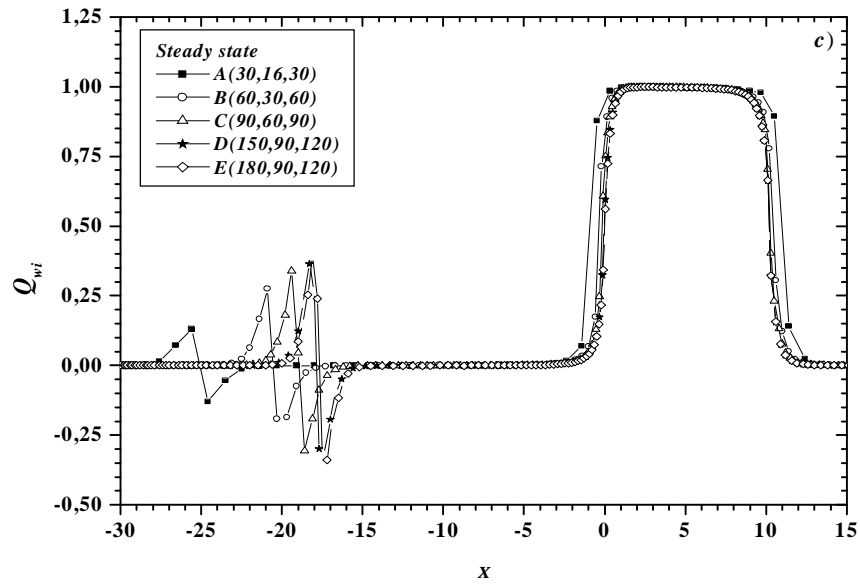
Figure 4.3c Influence of the grid distribution in the axial direction on the interfacial heat flux

---
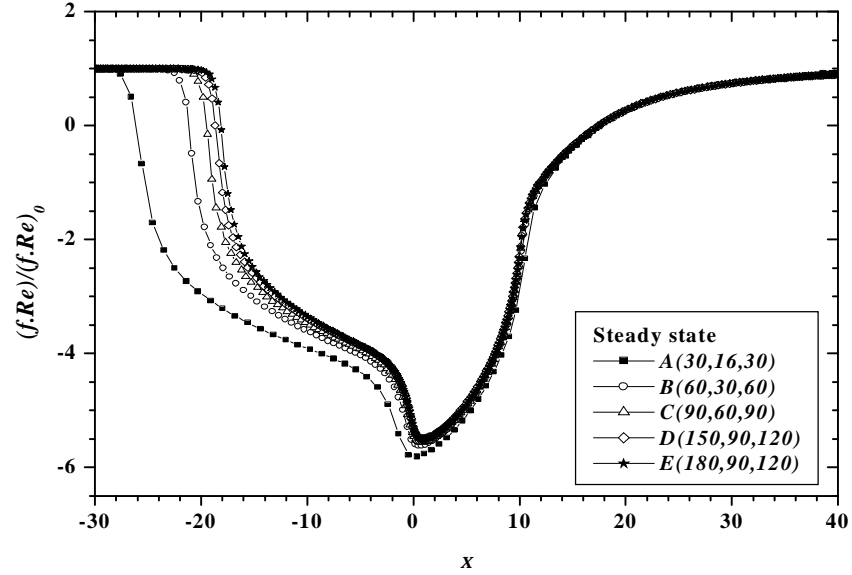
Figure 4.4 Influence of the grid distribution in the axial direction on the friction coefficient ratio
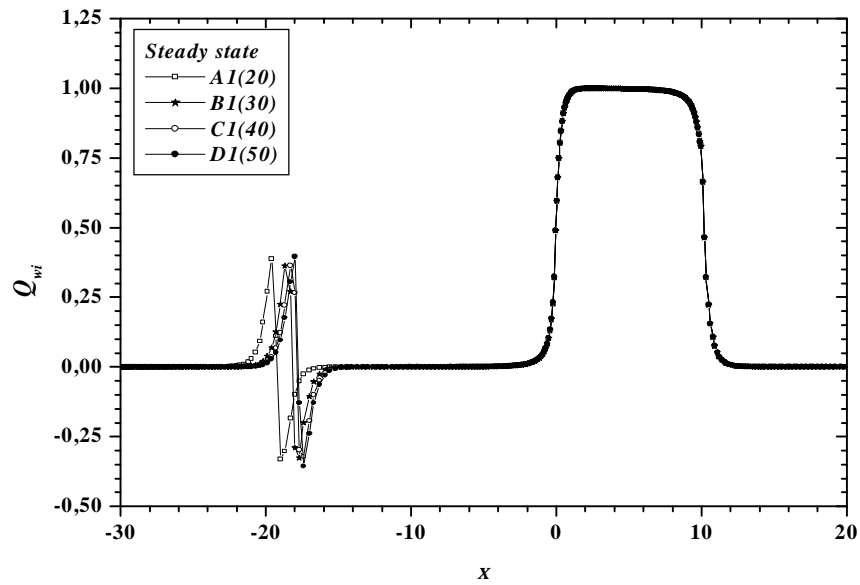
Figure 4.5 Influence of the grid distribution in the radial direction on the interfacial heat flux

----
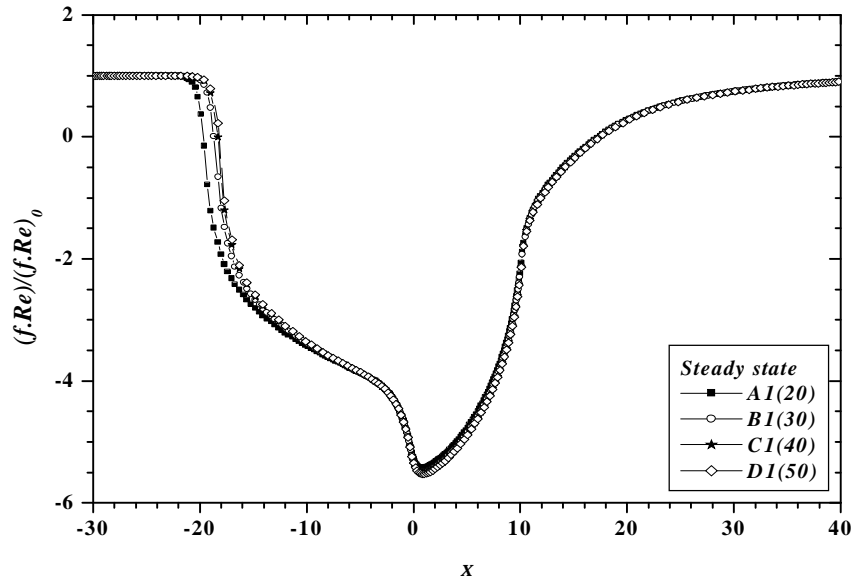
Figure 4.6 Influence of the grid distribution in the radial direction on the friction coefficient ratio

4.2.3 Effect of the initial time step

Since the size of time increments particularly important at the beginning of the transient, and t is of order magnitude of the time needed for the inside wall to respond to the sudden change of the applied heat flux at the outside surface of the heated section. A comparison was made for several first time intervals for the case *Pr=5, Gr=510^5, Re=100, D=0.05* and *K=50*. As shown in Figure 4.7 at $t = 0.1$, it is clear that a time interval of 510^{-4} is sufficiently accurate to describe the flow and heat transfer.

4.2.4 Validation

To check the accuracy of the numerical computation results, the interfacial heat flux and the axial velocity obtained at the steady state by the present developed code, are compared with the corresponding one of **LaPlante** [42]. As one can see in Figures 4.8 and 4.9 the agreement between our results and those of **LaPlante** is very satisfactory.

In the transient period, the computer model has been successfully validated by comparing the results obtained by the present developed code with the corresponding numerical data [50] of the simultaneously developing mixed convection flow of air inside a

----

vertical tube which is submitted to uniform but time-depending wall heat flux, at a specific axial position *x=19.5*, see Table 4.1.

As one can notice, the agreement between our results and those of **Nguyen** [50] may be qualified as very good.

In view of these comparisons, we conclude that the model and the computer code are reliable and can be used to analyse the problem under consideration.
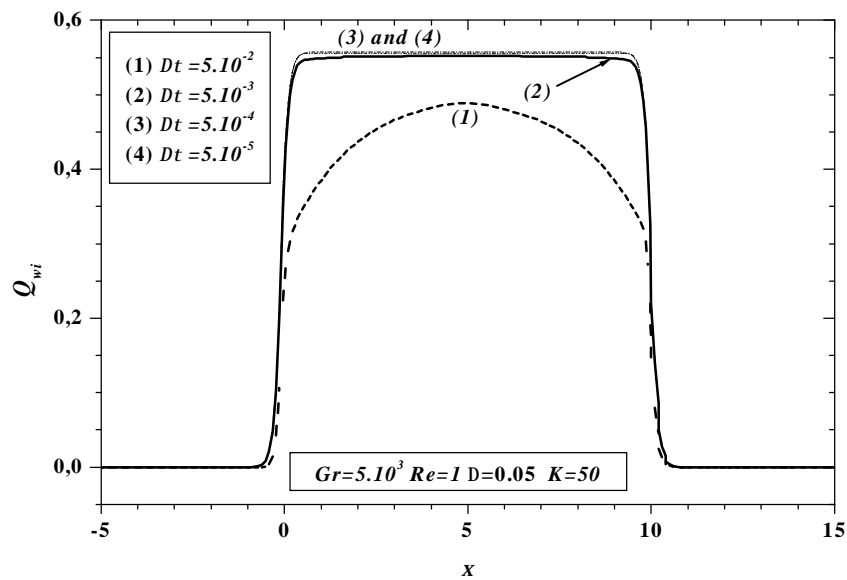
Figure 4.7 Effect of time steps Δt on the initial distribution of the interfacial heat flux at $t = 0.1$.

Chapter 4   *Numerical results*
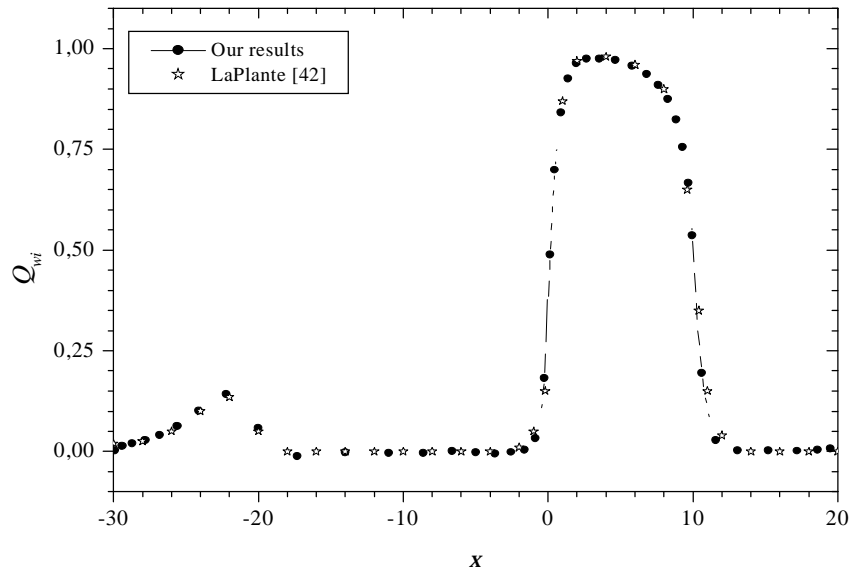
Figure 4.8 Validation of the computer code with available results
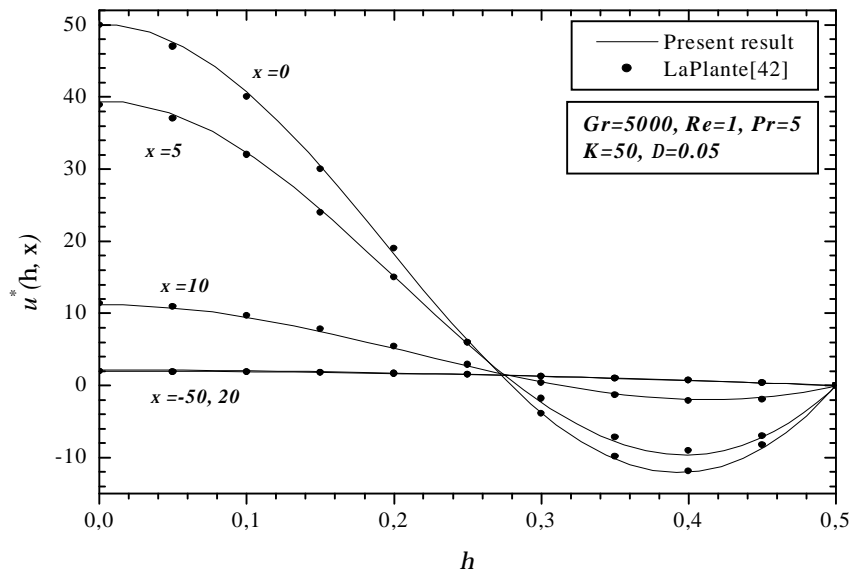
Figure 4.9 Validation of the computer code with available results

Table 4.1 Comparison of the radial distributions of the axial velocity u* obtained by the present code with those in reference [50].

55

Chapter 4 *Numerical results*

	Gr=0		Gr=10⁵		Gr=3.10⁵		Gr=4.510⁵		Gr=5.10⁵	
r/D	Ref [50]	Present study	Ref [50]	Present study	Ref [50]	Present study	Ref [50]	Present study	Ref [50	Present study
0.0	1.95	1.93	2.22	2.24	2.92	2.93	3.58	3.58	3.83	3.84
0.05	1.93	1.91	2.20	2.21	2.87	2.88	3.51	3.51	3.78	3.77
0.10	1.90	1.88	2.13	2.13	2.70	2.72	3.30	3.30	3.51	3.52
0.15	1.82	1.80	2.00	2.01	2.49	2.50	2.92	2.92	3.14	3.14
0.20	1.66	1.65	1.79	1.81	2.14	2.15	2.46	2.46	2.59	2.60
0.25	1.51	1.50	1.68	1.68	1.71	1.72	1.86	1.87	1.93	1.93
0.30	1.32	1.31	1.13	1.14	1.27	1.27	1.20	1.21	1.19	1.19
0.35	1.06	1.04	0.97	0.98	0.79	0.80	0.59	0.60	0.54	0.54
0.40	0.73	0.72	0.62	0.62	0.38	0.38	0.13	0.13	0.02	0.022
0.45	0.41	0.39	0.34	0.35	0.04	0.096	-0.098	-0.099	-0.18	-0.18
0.50	0.0	0.0	0.0	0.0	0.0	0.0	0.0	0.0	0.0	0.0

4.3 Numerical results and analysis

4.3.1 Introduction

This section presents the numerical results of the parametric study of the transient conjugated laminar mixed convection in vertical thick duct. A part of the presented results was the subject of publications [61-63, 75].

Local Nusselt number, as traditionally considered in the presentation of the convection heat transfer results is not a convenient tool for the conjugate problems [60], since it contains three unknowns in its definition. However, local interfacial heat flux gives more useful information. Therefore, the results are presented by the normalized interfacial heat flux and, for some cases, by the transient radial distribution of temperatures for thermal magnitudes and by the friction coefficient ratio $(f.Re)/(f.Re)_0$ and the vector velocities for the dynamical magnitudes.

Even, though calculations were performed from *x= -40* to *x= 40*. It is noted that for reasons of clearness, most of the results will not be plotted in this rang of *x*. Recall that $x = 0$ and $x = 10$ corresponds, respectively to the inlet and the exit of the heated section.

In a first step, we suggest a brief description of the transient behaviour of the flow in downward mixed convection. As $t < 0$, the flow is considered laminar, isothermal and

dynamically developed (parabolic profile of the axial velocity). As $t \geq 0$, we applied a uniform and constant heat flux on the outside surface of the heated section ($0 \leq x \leq 10$). With elapsing time, and as the fluid approaches the heated section it undergoes a local deceleration close to the pipe wall compensated by an increase of the velocity in the centre of the tube in order to obey the of the mass conservation law. The fluid deceleration in the near wall region is due to the Archimede's forces. Indeed, because of the heating, it establishes a difference of density inside the tube. The density of the fluid situated close to the pipe wall decreases in relation to the one of the flow in the core region. This variation of density combined with the gravitational field provokes upwards Archimede's forces on the fluid situated close to the pipe wall.

While approaching the heated section, Archimede's forces increase gradually in relation to the viscous forces. At a given axial position and instant of the transient period, the gradient of the axial velocity on the tube wall vanishes, indicating obviously that the flow reversal has just been initiated. While heading toward the downstream of this axial position, a reversing zone appears in the velocity profile. The thickness of this reversing zone increases with time and with the increase of the magnitude of Archimede's forces in relation to the viscous forces.

While continuing towards the downstream and while approaching the end of the heated section, the reversing zone becomes thins, whatever is the time. This is due to the fact that the viscous forces take gradually over on Archimede's forces. The reversing zone tends to disappear and while approaching of the exit of the tube, the flow becomes fully developed with parabolic velocity and uniform radial temperature profiles.

Let's note that for low values of Gr/Re^2, this cell disappears because Archimede's forces, in presence, are weak in relation to the viscous forces. Thus, for a given Pr, the transient extent and the intensity of this cell will be, therefore, function of the ratio Gr/Re^2, and of K and D. Indeed, when the axial wall conduction is important, one attends an important redistribution of the applied heat flux, what influences the position of the beginning of this cell.

In summary, in the reversing zone, which is situated close to the pipe wall, the fluid possesses an ascending movement. This ascending quantity of fluid is extracted from the central descendant flow, in the region of the end of the reversing zone. When this quantity of fluid arrives in the region of the beginning of the reversing zone, it loses gradually its

ascending quantity of movement and it is carried away by the descending central flow. Then, it establishes a buckle where a given quantity of fluid circulates in closed circuit. It is the recirculation cell.

4.3.2 Transient normalized interfacial heat flux Q_{wi}

In Figures 10a and 10b, axial distributions of the normalized interfacial heat flux $Q_{wi} = Q_i / Q = K(R_i / R_e)(\partial q_w / \partial h)|_{h=0.5}$ are given at several times for typical combination of parameters under consideration.

In this ratio Q is the uniform heat flux applied at the outside surface of the pipe wall ($r = R_e$) and Q_i is defined as follow: $Q_i = Q_{inner} (R_i / R_e)$, where Q_{inner} is the local heat flux transferred to the fluid at the inner surface of the pipe wall ($r = R_i$), given by the relation: $Q_{inner} = k_w (\partial T_w / \partial r)|_{r=R_i}$. A ratio of unity indicates that the applied heat flux goes directly to the fluid without any axial wall conduction.

At the early transient $t < 0.005$, where the heat transfer is globally dominated par radial conduction, one can note that the ratio Q_{wi} increases quickly in the heated section. With elapsing time, Q_{wi} continues to increase in the heated section with a symmetric upstream and downstream diffusion, indicating the beginning of the axial wall conduction effect.

At $t = 2$, one notes that Q_{wi} presents a weak minimum followed by a weak maximum in the vicinity of $x = 0$ with a notable corresponding reduction in the heated section before it decreases rapidly towards zero. One notes also, at this time instant, that the maximum of Q_{wi} shift towards the inlet of the heated section ($x = 0$). Such behaviour is due to the recirculation cell, which is established from the first instants of the transient period.

In fact, during these first moments, the recirculation cell is still confined in the heated section as can see it later in the representation of the vector velocities. As time goes on, its effect widens towards the upstream section, involving therefore the evacuation of a certain quantity of energy in the opposite direction of the main fluid flow (appearance of the minimum indicated previously). This quantity of energy added to that conducted by axial

wall conduction leads to increase more the interfacial heat flux (presence of the maximum).

With further increase in time, the intensity of the cell increases resulting in an increase of the evacuated energy in the direction opposite to the main fluid flow. Then, the fluid temperature in the vicinity of the wall is higher than the inner wall temperature and therefore negative interfacial heat flux Q_{wi} values are obtained, indicating that the heat transfer is from the fluid to the pipe wall. This transferred quantity of energy to the pipe wall is then diffused by axial conduction in the upstream section of the duct, resulting in a significant redistribution of the applied heat flux in this adiabatic section, Figure 4.10a.
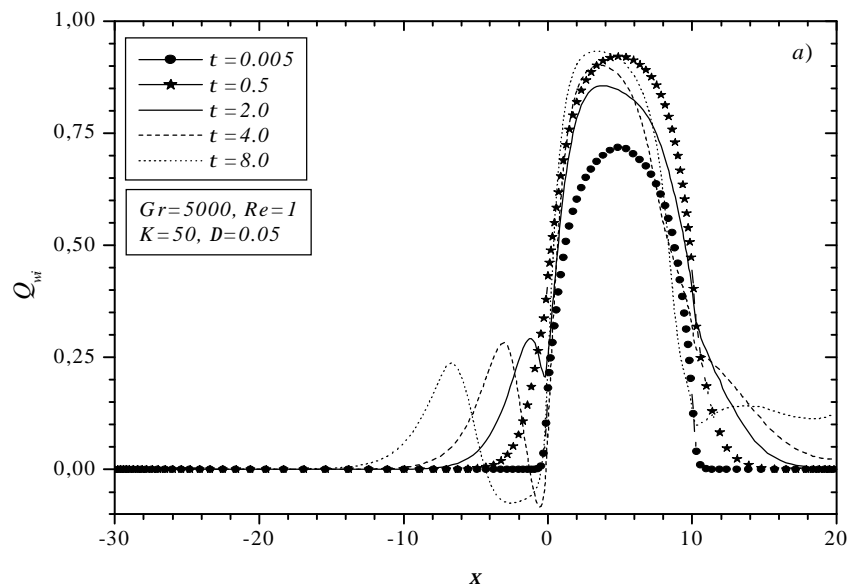
Figure 4.10a Transient axial distribution of interfacial heat flux

The process of the heat flux redistribution in the upstream section continues with elapsing time, until the steady state is reached. At this final time, Figure 10b, one notices that a significant quantity of the applied heat flux of the order of 15%, represented by a maximum of the curve $Q_{wi} = f(x)$ is redistributed in the upstream section far from the inlet of the heated section, before being released upstream of the beginning of the recirculation cell.

We notice that at $t = 2$ and 4, the negative values of Q_{wi} in the vicinity of $x = 0$ are about *10%* of the applied heat flux, whereas, with further increase in time, it tends to decrease rapidly and reach very low values at the steady state. This is due to the fact that, at the beginning of the transient state, the temperatures difference at the wall-fluid interface is important, while with further increases in times, the hot fluid contained in the recirculation cell tends to decrease this difference. Such effects result in a gradient of the radial temperature at the wall-fluid interface ($(\partial q / \partial h)_{h=0.5}$) approximately equal to zero, as one can see it later at the time of the representation of the radial distribution of temperatures. In addition, we note that the maximum of the redistributed heat flux in the upstream section decreases according to time, whereas the zone through which the heat transfer at the wall-fluid interface is produced increases (Figure 4.10a-b).

In the downstream section, the energy diffused by axial conduction in the pipe wall increases with elapsing time until the instant $t = 8$. From this time, one notices a decrease of the ratio Q_{wi} in the vicinity of $x = 10$, whereas for $x > 10$, an increase is observed ($t = 12.5$ and 25). From $t > 25$ until the steady state, the ratio Q_{wi} presents a weak widening of its redistribution towards the downstream section ($x > 10$) and tends to zero on the remainder of this section.
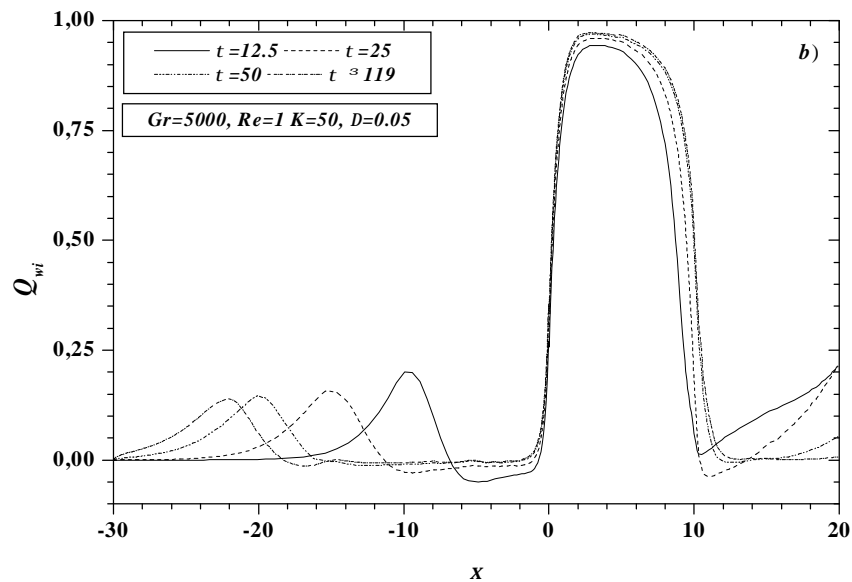
Figure 4.10b Transient axial distribution of interfacial heat flux.

This behaviour of Q_{wi} is due to the fact that at the beginning of the transient, for example at $t = 0.1$, the fluid decelerates near the wall at the point where the axial velocity becomes negative in the vicinity of $x = 10$, Figure 4.11. With elapsing time, the fluid axial velocity increases from negative to positive values, as can be seen, for example at $t = 4$, whereas from $t \geq 8$ until the steady state, one can observe that the fluid axial velocity presents, again, negative values. This effect leads to the apparition, the disappearance and, finally again, the apparition of the recirculation cell in the vicinity of this axial position, which affects the transient evolution of the normalized interfacial heat flux Q_{wi}.
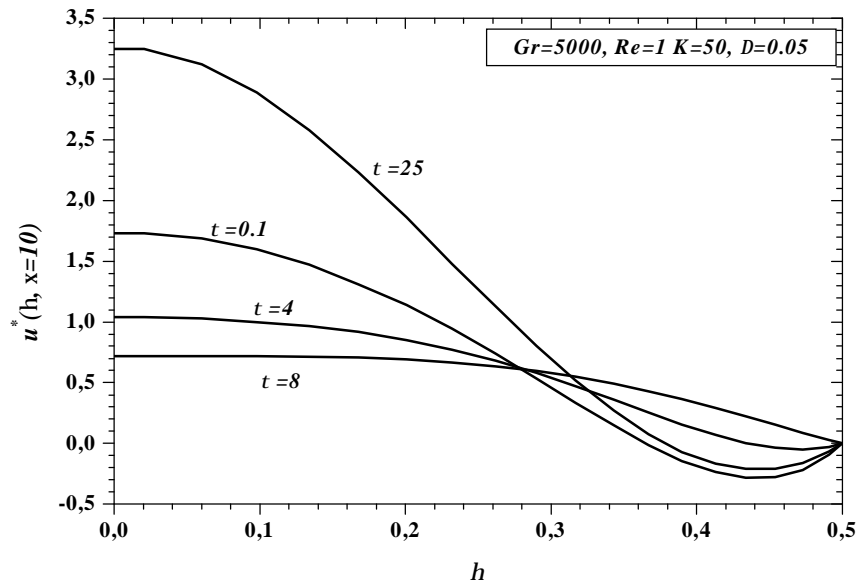
Figure 4.11 Transient distribution of the axial velocity profiles at the exit of the heated section (*x*=*10*)

4.3.3 Transient axial distribution of friction coefficient and vectors velocities

Shown in Figures 4.12a and 4.12b are the transient axial distributions of the friction coefficient ratio$(f.Re)/(f.Re)_0$. In this ratio $(f.Re)_0$ is the friction coefficient relating to the case of the forced convection and $(f.Re)$ is defined as follows: $(f.\text{Re}) = 2\left[- \partial u * / \partial h\right]_{h=0.5}$.

During the early transient period, $t < 0.005$, one notes that the friction coefficient is equal to 1 while from $t = 0.1$, it becomes negative indicating that the flow is reversed in

the vicinity of the wall, as one can see it in Figure 4.13, where we represent the radial distributions of u^* at $t = 0.1$, from $x = -5$ to $x = 20$.

This behaviour of the friction coefficient ratio continues with elapsing time where it is noted that this later presents more and more negative values in the heated and in the upstream sections. However, one can note, that the friction coefficient ratio decreases quasi-linearly from the value 1 in the downstream section to a negative maximum value at the vicinity of $x=0$ and then it increases again to the value 1 in the vicinity of the inlet of the upstream section (limit case of forced convection).

This maximum negative value can be explained by the fact that at the inlet of the heated section ($x = 0$), the temperatures difference between the fluid located close to the wall and that in the core region is more important than the corresponding one at the centre ($x=5$) and the exit ($x = 10$), as can be seen in Figures 4.14 and 4.15, respectively for a representative instant $t = 2$ in the transient period and at the steady state. In Figure 4.14, it is noted that the recirculation cell has not reached yet the axial position $x = -5$.
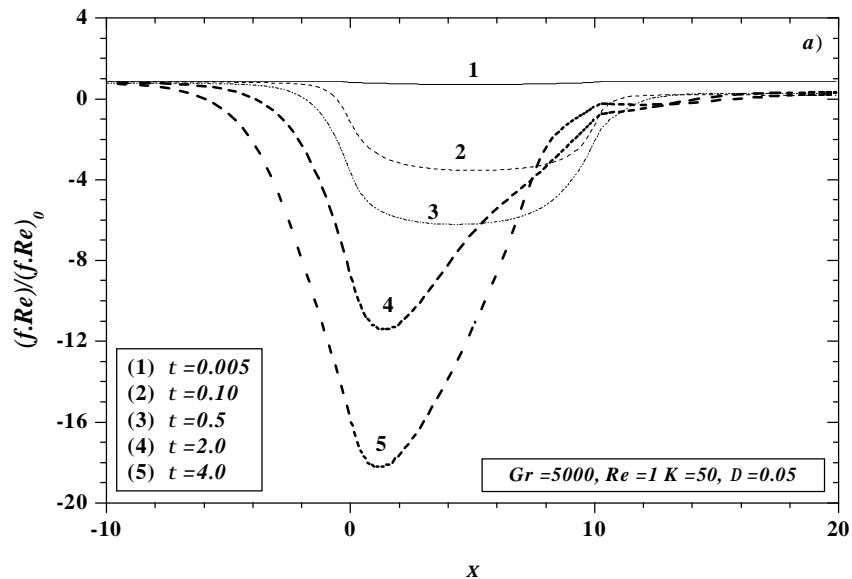
Figure 4.12a Transient axial distributions of the friction coefficient ratio.

At the steady state, Figure 4.12b, one can note that the ratio $(f.Re)/(f.Re)_0$ presents negative values in the heated section and along the most length of the upstream section,

indicating that the flow is reversed in the vicinity of the wall. In particular, one finds the stationary asymptotic values corresponding to forced convection flow in the vicinity of the inlet of the duct $x = -30$ and in the downstream section, $10 < x \leq 20$.
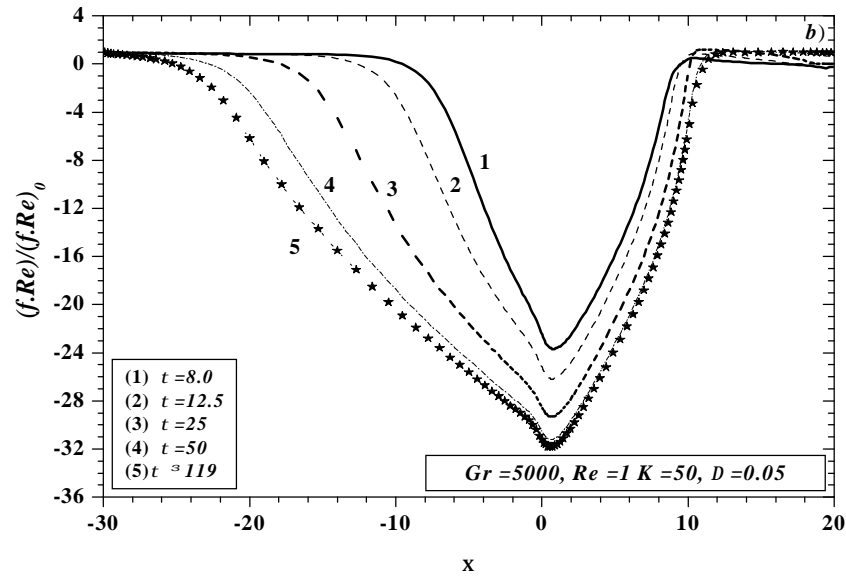
Figure 4.12b Transient axial distributions of the friction coefficient ratio.
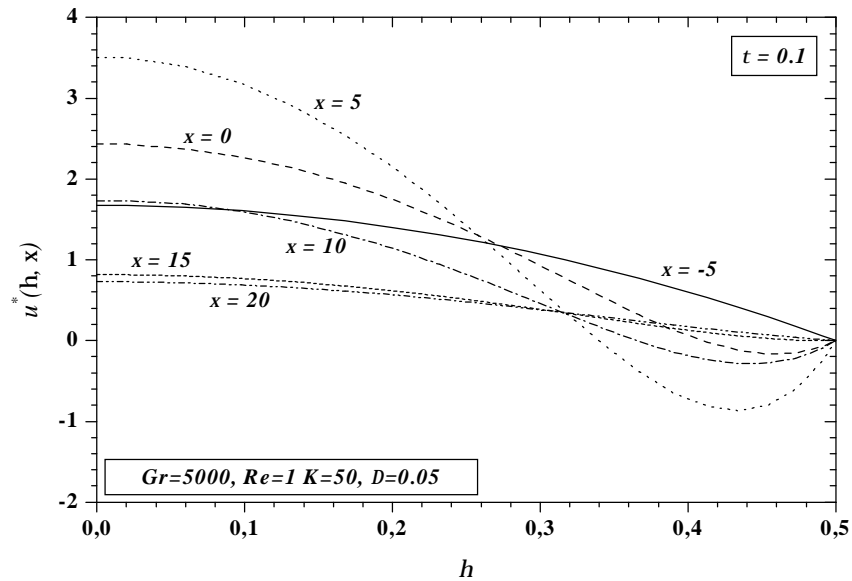
Figure 4.13 Radial distribution of the axial velocity profiles at different axial positions at $t = 0.1$

The widening of the recirculation cell towards the upstream section mentioned above is confirmed by Figures 4.16a-c. In these figures we present the development of the vector velocities at the moments $t = 0.1$, *4*, and *119* (steady state). Inspection of these figures shows that:

-As $t < 0.5$, the recirculation cell is very weak and remains confined in the heated section, Figure 4.16a at $t = 0.1$.

-From $t \geq 0.5$, an increase of the intensity of this recirculation cell at the inlet and the centre of the heated section is observed. As a consequence, the cell spreads toward the adiabatic upstream section, as can be seen, in Figure 16b at $t = 4$. It is also shown on this figure that the recirculation cell tends to shift towards the upstream section before returning gradually downwards with elapsing time. This behaviour is a consequence of the temperatures difference at the beginning of the transient period explained previously (Figure 4.14).

-As time goes on, the recirculation cell becomes more intense with however a weak widening toward the downstream section compared with the corresponding one toward the upstream section until the steady state is reached. At this final time the cell covers more than two-thirds of the length of the adiabatic upstream section (Figure 4.16c).
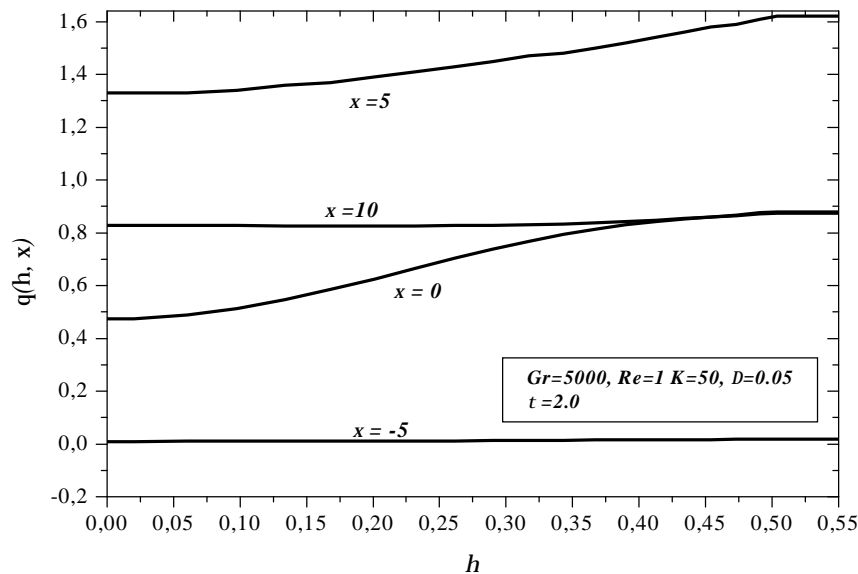
Figure 4.14 Radial distribution of temperature profiles for different axial positions at $t = 2$.
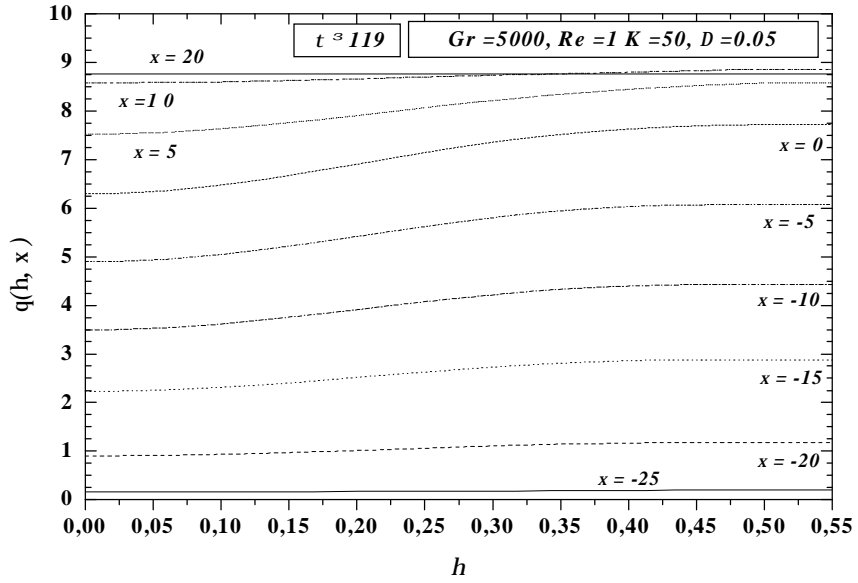
Figure 4.15 Steady radial distribution of temperature profiles for different axial positions ($t =119$ or greater)
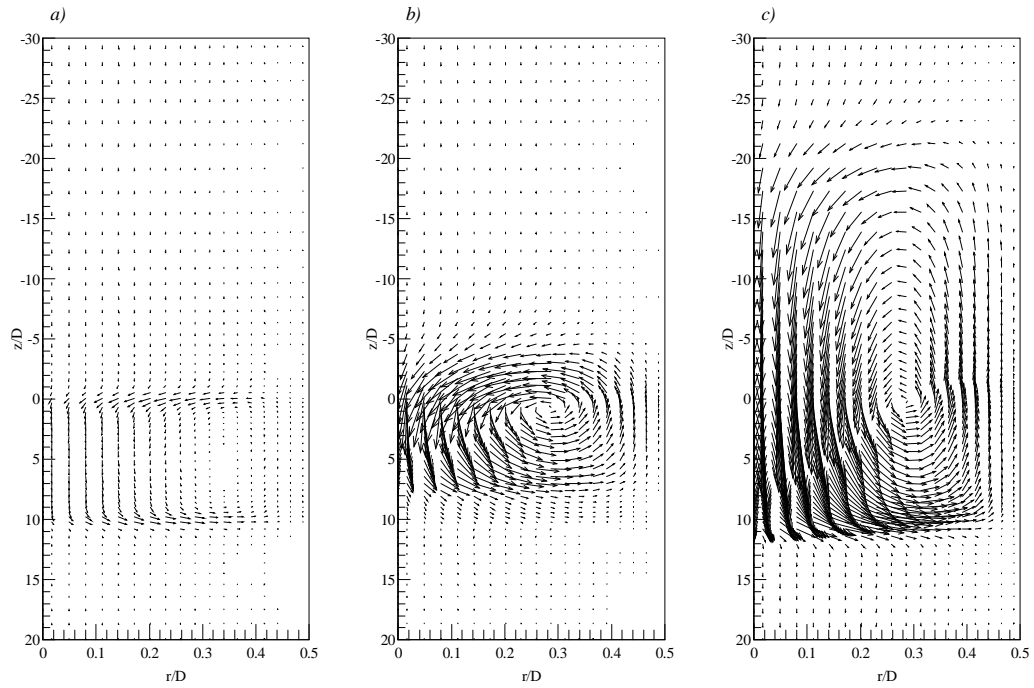
Figures 4.16a-c Vector velocities at: a) $t =0.1$, b) $t =4$, c) $t =119$ (steady state)

The upstream extent of the cell can be explained by a transfer of energy between the hot fluid contained in the recirculation cell and the pipe wall, as described previously in relation to the Figures 4.10a and 4.10b. This energy is conducted thereafter by axial conduction in the wall in the opposite direction to the main flow, involving again the heating of the fluid in near wall, situated forward of the beginning of the recirculation cell. This effect results in a deceleration of the fluid located close to the wall at the point where the axial velocity becomes negative. As a consequence, the cell moves in the upstream section toward the inlet of the duct. Thus, the thermal gradient at the wall $[(\partial q / \partial h)_{h=0.5}]$ becomes then increasingly weak, tending toward zero inside the cell with elapsing time, see Figure 4.15, representing the radial distribution of the temperatures at the steady state for the interval $-25 < x \leq 20$.

On Figure 4.15, it is also noted that the radial distribution of temperatures at the exit of the duct ($x = 20$) is constant. This behaviour is due to the fact that, at this axial position, the forced convection is dominant, and consequently, the flow field is fully developed.

4.3.4 Effect of the thermal diffusivity ratio A

In order to investigate the effects of thermal diffusivity ratio, one presents in Figures 4.17a-c the transient axial distributions of normalized interfacial heat flux Q_{wi} for three values of A at several time steps, including the steady state.

An overall inspection of these curves discloses that the values of the interfacial heat flux are higher for higher values of A. This is due to the fact that thermal resistance and heat capacity of the pipe wall $(rC_p)_w$ are small for higher values of A. Thus, during the transient period, the heat flux supplied from the outer surface of the heated section is easily transferred to the fluid. This in turn causes a large thermal lag in the system. A similar trend has been found by, **Lee** & **Yan** [54].

For example at $t = 4$, see Figure 4.17a, the amount of heat transferred to the wall-fluid interface in the heated section for $A = 0.1$, is of order of 50% than the corresponding one for $A = 4$. Thus, the quantity of energy transported by the recirculation cell in the opposite direction of the main flow is more important for $A = 4$. This results in a negative value of the interfacial heat flux Q_{wi} in the vicinity of $x = 0$ for $A = 4$, while for $A = 0.3$

and $A = 0.1$, the corresponding values of Q_{wi} are even positive, indicating that the heat transfer is still from the pipe wall to the fluid at this time instant.

In the downstream section, the effects of the thermal diffusivity ratios on the thermal response are also more pronounced. For example, at $t = 4$ and $t=50$, the heat transfer is from the fluid to the pipe wall over a large length of this section for $A = 0.1$, contrary to the case of $A = 4$, where Q_{wi} is positive (Figure 4.17b). Indeed, at this period of the transient, the quantity of heat conducted by axial conduction in the pipe wall for $A = 0.1$ is small compared with that evacuated by the recirculation cell toward this section. This is a direct consequence of the effect of the pipe wall heat capacity.

In the upstream section, one can observe that the thermal lag between the curves of Q_{wi} corresponding to the three values of A increases with elapsing time. As a consequence, the heat flux redistribution in the upstream section slows down with the decrease of A (Figure 17b), and consequently, affects the upstream widening of the recirculation cell, as one can see it later on the corresponding vectors velocities (Figures 4.19a-c).

With further increase in time, heat transfer between the pipe wall and the fluid continues with thermal lag effect between the curves of Q_{wi} relative to the three ratios of A until the steady state is reached. At this time one can observe, as expected, that the curves of Q_{wi} corresponding to the three values of the wall-to-fluid thermal diffususivity ratio are superposed, see Figure 4.17c. Indeed, it can be made plausible by noting that the governing equations for the system at the steady state, is independent of A.

Figures 4.18a-c, presents the transient distribution of the friction coefficient ratio for the same three values of the thermal diffusivities ratio at several times of the transient period. In these figures, one notes that as time goes on, the friction coefficient corresponding to $A = 0.1$ has the lowest negative values. At the steady state, the curves of Q_{wi} corresponding to the three ratios of A are superposed.
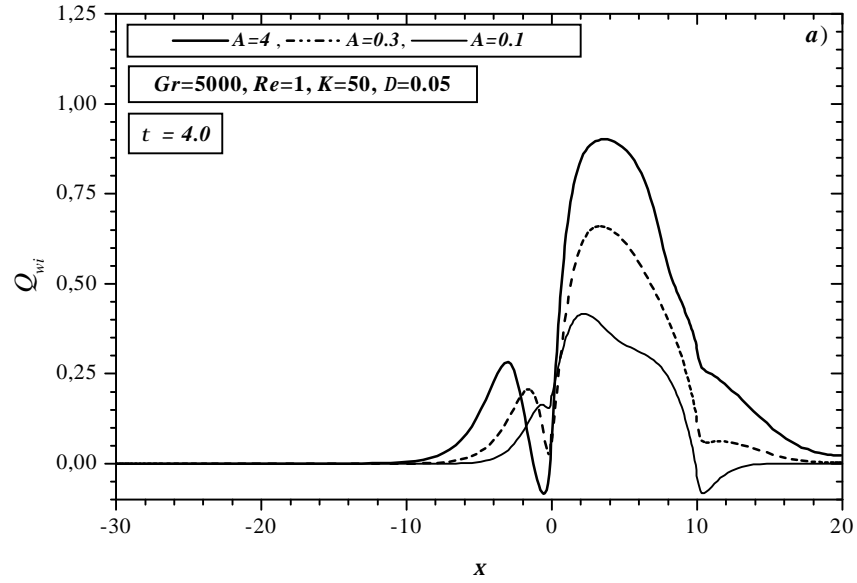
Figure 4. 17a Influence of the thermal diffusivities ratios *A* on the axial distribution of the interfacial heat flux at $t = 4$.
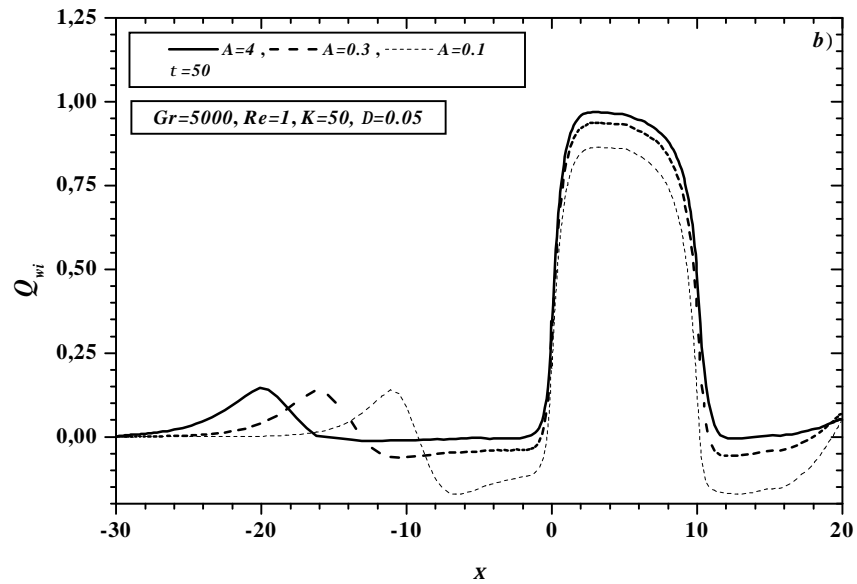
Figure 4.17b Influence of the thermal diffusivities ratios *A* on the axial distribution of the interfacial heat flux at $t = 50$.
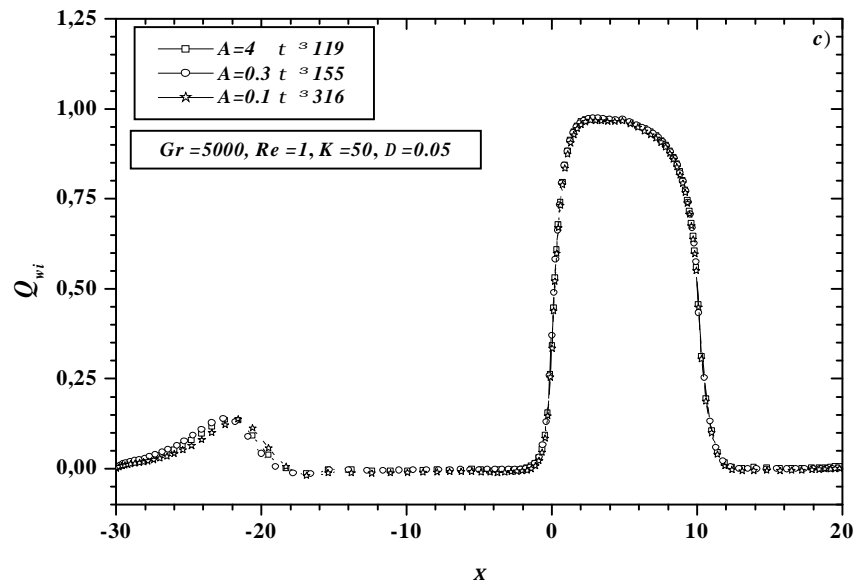
Figure 4.17c Influence of the thermal diffusivities ratios *A* on the axial distribution of the interfacial heat flux at the steady state.
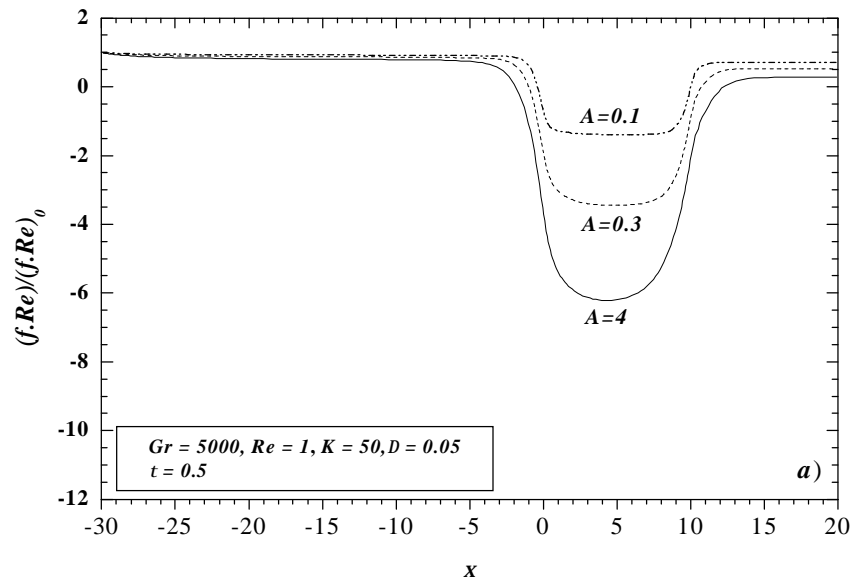
Figure 4.18a Influence of the thermal diffusivities ratios *A,* on the axial distribution of the friction coefficient ratio at $t = 0.5$.
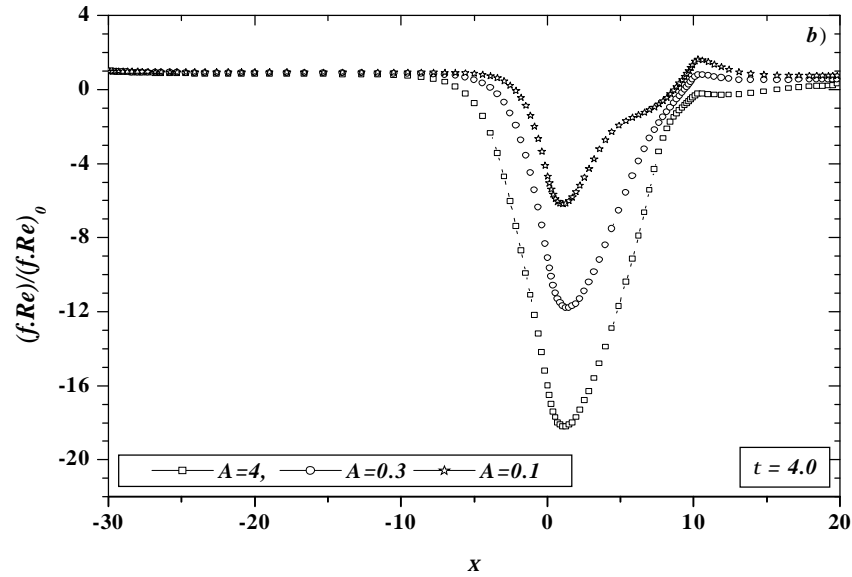
Figure 4.18b Influence of the thermal diffusivities ratios *A* on the axial distribution of the friction coefficient ratio *t = 4*.
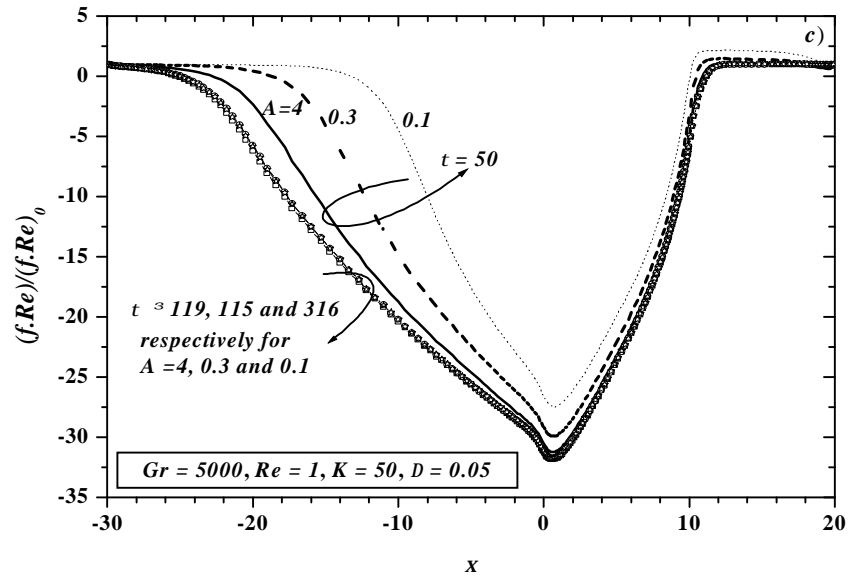
Figure 4.18c Influence of the thermal diffusivities ratios *A* on the axial distribution of the friction coefficient ratio at *t =50* and in the steady state.

The Figures 4.19a-c, are presented to analyse the effect of the thermal diffusivity ratios on the transient development of the recirculation cell inside the duct for a

----

representative instant of the transient period $t=4$. For low values of *A* and during the whole transient period, the intensity and the upstream and downstream widening of the cell remain the lowest. This is due to the weak diffusion of energy by axial wall conduction caused by the high heat capacity of the wall. Thus, in Figures 4.19a-c, one can observe that the recirculation cell is mainly confined inside the heated section for *A=0.1*, whereas for *A=4* its effect already reached the axial position $x = -5$.

The effect of thermal lag on the transient development of the cell continues with further increase in time until the steady state is reached. At this final time, the cells relative to the three ratios of thermal diffusivity, not represented here, present the same intensity and the same level of extent toward the two adiabatic sections.

Note that the time needed to reach the steady state increases with the decrease of the ratio *A*.
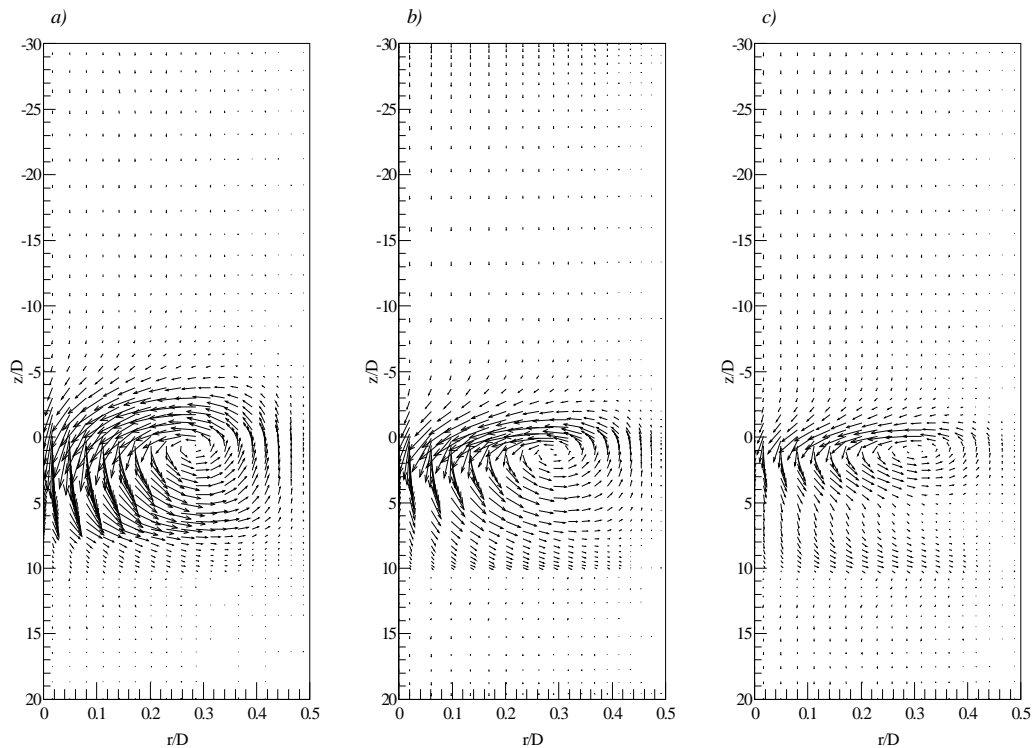
Figures 4.19a-c Influence of the thermal diffusivities ratio *A* on the vector velocities at $t =4$: a) *A=4*, b) *A=0.3,* c) *A=0.1*

4.3.5 Effect of the Grashof number *Gr*

The effect of the Grashof number on the transient axial distribution of the normalized interfacial heat flux, Q_{wi} are shown in Figures 4.20a-b, respectively for a representative instant of the transient period $t = 25$ and at the steady state.

At the initial transient stage, not represented here, the curves of Q_{wi} for the various values of the Grashof number under consideration are indistinguishable. This is due to the fact that the heat transfer is dominated by the radial conduction. With elapsing time, the effect of buoyancy increases with the increase of *Gr*, especially in the upstream section, where one can observe that the redistribution of the applied heat flux is more and more localised far from the inlet of the heated section as the Grashof number increases.

This process continues until the steady state regime, where one can observe no maximum of Q_{wi} in the upstream section for *Gr=1000*, while in the heated section it remains the lowest. This is a direct consequence of the recirculation cell that remains confined in the heated section.
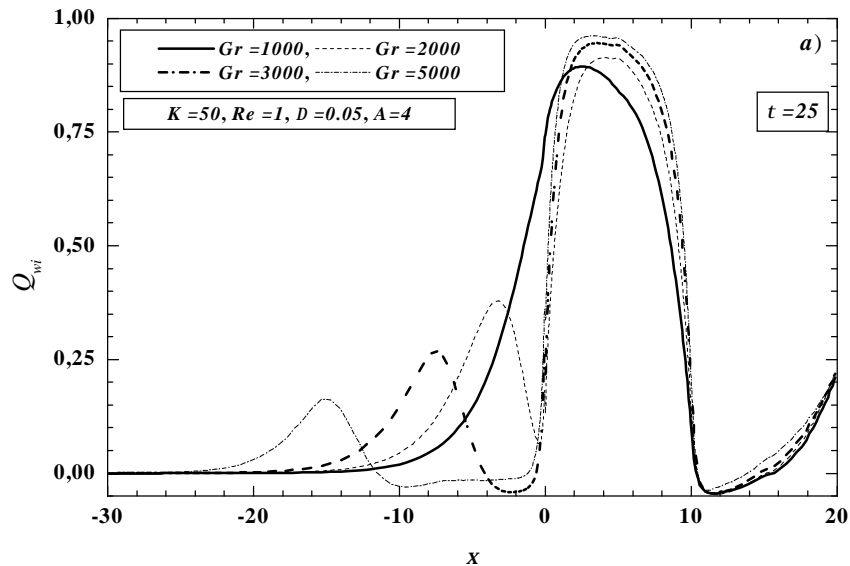
Figure 4.20a Influence of *Gr* on the axial distribution of Q_{wi} at $t = 25$.
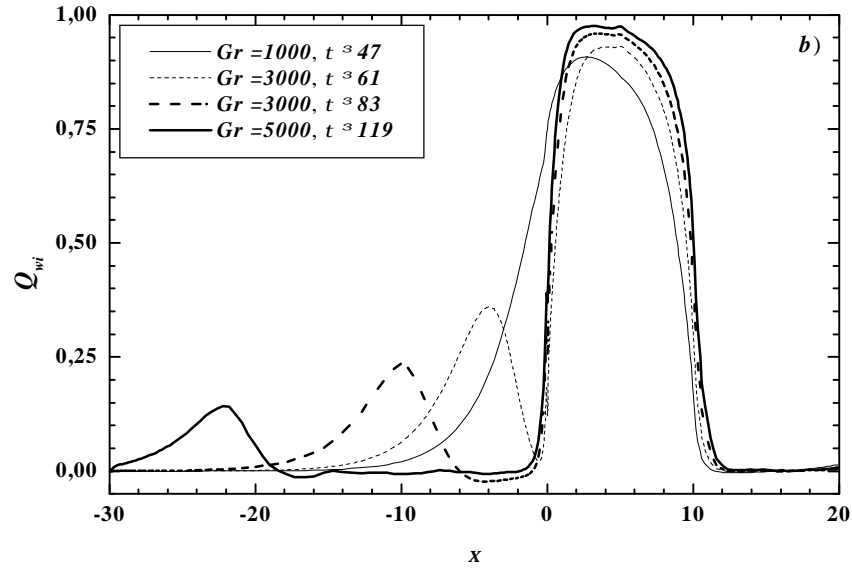
Figure 4.20b Influence of *Gr* on the axial distribution of Q_{wi} at the steady state

The corresponding steady state axial distribution of the friction coefficient ratio for the stated values of the Grashof number, Figure 4.21, shows clearly that with the increase of Grashof number, the intensity and the region of the flow reversal increase in its turn.
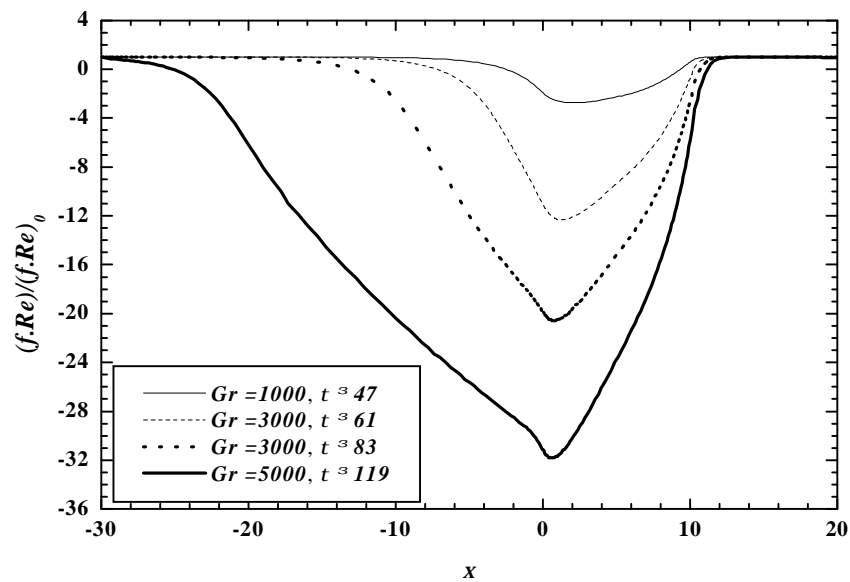
Figure 4.21 Influence of *Gr* on the axial distribution of the friction coefficient ratio in the steady state

The Figures 4.22a-c, present the effect of Grashof number on the widening of the cell upstream and downstream of the heated section at the steady state. The inspection of these figures reveals that the extent and the intensity of the cell increase with the increase of Gr. This confirms the upstream redistribution of the applied heat flux, observed previously for different values of the Grashof number Gr.
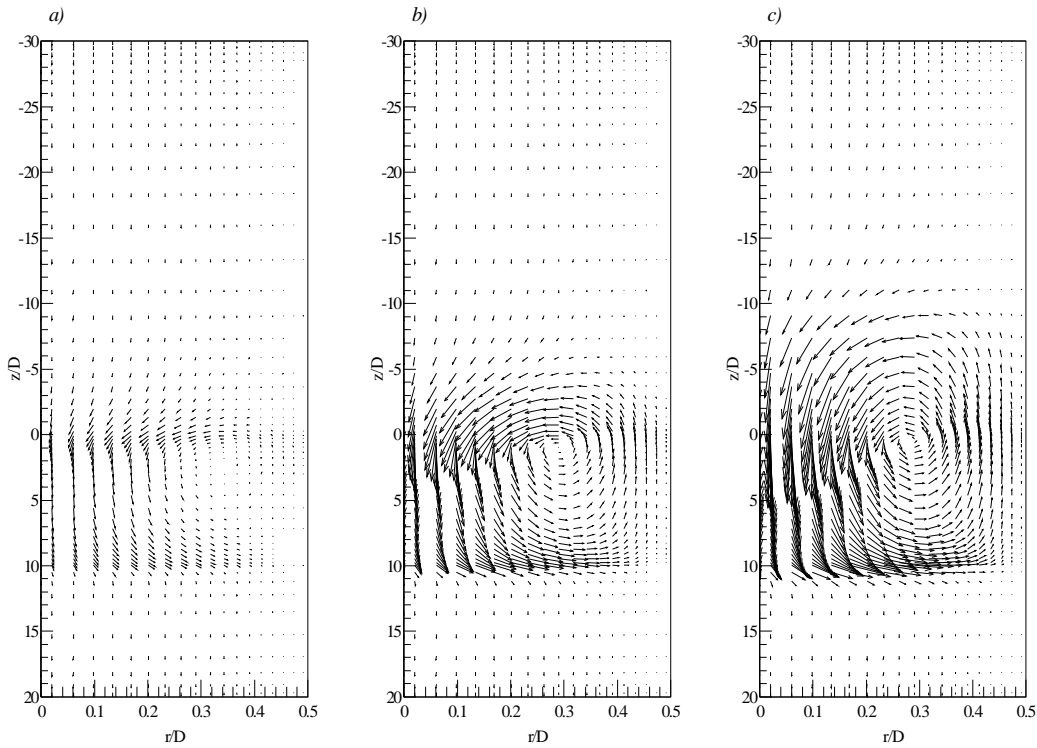
Figures 4.22a-c Influence of *Gr* on the vector velocities at the steady state
a) *Gr=1000*, b) *Gr=2000,* c) *Gr=3000*.

4.3.6 Effect of wall-to-fluid conductivity ratio

The axial distribution of the normalized interfacial heat flux Q_{wi} for different values of *K* and for different instants of interest is shown in Figures 4.23a-d.

An overall inspection of these figures show that, in the whole transient period, higher values of the normalized interfacial heat flux are obtained in the heated section for lower values of *K*, since the low values of *K* [$K=A.(rc_p)_w/(rc_p)_f$] with *A* fixed, decrease the thermal capacity of the wall $(rc_p)_w$. Such effect leads to a large thermal lag in the system as

one can see it by comparing the curves of Q_{wi} corresponding to the three values of K (Figures 4.23a-d).

Furthermore, at the early transient period (t £ 0.5), the magnitude of the normalized interfacial heat flux Q_{wi} increases quickly in the heated section, while in the upstream and downstream sections it increases symmetrically with the increase of K (Figure 4.23a at $t = 0.5$). This behavior is due to the fact that the heat transfer in the pipe wall and in the flow is essentially dominated by conduction at small t.

Later ($t>0.5$), one can observe a decrease of Q_{wi} in the heated section, which is more substantial for high values of K, as one can see it in Figure 4.24, representing the transient evolution of Q_{wi}, from $t = 0$ to $t = 8$ in the medium of the heated section ($x=5$). In the adiabatic upstream and downstream sections an important diffusion of heat is noticed, Figure 4.23b, at $t = 2$.

It is also shown in Figure 4.23b ($t = 2$) that the normalized interfacial heat flux Q_{wi} present a local minimum and maximum in the vicinity of the inlet of the heated section before decreases rapidly towards zero. At this time, the minimum of Q_{wi} corresponding to $K=10$ is more pronounced compared to the corresponding one for $K=50$ and 100. Thus, for $K=10$, Q_{wi} presents a negative value (minimum), indicating that the heat transfer is from the fluid to the pipe wall. This later quantity of energy, that has been transferred from the fluid to the pipe wall, is then diffused by axial wall conduction, resulting in a positive value of Q_{wi} (maximum), while for $K=50$ and 100, Q_{wi} still positive.

This presence of these negative values of Q_{wi} is attributed to the recirculation cell. In fact, at the early transient period, the recirculation cell is confined in the heated section, and its intensity is very low, as one can note it in Figures 25a-b ($t = 0.5$) for the limiting cases, $K=10$ and $K=100$. With elapsing time, the intensity of the cell increases and spreads towards the adiabatic upstream section (Figures 4.26a-b, $t = 4$), involving the evacuation of some quantity of energy in the direction opposite to the main flow, which is more important than that diffused by axial wall conduction for $K=10$. Then, Q_{wi} is negative at the vicinity of $x=0$ for $K=10$ at this period of the transient, contrary to the other values of K, where the energy diffused by axial wall conduction is too large than that transported by the cell.

Chapter 4   *Numerical results*
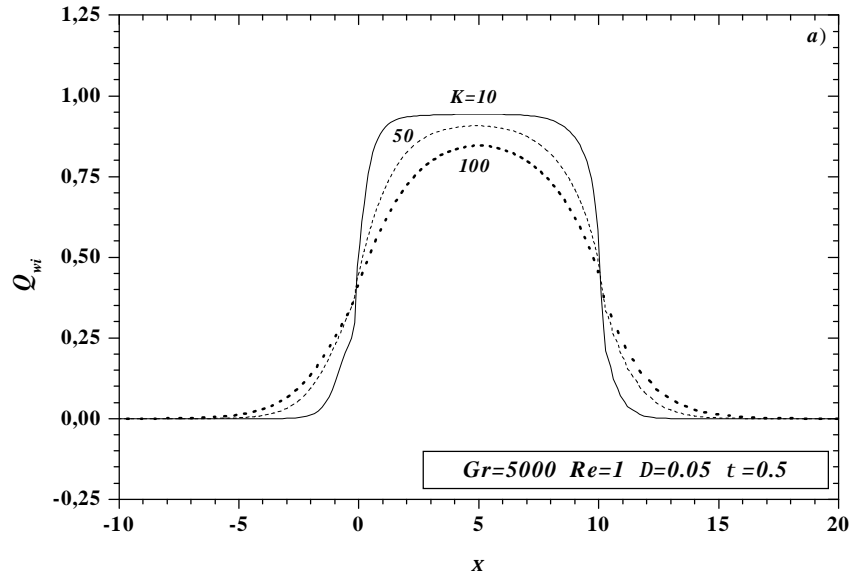
Figure 4.23a Influence *K (K=10, 50* and *100)* on the axial distribution of Q_{wi} at *t=0,5.*
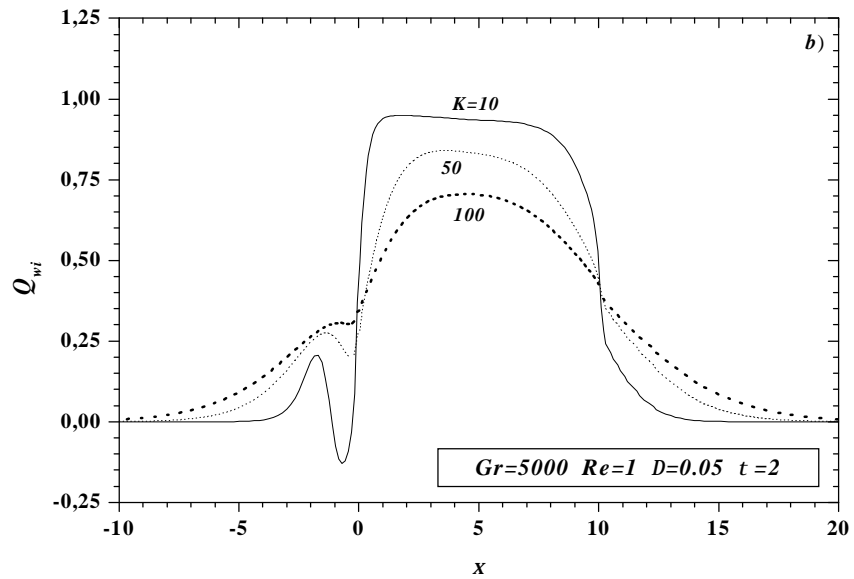
Figure 4.23b Influence *K (K=10, 50* and *100)* on the axial distribution of Q_{wi} at *t=2.*

Chapter 4   *Numerical results*
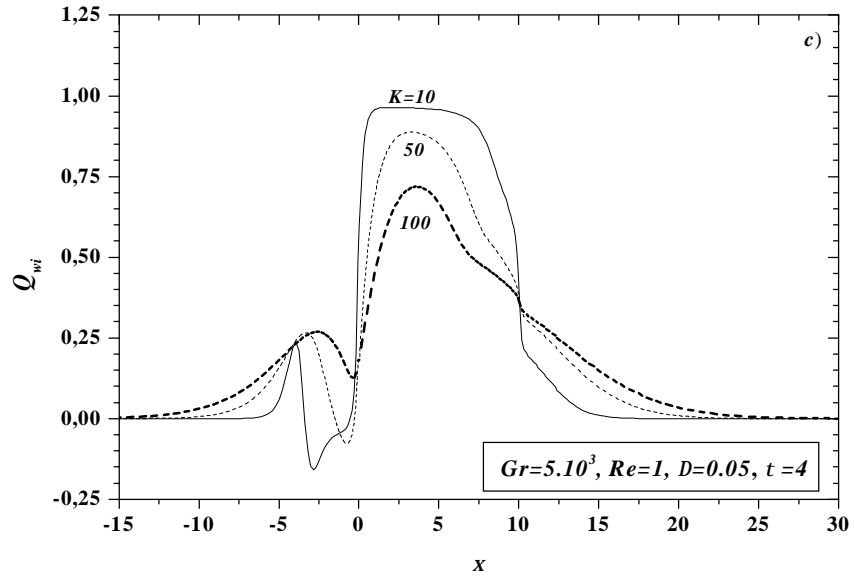
Figure 4.23c Influence *K (K=10, 50* and *100)* on the axial distribution of Q_{wi} at $t = 4$.
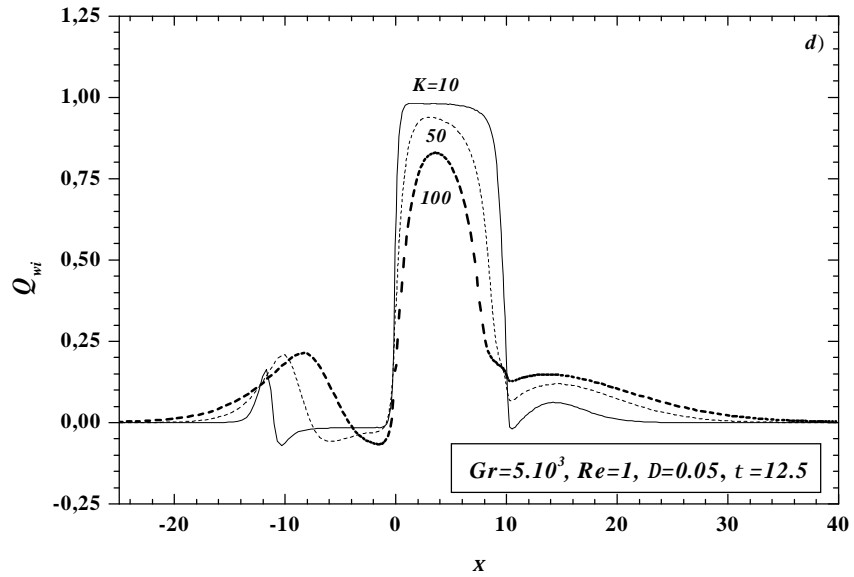
Figure 4.23d Influence *K (K=10, 50* and *100)* on the axial distribution of Q_{wi} at $t=12.5$.
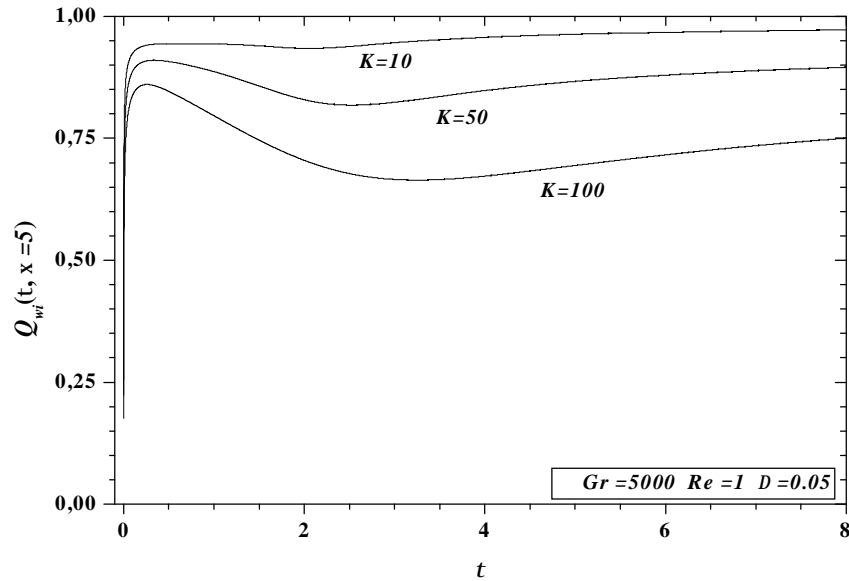
Figure 4.24 Transient distribution of the Q_{wi} at ($x=5$) for $Gr=5.10^3$, $Re=1$.

On Figures 4.26a-b, relative to another instant of the transient, it is noticed that the intensity of the cell for $K=10$ is more important than the corresponding one for $K=100$. This is also due to the fact that for low value of K [$K=A(rc_p)_w/(rc_p)_f$] with A fixed, the heat capacity of the wall is lower by comparing with that of the fluid. So, the supplied heat flux from the outside surface of the heated section is easily transported in the wall and, consequently to the fluid.

This effect results in a difference of temperatures between the fluid located close to the wall and that in the core region, more important for lower K than for higher K, as can be seen, for example, at $t=4$ in Figure 4.27a. Therefore, the local deceleration of the fluid in the near wall region is more important for $K=10$ than for $K=100$. Consequently, the acceleration of the fluid on the tube centreline is greater for $K=10$.

With elapsing time, it may be observed in the upstream section that the local minima and maxima of Q_{wi}, shown previously for each value of K, are more pronounced, resulting in a negative value of Q_{wi} for $K=50$, while for $K=100$ it remains positive, see Figure 4.23c.

As time goes on, one can observe that the present quantity of energy at the vicinity of the inlet of the heated section is redistributed in the adiabatic upstream section, for all

values of *K* (Figure 4.23d). This redistribution of the applied heat flux is due to the fact that, the hot fluid circulating inside the cell, tends to diminish the radial gradient of temperature, see Figure 4.27b at *t =25*, for *K=10* and *100*. Thus, the cell acts like an insulator and, with elapsing time, as the cell moves towards the inlet of the adiabatic upstream section, the heat flux inside the wall is redistributed further upstream of the region of the beginning of the cell.

Further inspection of Figure 4.27b, show also that for *K=100*, the cell has not yet reached the axial position *x = -10*, and the temperature at the exit of the heated section *(x =10)* corresponding to *K=10* is greater than the corresponding one for *K=100*. This is the direct consequence of the quantity of energy transferred to pipe-wall interface.

It is also shown in Figures 4.23a-d that from *t ^{3} 4*, Q_{wi} increases in the heated section for all values of *K* due to the effects of the widening of the cell towards the upstream section.
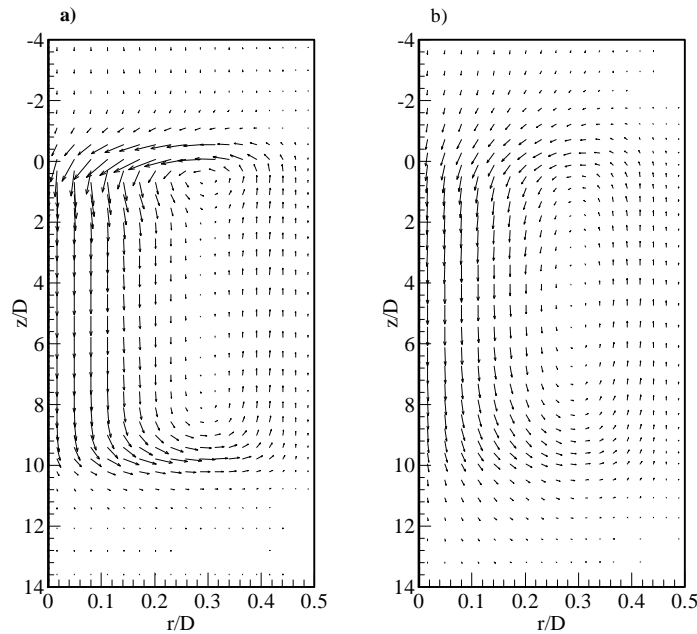
Figures 4.25a-b Vector velocities at *t =0.5:* a) *K=10,* b) *K=100* for *Gr=5.10³, Re=1.*
Scale: Relative (Grid units/Magnitude)=0.10
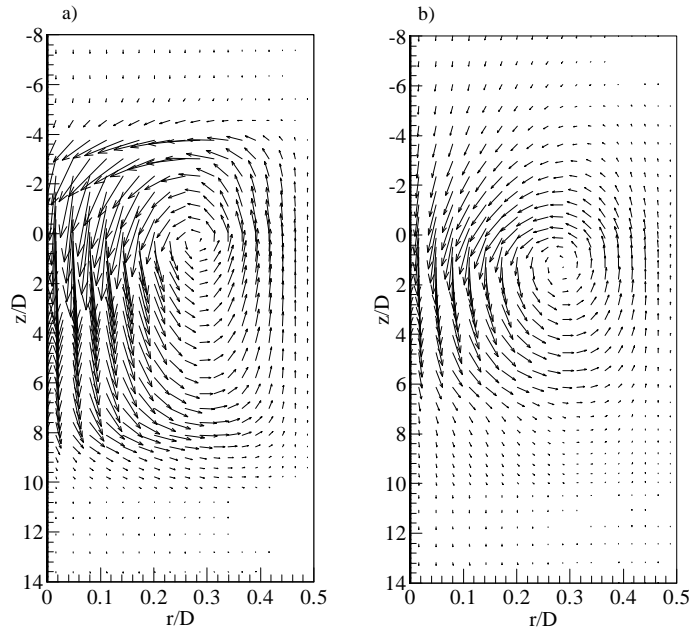
Figures 4.26a-b Vector velocities at $t = 4$: a) $K=10$, b) $K=100$, for $Gr=5.10^3$, $Re=1$. Scale: Relative (Grid units/Magnitude)=0.10.
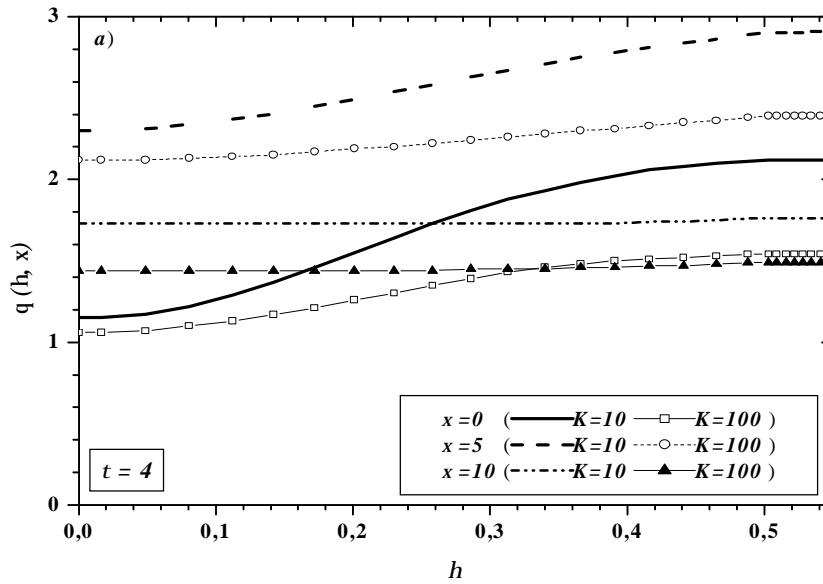
Figure 4.27a Influence of K $(K=10, 100)$ on the radial distribution of temperature for $Gr=5.10^3$, $Re=1$ from $x=0$ to 10, at $t=4$
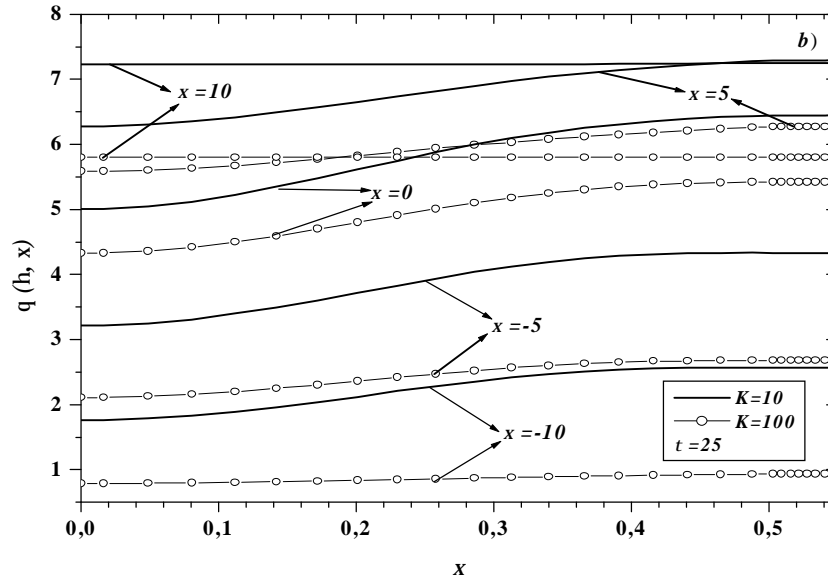
Figure 4.27b Influence of *K (K=10, 100)* on the radial distribution of temperature for *Gr = 5.10³, Re=1* at *t =25* from *x =-10* to *10*.

In the downstream section, one can observe that the energy diffused by axial conduction continues to increases at the first period of the transient, say for $t \leq 8$, and then, decreases with elapsing time until the steady state is reached where it becomes zero, Figure 4.23d and Figure 4.28.

This behaviour of Q_{wi} at this period of the transient is due to the effect of the axial wall conduction and the recirculation cell. Thus, for all values of *K*, and after the initial period of the transient where the cell is confined in the heated section, Q_{wi} continues to increase in the upstream and downstream sections due to the effect of axial conduction. Whereas, as time goes on, the cell becomes more intense, especially at the inlet of the heated section (*x=0*) than at the middle (*x =5)* and the exit (*x =10)*, Figures 4.26a-b, resulting in a displacement of the cell upwards, at the point where the reversed flow region near the wall, spreads toward the downstream region and leads consequently to increase Q_{wi} in this section (Figure 4.23c).

Chapter 4   *Numerical results*
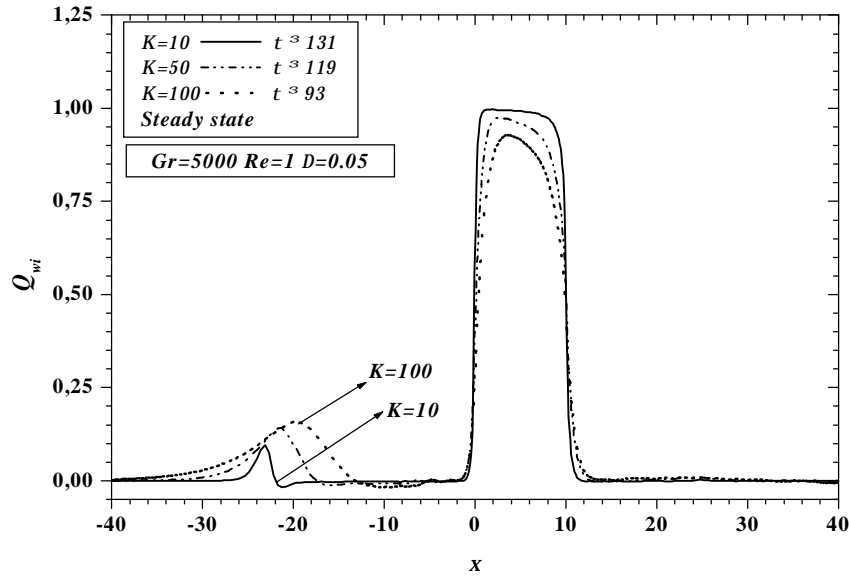
Figure 4.28 Influence of *K (K=10*, *50* and 100) on the axial distribution of Q_{wi} in the steady state.

As time goes on, we have observed that the cell starts to spread towards the exit of the heated section, see Figures 4.29a-b, leading consequently to the disappearance of the reversed flow near the wall region. This effect results in the evacuation of the energy diffused by axial conduction towards the downstream section during the early period of the transient (Figure 4.23d).

Note that for *K=100* and, with further increase in time, the energy evacuated by the cell becomes also higher than that conducted by axial wall conduction. Then, the interfacial heat flux Q_{wi} becomes also negative in the vicinity of *x =0* (Figure 4.23d), before being redistributed, in its turn, in the upstream section, in the same way as for the other values of K (*K=10* and *50*).
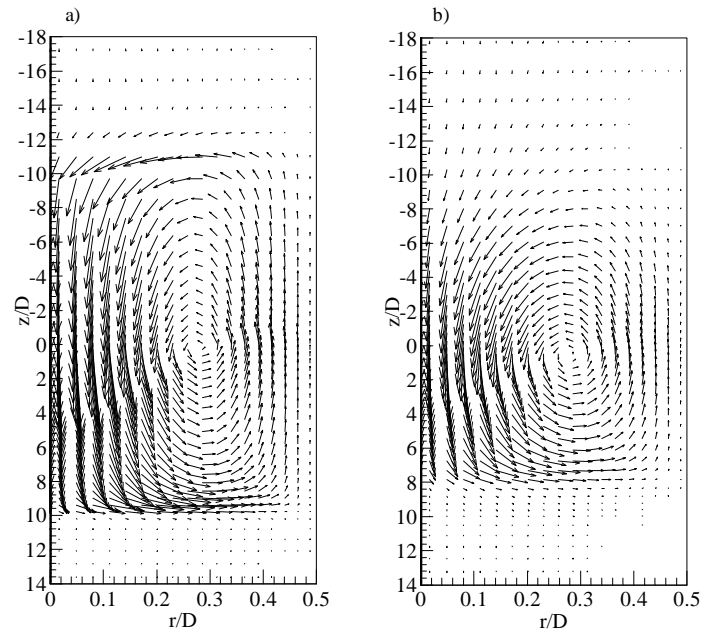
Figures 4.29a-b Vector velocities at τ =12.5: a) K =10, b) K =100, for Gr=5.10^3, Re=1. Scale: Relative (Grid units/Magnitude)=0.10
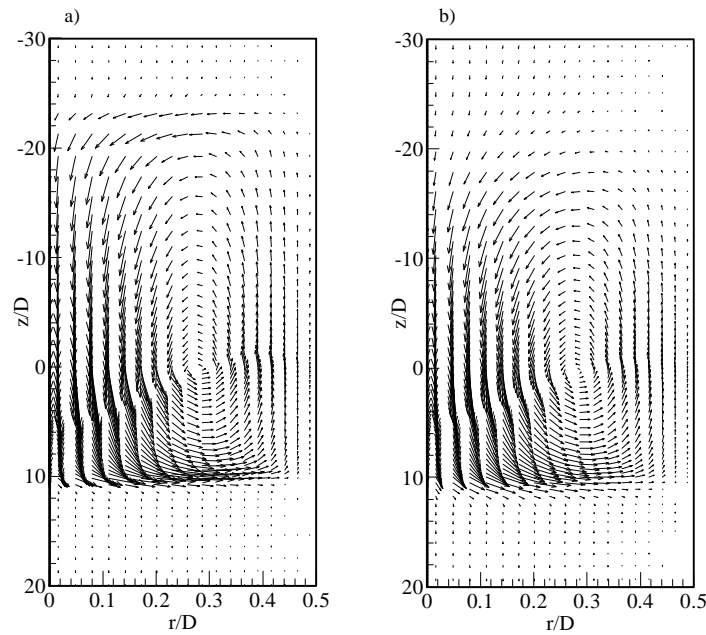
Figures 4.30a-b Vector velocities at the steady state: a) *K=10*, b) *K=100* for *Gr=5.10^3*, *Re=1*. Scale: Relative (Grid units/Magnitude)=0.10.

The process of the widening of the cell and consequently the heat flux redistribution continues as time goes on until the steady state is reached. At this final time, one can observe that the redistributed quantity of energy corresponding to low values of K is the lower and, for all values of K, this later, is also represented by a maximum of the curve $Q_{w\,i} = f(x)$, see Figure 4.28. The cell begins far upstream of the inlet of the heated section and extends downstream from this latter, see Figures 4.30a-b. A similar trend was found, at the steady state by, **LaPlante** [42].

Finally, it is worth noting in these figures that in the whole transient period, the widening of the cell and consequently the heat flux redistribution in the upstream section slow down with the increase of K.

The transient axial distribution of the friction coefficient ratio $(f.\text{Re})/(f.\text{Re})_0$ is shown on Figures 4.31a and 4.31b.

As can be shown previously and, due to the fact that at small t, the heat transfer is essentially made by conduction, the friction coefficient ratio for $t \leq 0.5$ presents a weak distortion over the most of the length of the heated section. As time goes on ($t = 2$), one can find the results discussed above, relating to the behaviour of the recirculation cell during the transient period. It is also shown at this representative instant ($t = 2$) that the friction coefficient ratio present negative values for all K in the downstream adiabatic section, indicating that the reversed flow region spreads towards this section, as mentioned above.

With further increase in time and as a consequence of the spreading of the cell toward the upstream and downstream sections, the friction coefficient ratio follows the same behaviour until the steady state is reached. At this final time, see Figure 4.31b, one can note that the friction coefficient is negative over an important length of the upstream section, especially for higher values of K, before tending asymptotically to the corresponding value of forced convection in the vicinity of the inlet of the duct $(x = -40)$. In the downstream section $(10 < x \leq 40)$, the friction coefficient ratio is equal to 1, indicating that the flow is fully developed.
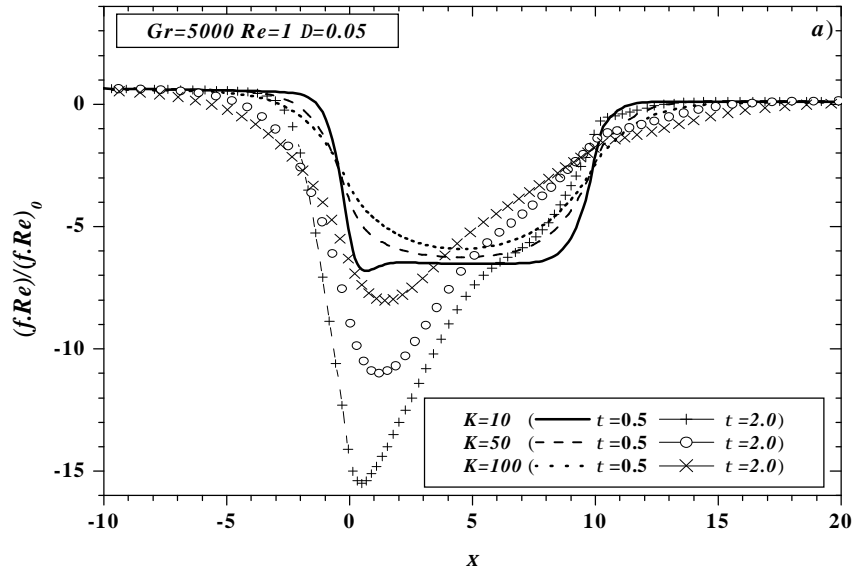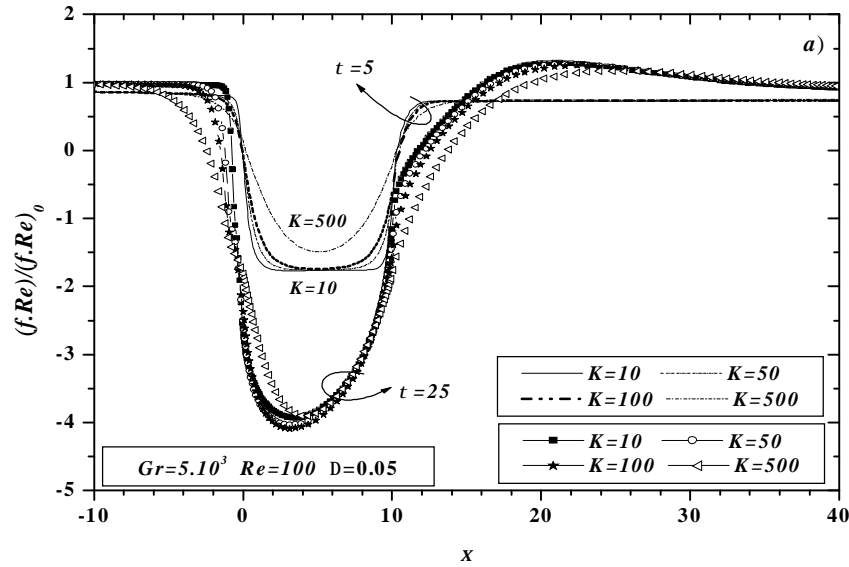

Figure 4.31a Influence of *K (K=10*, *50* and *100)* on the axial distribution of the friction coefficient ratio for *Gr=5.10³*, *Re=1* at *t = 0.5* and *2*
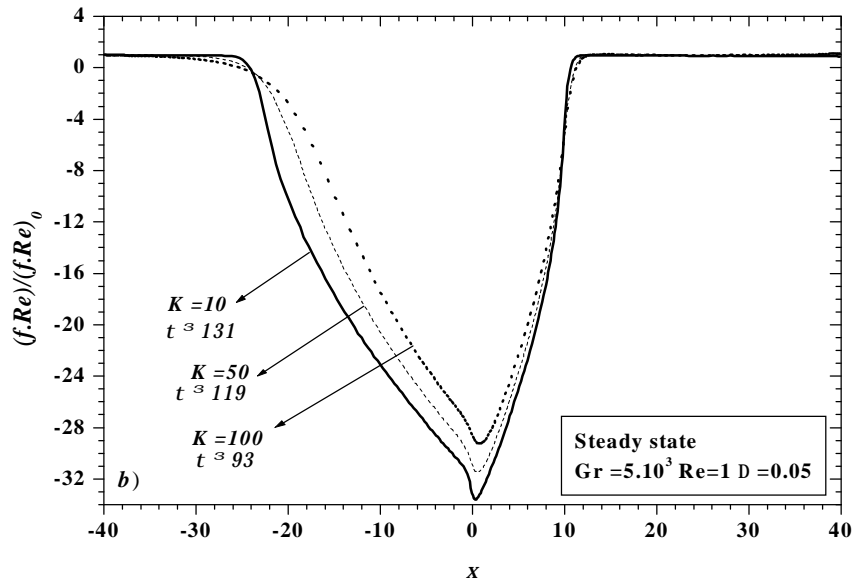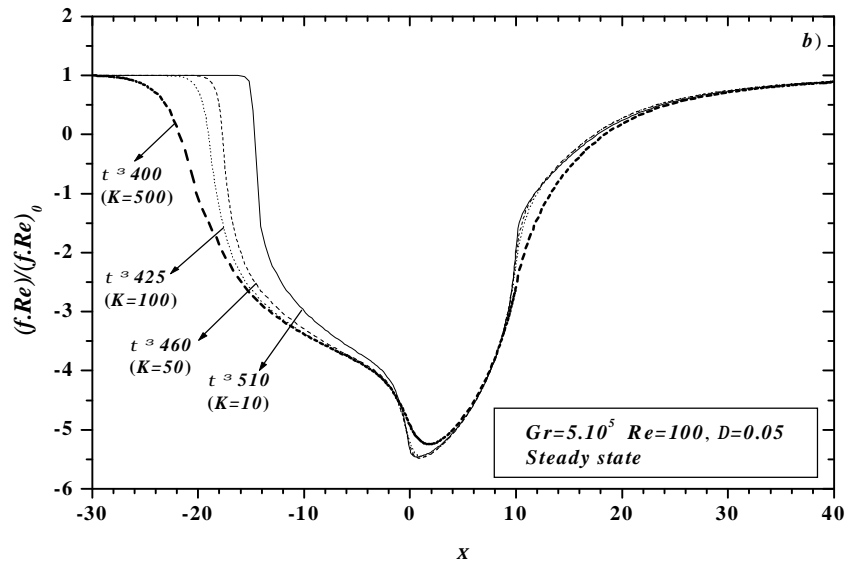

Figure 4.31b Influence of *K (K=10*, *50* and *100)* on the axial distribution of the friction coefficient ratio for *Gr=5.10³*, *Re=1* at the steady state.

4.3.7 Effects of high Reynolds and Grashof numbers

In order to examine the effect of the thermal conductivity ratio K on the transient behaviour of the previous dynamical and thermal magnitudes for high Gr and Re numbers, one present for $Gr = 5.10^5$, $Re = 100$, the axial distribution of the normalized interfacial heat flux, Figure 4.32 for a representative instant $t = 25$ in the transient period where the convection in the flow becomes increasingly important. For the early transient period note represented here, we have noted that, Q_{wi} increases rapidly for all values of K.
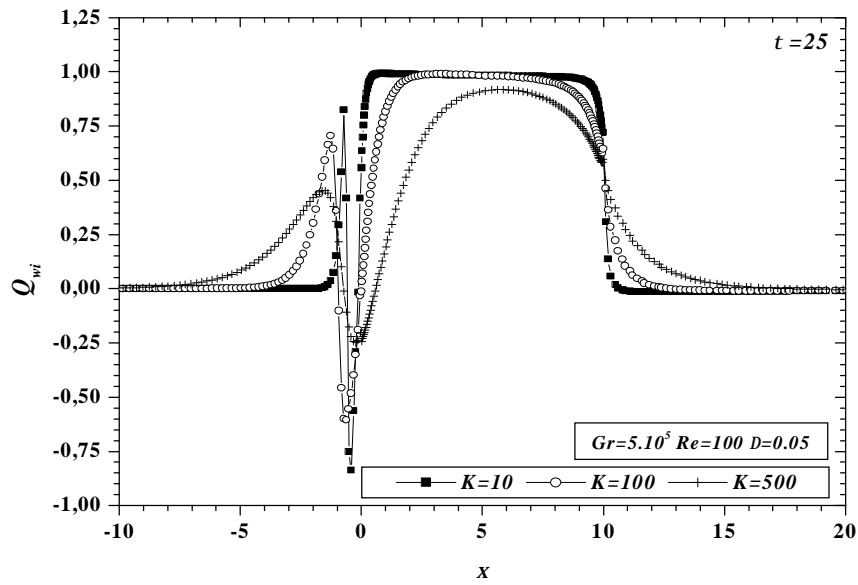
Figure 4.32 Influence of K ($K=10$, 100 and 500) on the axial distribution of Q_{wi} at $t=25$ for $Gr=5.10^5$, $Re=100$.

A comparison of the results of this case (Figure 4.32) with the corresponding one, (Figures 4.23b-d) for $Gr=5\ 10^3$, $Re=1$, shows that:

- The time required for the appearance of the minimum and maximum of Q_{wi} is much longer ($t \leq 2$ for $Gr=5\ 10^3$, $Re=1$) and ($t \leq 25$ for $Gr=5\ 10^5$, $Re=100$).

- The values of the minimum and maximum corresponding to each value of K are more important.

It is also worth noting in Figure 4.32 that for the limiting case $K=500$, the interfacial heat flux is negative in the heated section. In fact, for these values of Re ($Re=100$) and Gr

$(Gr=5.10^5)$, the negative values of Q_{wi} in the heated section have also been observed for the other values of K (*10, 50* and *100*) before $t=25$.

Indeed, as can be seen in Figures 4.33a and 4.33b, respectively for $K=10$ and *500*, the interfacial heat flux is negative in the heated section from $t >10$ for $K=10$, while for $K=500$, it becomes negative from $t >20$. This difference in time between the two values of K is due to the thermal lag effect. Recall that the negative values of Q_{wi} indicate that the heat transfer is from the fluid to the pipe wall.

The presence of these negative values of Q_{wi} in the heated section in this case $(Gr=5.10^5, Re=100)$, contrary to the case $(Gr=5.10^3, Re=1)$ is due to the fact that the axial conduction in the fluid is negligible $(Pe =500)$. Indeed, at the beginning of the transient state, the cell is not yet sufficiently intense to overcome the forces exerted by the fluid flow coming from the entry of the duct. So the cell remains confined longer in the heated section and, spreads slowly toward the upstream section, see Figures 4.34a and 4.34b.

This effect leads to an increase in the fluid temperature with a maximum in the vicinity of the wall-fluid interface at $x=0$, as can be seen, for example, in Figure 4.35a for $K=10$ at $t =17.5$ and *20* and, in Figure 4.35b for $K=500$ at $t =25$. In these figures one can note that the maximum corresponding to $K=10$ is more pronounced and still much longer than the corresponding one for $K=500$.

This behaviour explain the large values of the minimum and maximum and the very sharp changes of Q_{wi} in this case, contrary to the case of Figures 4.23b-d $(Gr=5\ 10^3, Re=1)$, where the axial conduction in the fluid is important.

With elapsing time, the cell becomes more intense and starts to spread toward the upstream section, involving the evacuation of the accumulated energy and, leading consequently to the disappearance of the maximum of the temperature at $x=0$, see Figures 4.35a-b.
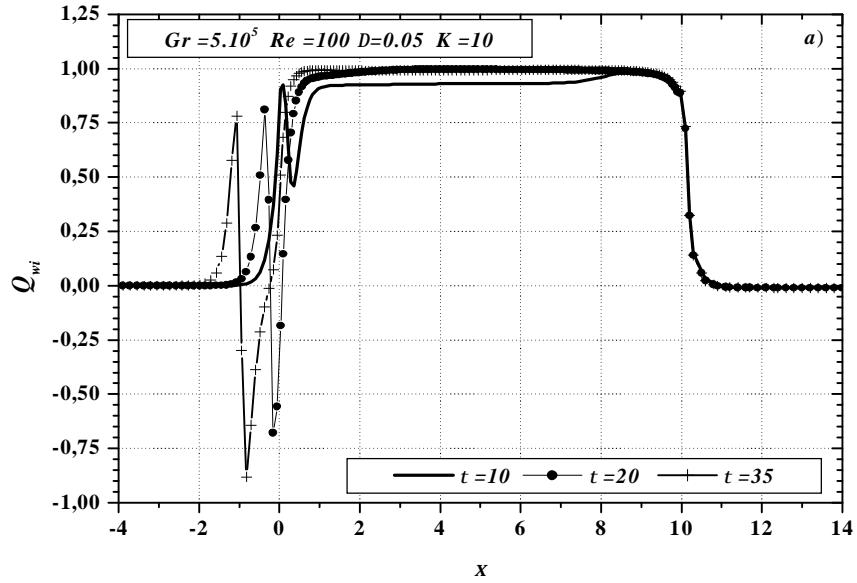
Figure 4.33a Axial distribution of Q_{wi} for *K=10* at **t=10, 20** and *35* for $Gr=5.10^5$, *Re=100*.
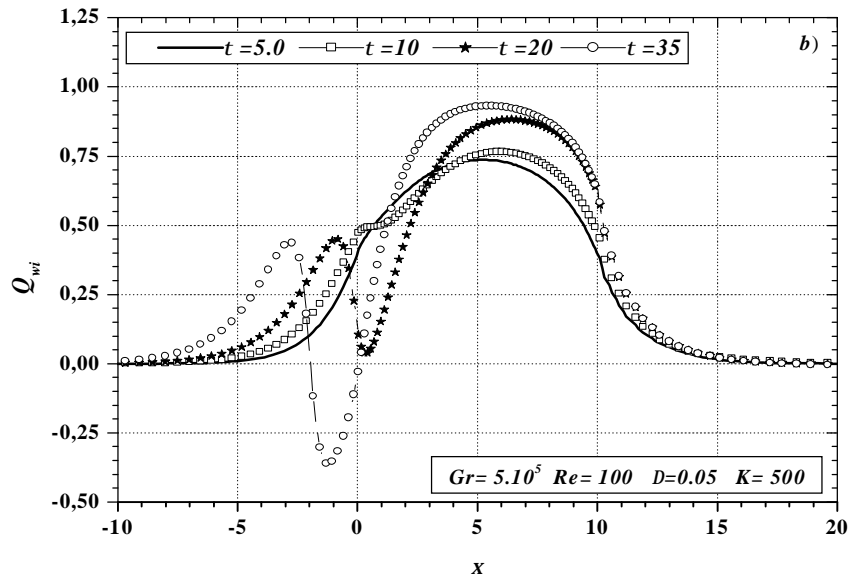
Figure 4.33b Axial distribution of Q_{wi} for *K=500* at **t=5, 10, 20** and *35* for $Gr=5.10^5$, *Re=100*.

Chapter 4   *Numerical results*
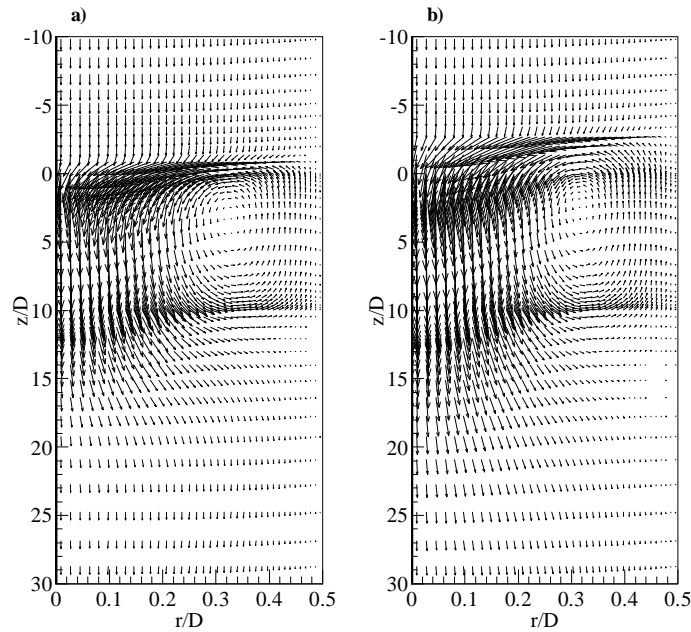
Figures 4.34a-b Vector velocities for $Gr=5.10^5$, $Re=100$, $K=50$: a) at $t=25$, b) at $t=50$. Scale: Relative (Grid units/Magnitude)=0.40

It is also shown in Figures 4.33a-b that the appearance of the first minimum and maximum of Q_{wi} is accompanied by a corresponding reduction of this later in the heated section. With further increase in time, the cell spreads toward the upstream section, leading to increase Q_{wi} in the heated section for the two values of K. This is due to the fact that the cell acts like an insulator between the pipe wall and the fluid, as it has been explained previously for the case ($Gr=5.10^3$, $Re=1$).

Other inspections of Figure 4.32 and Figures 4.33a-b show that the extreme values of Q_{wi} increase with the decrease of K. This is due to the fact that for low K the heat transmission in the wall by axial conduction is slower, whereas the energy transferred from the hot fluid to the pipe wall is conducted in the pipe wall more rapidly for large value of K. This effect results in lower extreme values of the redistributed energy in the upstream section for large values of K and, consequently slowly sharp changes between the maximum and minimum points, contrary to the case of low values of K.
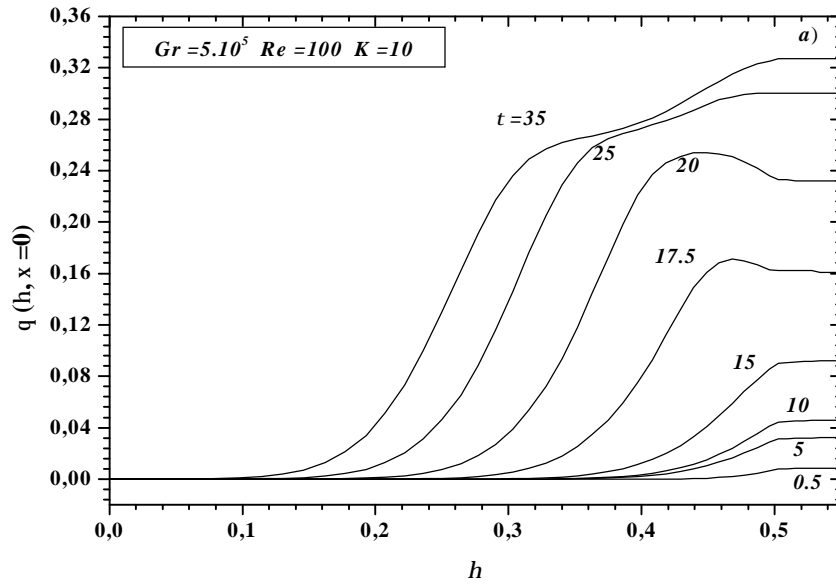
Figure 4.35a Radial distribution of temperature at the inlet of the heated section ($x=0$) at different instants of the transient period, for $Gr=5.10^5$, $Re=100$, $K=10$.
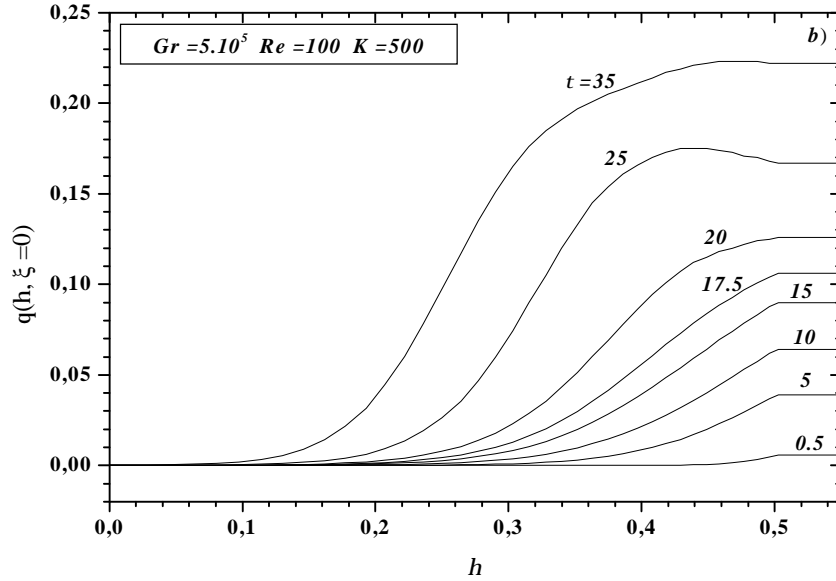
Figure 4.35b Radial distribution of temperature at the inlet of the heated section ($x=0$), at different instants of the transient period, for $Gr=5.10^5$, $Re=100$, $K=500$.

At the steady state, Figure 4.36 and, contrary to the result shown in Figure 4.28 (*Gr=5.10³*, *Re=1)*, one can observe that the heat flux redistribution in the upstream adiabatic section slows down with the decrease of *K* and it is more close to the entry of the heated section. This is the consequence result of the axial conduction. Thus, in this case (*Gr=5.10⁵*, *Re=100)*, the heat flux redistribution is done mainly by axial wall conduction (*Pe=500*).

More inspections of the Figure 4.36 reveal that the time needed to reach the steady state regime is more important compared to the corresponding one of the case (*Gr=5.10³*, *Re=1)*. This is also a direct consequence of the pipe wall and fluid axial conductions.
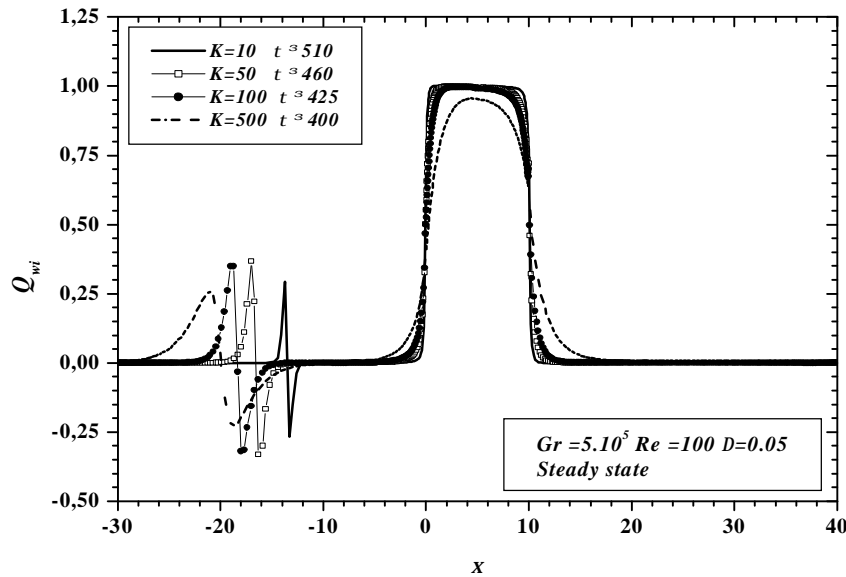
Figure 4.36 Axial distribution of Q$_{wi}$ at the steady state for K=10, 50, 100 and 500 for Gr=5.*10⁵*, *Re=100*.

The axial distribution of the friction coefficient ratio for *Gr=5.10⁵* and *Re=100* at a representative instants t =*5, 25* in the transient period and, at the steady state, Figures 37a-b, shows:

-The same behaviour to the one corresponding to the previously studied case (*Gr=5.10³*, *Re=1)* at the early transient period.

-Local values higher than the unity (>1) in the downstream section, during a period of the transient, before decrease asymptotically to the unity at the outlet of the duct.

Chapter 4   *Numerical results*

-At the steady state, a local minimum in the vicinity of the inlet of the heated section. This later is more pronounced than the corresponding one shown in Figure 4.31b, before tending slowly towards the limiting case corresponding to the forced convection at the exit and the inlet of the duct.

Figure 4.37a Influence of *K (K=10, 50, 100* and *500)* on the axial distribution of the friction coefficient ratio for $Gr=5.10^5$, $Re=100$ at $t=5$ and *25*.

Figure 4.37b Influence of *K (K=10, 50, 10*0 and 500) on the axial distribution of the friction coefficient ratio for $Gr=5.10^5$, $Re=100$ at the steady state.

In order to improve our understanding of heat transfer characteristics in the unsteady mixed convection and to prove that the large values of Q_{wi} in the upstream section for this case *(Gr=5.10^5, Re=100)* is due to an important heat transfer at the wall-fluid interface, we present the transient evolution of the temperatures difference Dq_{wi} at the wall-fluid interface, Figure 4.38a and of Q_{wi}, Figure 4.39a at three axial positions (*x =0, x = -5* and *x = -10*).

As can be seen in these figures, it is obvious that the large values of the maximum and minimum points of Q_{wi} are due to a large temperatures difference Dq_{wi} at the wall-fluid interface. Furthermore, it is also observed that for the three axial positions, Dq_{wi} and consequently Q_{wi}, increases with time and reach a maximum value. Thereafter, it decreases rapidly towards a minimum value and finally it increases again asymptotically towards zero.

This behaviour of Dq_{wi} and Q_{wi} is explained by the fact that, for each axial position, the heat transfer is firstly dominated by conduction in the pipe wall, which results in a lower rate of increase in the fluid temperature than in the interfacial temperature. Then, Dq_{wi} increases with elapsing time until the recirculation cell reach the corresponding axial position. At this transient period, the energy transported by the cell becomes more important than that diffused by conduction in the pipe wall from the adjacent heated section. This effect result in negative values of Dq_{wi} and consequently Q_{wi}, indicating that the heat transfer is from the fluid to the pipe wall.

As time goes by, the cell continues to move towards the inlet of the upstream section, resulting in a decrease of Dq_{wi} and consequently Q_{wi} until they become zero after a certain period of time. This is due to the fact that, as the cell passes the corresponding axial position *(x=0, x= -5* or *x= -10)*, it acts like an insulator, as it has been explained previously for the case *(Gr=5.10^3, Re=1)*.

Figure 4.38b and Figure 4.39b gives, respectively the transient evolution of Dq_{wi} and Q_{wi} at the same conditions and axial positions for *Re=50*. It is observed that the decreases of *Re* leads to decrease the extreme values of Q_{wi}. This is due to the fact that as *Re* decreases, the forces exerted by the fluid flow coming from the inlet of the duct decrease also in its turn. Therefore, the cell spreads in the upstream section more rapidly, as can be seen in Figure 39b. Consequently, the accumulated energy at each axial position is lower.

It is also seen in these figures that for *Re=50*, $\boldsymbol{Dq_{wi}}$ and consequently Q_{wi} are positive at the axial position *x=0,* Figure 4.38b contrary to the case of Figure 4.38a (*Re=100*), indicating that the interfacial heat flux is positive in the heated section for *Re=50*.
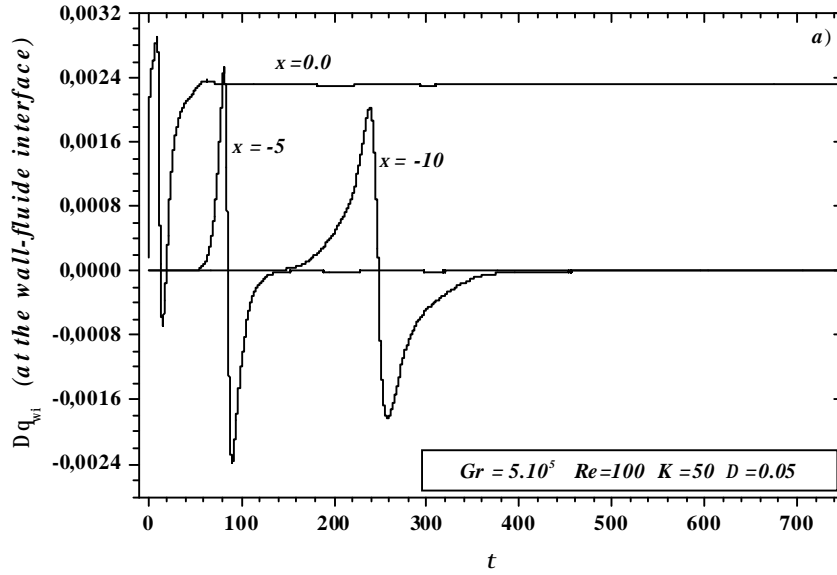
Figure 4.38a Transient evolution of the temperature difference at the wall-fluid interface at *x=0, - 5* and *x=- 10* for $Gr=5.10^5$, *K=50, Re=100*.
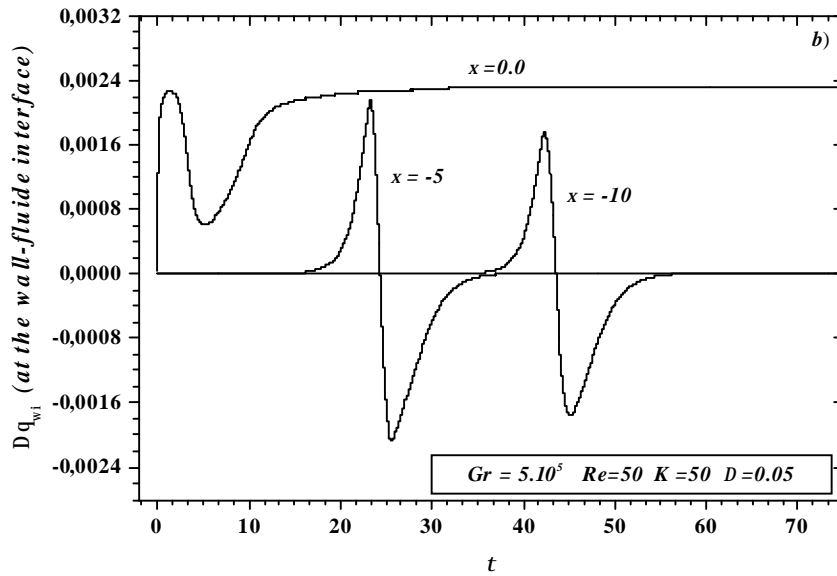
Figure 4.38b Transient evolution of the temperature difference at the wall-fluid interface at *x=0, - 5* and *x=- 10* for $Gr=5.10^5$, *K=50, Re=50*.
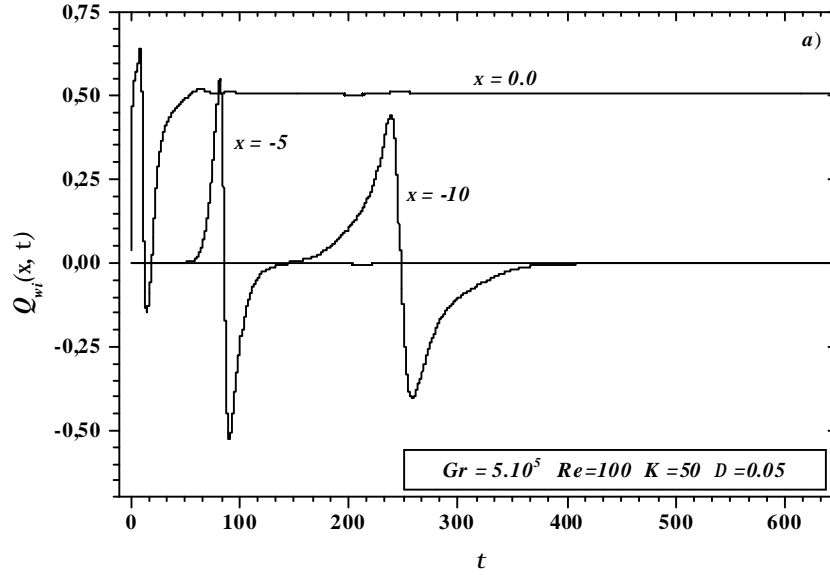
Figure 4.39a Transient evolution of the interfacial heat flux at $x=0, -5$ and $x = -10$, for $Gr=5.10^5$, $K=50$, $Re=100$.
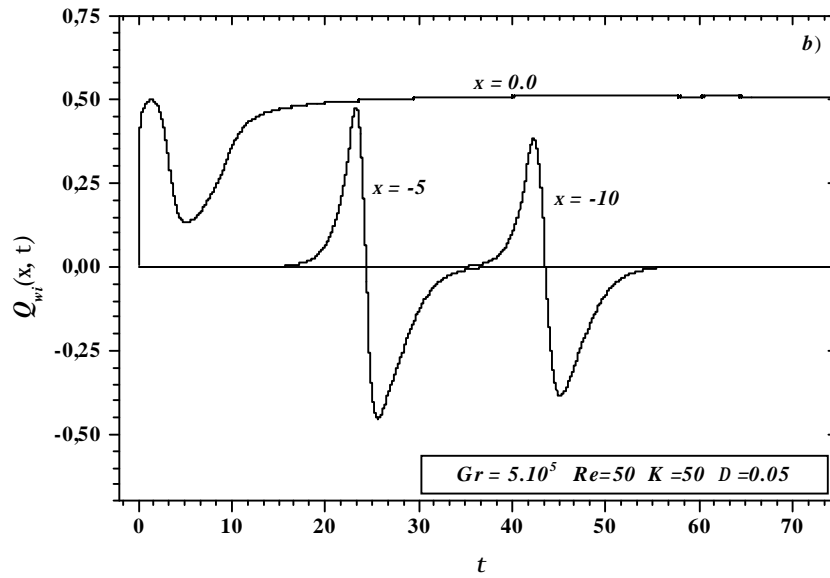
Figure 4.39b Transient evolution of the interfacial heat flux at $x=0, -5$ and $x = -10$ for $Gr=5.10^5$, $K=50$, $Re=50$.

4.3.7.1 Observations on the maximum of the radial temperature in the upstream section

The maximum of the radial distribution of temperatures to the neighbourhood of the pipe wall observed previously to the entry of the heated section during a weak period of the transient period has also been observed in the upstream section.

Indeed, for every axial position, the radial temperature presents a distribution similar to the one of the forced convection in the absence of the recirculation cell as one can see it in Figures 4.40a *(x= -5)* and 4.40b *(x = - 10)*, respectively at *t = 80* and *180*. The corresponding vectors velocities are represented in Figures 4.41a-b and 4.41c-d. The Figures 4.41b and 4.41d represents an enlarging of the zones situated between $-5 \le x \le 0$ and between $-15 \le x \le -5$.

In Figures 4.41a-c, one notes that the velocity profiles at the axial positions *(x= -5)* or *(x = - 10)* are parabolic, indicating that the recirculation cell has not reached these two axial positions again. As the recirculation cell reaches a given axial positions, *(x=-5)* or *(x= -10)*, the radial temperature profiles undergo a distortion in the neighbourhood of the pipe wall, represented by a maximum, see Figures 4.40a-b, respectively at *t =90* and *t =190*. This distortion subsists until the moment where the cell passes the corresponding axial position.

With elapsing time, for the reasons that we evoked previously, the cell moves toward the upstream section, Figures 4.42a-b. Such effect results in the evacuation of the accumulated energy to the neighbourhood of the pipe wall. Consequently, these maxima undergo a decrease and finish by disappearing completely with elapsing time, Figures 4.40a-b, respectively from *t>100* and *t>210*.

Later, *t* ³*110* (Figure 4.40a) and *t*³*250* (Figure 4.40b), the radial distribution of temperatures to the neighbourhood of the pipe wall presents a flat profile, indicating that the gradient of temperature between the pipe wall and the fluid is nearly equal to zero. This is due to the fact that, when the recirculation cell passes a given axial position, it acts like an insulator between the pipe wall and the fluid. In Figures 4.43a-b (*t=110)* and 4.43c-d (*t=250)*, representing the vector velocities, one can see that the reversed flow region has already passe the two axial positions *x=-5* and *x=-10*.

This flat profile in the near wall maintains itself until the steady state is reached for every axial position reached by the recirculation cell.
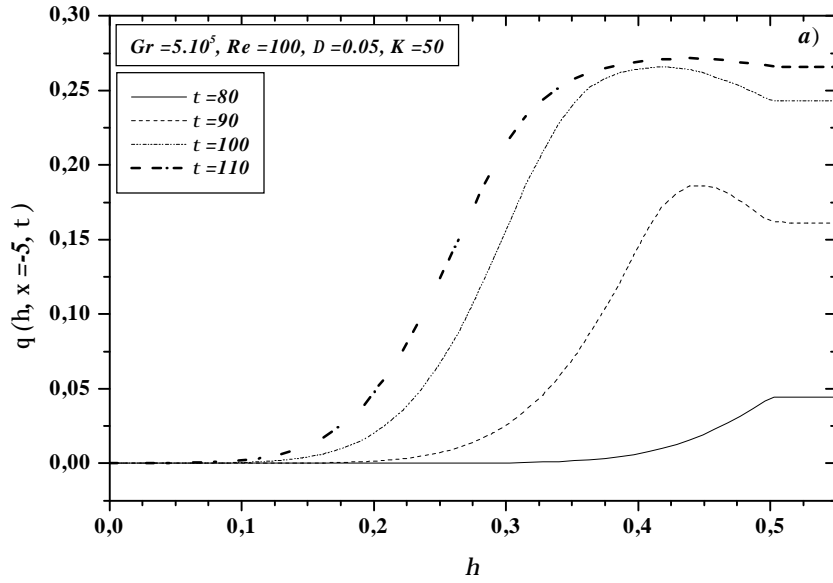
Figure 4.40a Transient evolution of temperature profiles at *x=-5*.
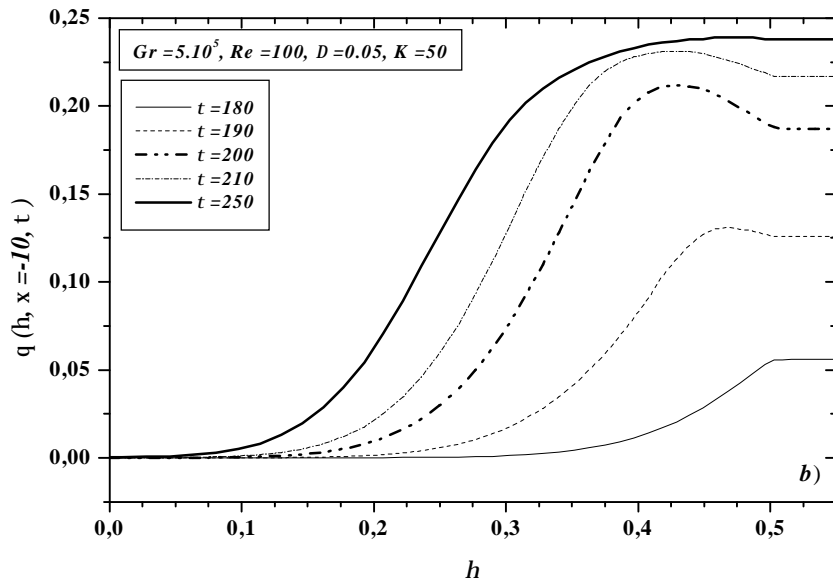
Figure 4.40b Transient evolution of temperature profiles at *x=-10*.
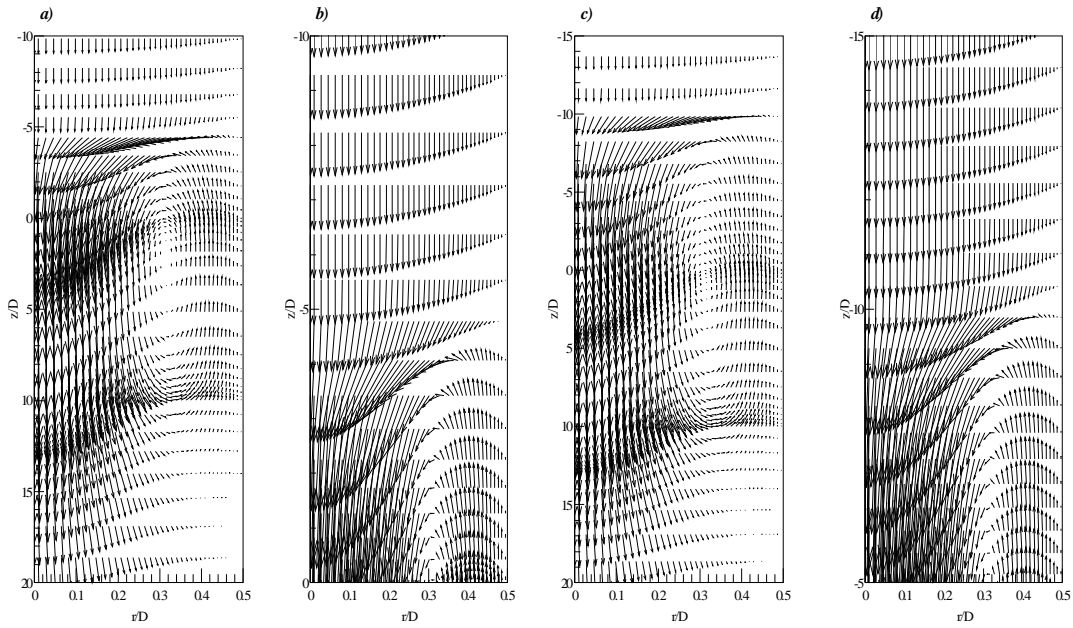
Figures 4.41a-d Vectors velocities for two instants of the transient period
a-b) Vector velocities and enlarging of the zone $-10 \leq x \leq 0$ at $t = 80$
c-d) Vector velocities and enlarging of the zone $-15 \leq x \leq -5$ at $t = 180$
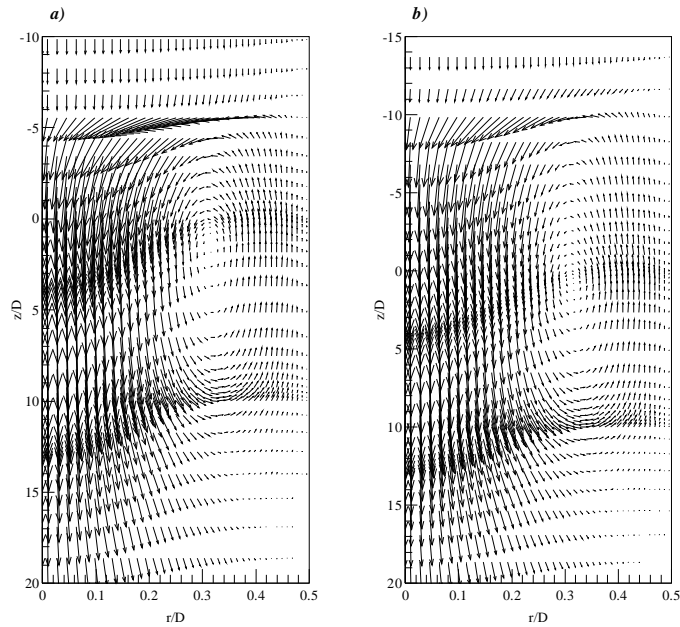
Figures 4.42a-b Vectors velocities for two instants of the transient period
a) $t = 100$ b) $t = 210$
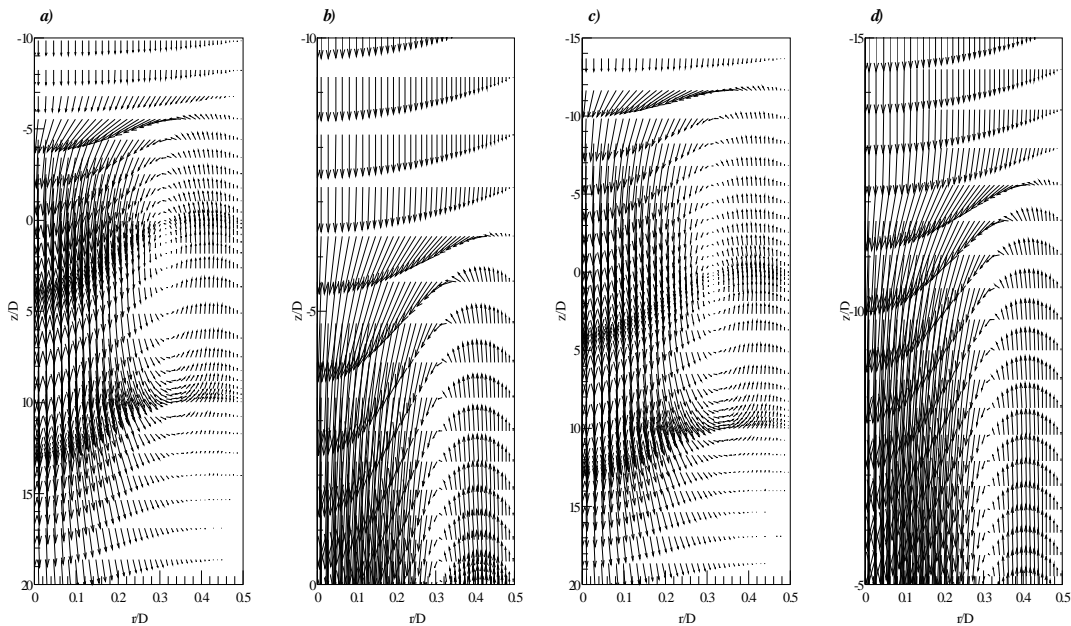
Figures 4.43a-d Vectors velocities for two instants of the transient period
a-b) Vector velocities and enlarging of the zone $-10 \leq x \leq 0$ at $t = 110$
c-d) Vector velocities and enlarging of the zone $-15 \leq x \leq -5$ at $t = 250$

4.3.7.2 Observations on the maximum of the radial temperature in the heated section

The analysis of the numerical results showed that the transient evolution of the radial distribution of temperatures in the heated section is different from the one in the adiabatic upstream section, except in the first instants of the transient period.

Indeed, during the first instants of the transient period where the heat transfer is globally dominated by radial conduction we have noted that the flow corresponds to the case of 'pure forced convection' without the effect of the natural convection as one can see it in Figure 4.44 representing the radial axial velocity profiles at $t = 0.5$. On the Figure 4.45, relative to the radial temperature profiles at the same instant, one notes as for the case of the upstream section, a similar profile to the one of the forced convection.

With elapsing time, the energy transferred to the wall-fluid interface increases. Consequently, the effect of the natural convection in the vicinity of the wall starts to appear and, acts on the main descendant flow, in particular from the middle to the exit of the heated section. This results in a deceleration of the fluid close to the pipe wall compensated by an

----

acceleration in the centre of the duct in order to satisfy the conservation of the continuity equation, see Figure 4.44 at t =5.
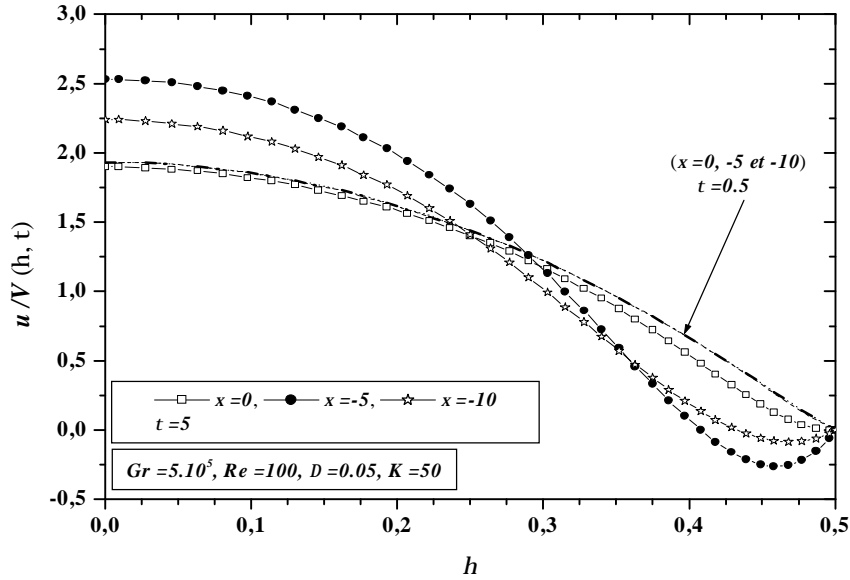
Figure 4.44 Radial distributions of axial velocity profiles inside the heated section for two instants of the transient period.
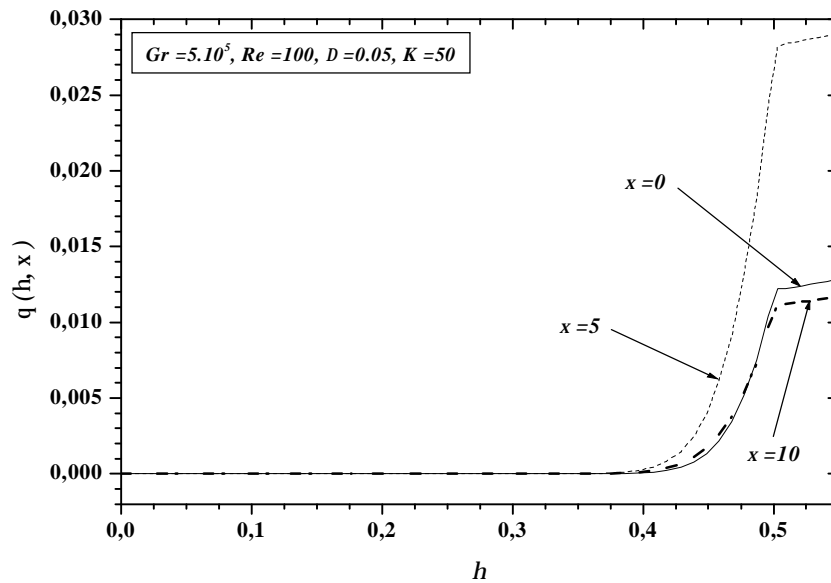
Figure 4.45 Radial distribution of temperature profiles inside the heated section at $t=0.5$

At this instant (t =5), where the axial velocity at the middle of the heated section (x=5) is negative (Figure 4.44) and, where the gradient of the axial velocity to the exit of the

heated section (*x=10*) is zero, there is practically no noticeable effect on the radial distributions of the temperature, see Figure 4.46.
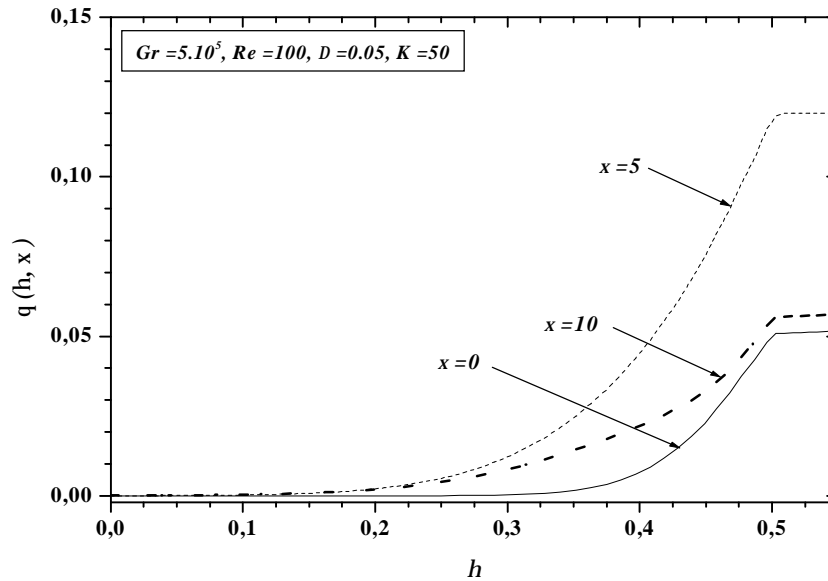
Figure 4.46 Radial distribution of temperature profiles inside the heated section at *t=5*

As the time goes on, the negative values of the axial velocity to the vicinity of the pipe wall become more visible. Consequently, the reversed flow region thickness increases considerably, see Figure 4.47. The presence of this reversed flow region in the vicinity of the pipe wall has strongly distorted the radial temperature profiles. Such effect results in a clear change in the shape of the fluid temperature profiles in the whole heated section. So, at the entry of the heated section, one notes a local maximum in the near wall region (observed previously) and a local minimum close to the axis of the duct. From the middle to the exit, the temperature profiles present two local minima, Figure 4.48.

From *t>17.5*, the recirculation cell, spreads toward the upstream section (Figures 4. 49a-b), leading to the disappearance of the local maxima of the temperature profiles at the inlet of the heated section and, indicating the end of the period where the heat transfer at the vicinity of the inlet of the heated section is from of the fluid to the pipe wall.

After this period and until the steady state the temperature profiles along the heated section presents two local minima: one observed on the centreline of the duct and the other

----

one located in the near wall region, see Figure 4.50. Consequently, the heat transfer at the wall-fluid interface is again from the pipe wall to the fluid.
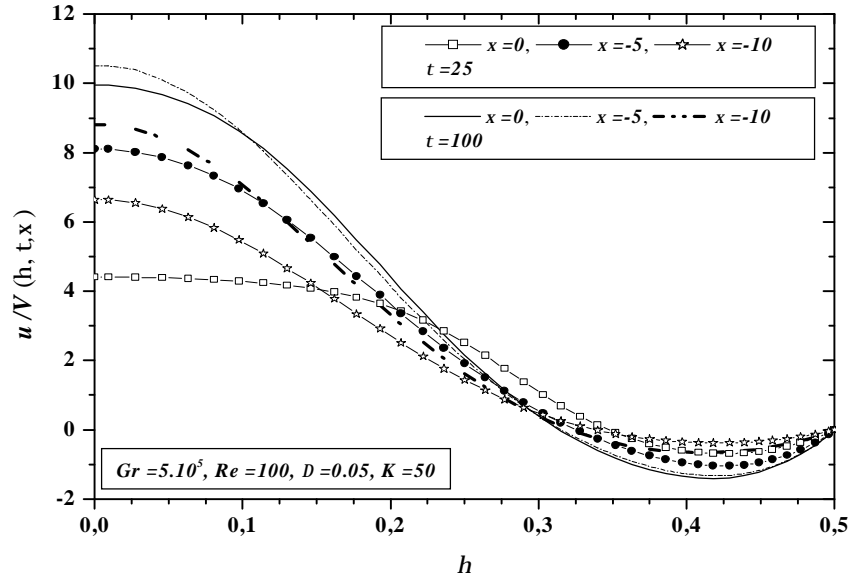
Figure 4.47 Radial distribution of the axial velocity profiles inside the heated section
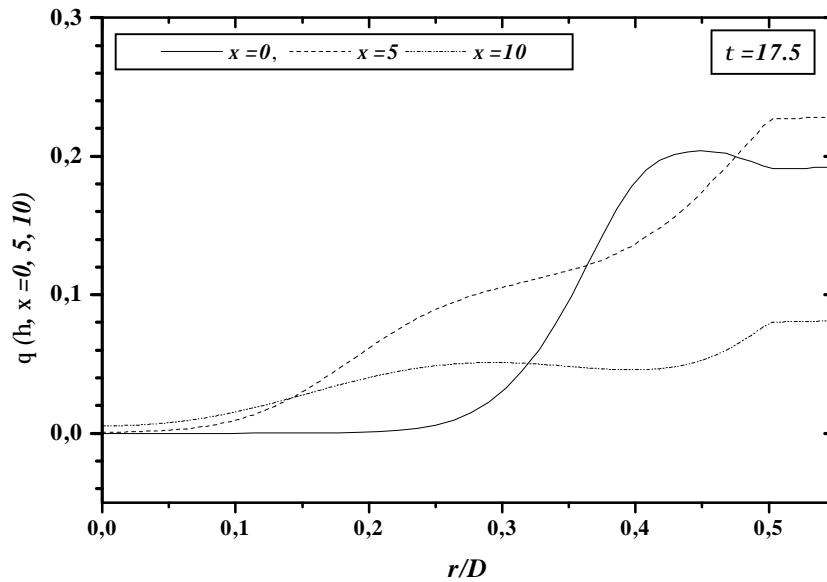
Figure 4.48 Radial distribution of the temperature profiles inside the heated section
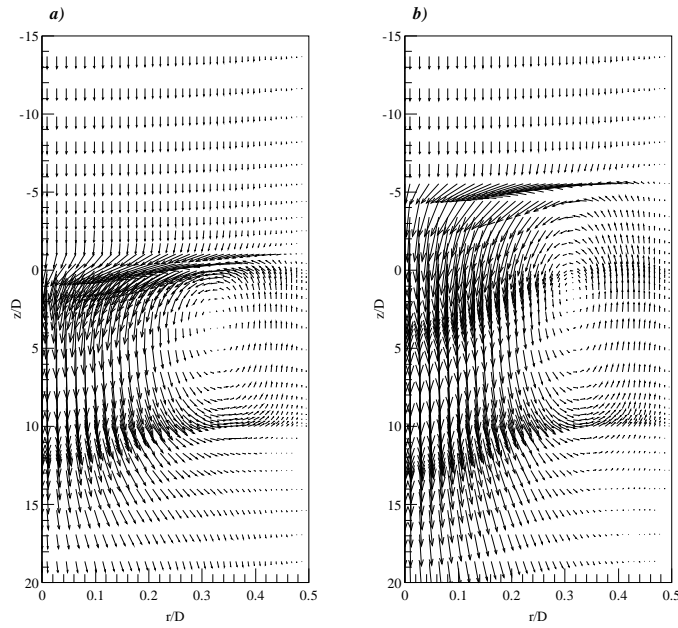
Figures 4.49a-b Vectors velocities for two instants of the transient period *a)t=25, b)=100*
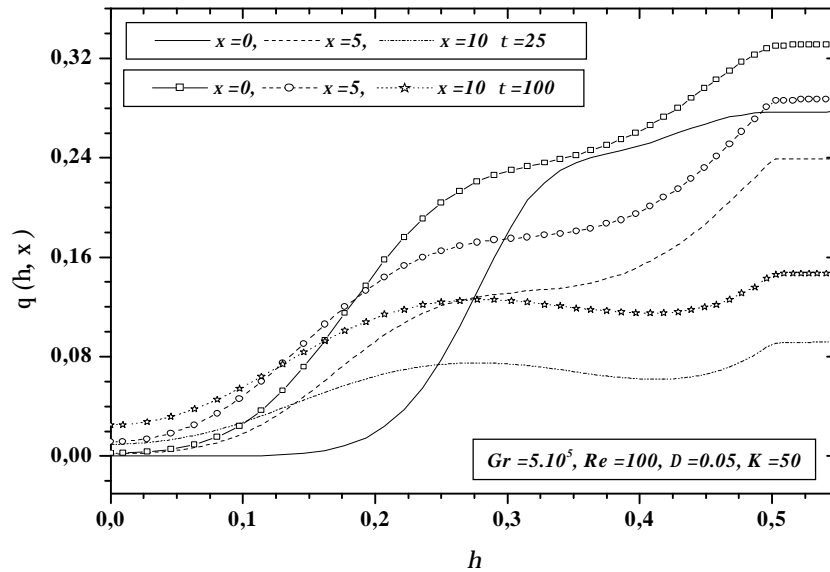
Figure 4.50 Radial temperature profiles inside the heated section at *t=25* and *100*.

      Such behaviour (presence of two local minima), concerning the radial temperature profiles in this case is due to the fact that the recirculation cell brings the colder fluid from the outer space adjacent to the end of the recirculation cell (*x³10)* and, injects it in the heated

Chapter 4   *Numerical results*

----

section. This effect results in weak values of temperatures at the exit of the heated section *(x=10)* over a large zone of the cross-section of the duct, compared to the corresponding one at the middle (*x =5)* and the exit (*x=0),* see Figure 4.50.

As the fluid moves toward the inlet of the heated section *(x=0)*, the radial temperature increases and reach its maximum values at this axial position. The fact that the temperature at the inlet of the heated section *(x=10)* is the higher compared to one at the middle (*x =5)* and the exit (*x=0)* can be explained by the fact that the heat coming from the wall continuingly heats the fluid brought from the outer space adjacent to the exit of the heated section into the reversed flow region. A similar trend has been found, at the steady state by, **Nguyen & al** [50].

Let's note that on a weak region of the cross-section at *x=10*, the radial temperature is slightly greater than the corresponding one at *x=5* and *x=0* (Figure 4.50). This is a result of the permanent contact of the beginning of the recirculation cell with the cold fluid, coming from the entry of the duct.

It is also noted on the Figure 4.45 at *t =0.5* (at the beginning of the transient period), that the pipe wall temperature at *x=0* is higher than the corresponding one at *x=10*, whereas at *t =5,* Figure 4.46, one notes the inverse. As the time goes on, one realizes that the radial temperature at *x=0* is again higher than that at *x=10* over a large zone of the cross-section, say between $0.2 \leq \eta \leq 0.55$, Figure 4.50.

This can be explained by the fact that at the beginning of the transient period, the heat transfer is made without natural convection effect and, that upstream of the heated section one recovers the colder fluid, what favourites the heat transfer. After a short time, the effect of the natural convection begins to appear, resulting in a more important reduction of the axial velocity at the vicinity of the pipe at *x=10* than at *x=0 (*Figure 4.44 at *t =5)*, leading thus to an increase of temperature at *x=10*. Later, the intensity of the cell becomes more pronounced, resulting in an important extent toward the upstream section. This results therefore in an important evacuation of energy toward the entry of the heated section. Consequently, the temperature at *x=0* is again greater than that at *x=10.*

Chapter 4   *Numerical results*

4.3.8 Effect of the pipe wall thickness-to-diameter ratio D

In order to examine the effect of the pipe wall thickness-to-diameter ratio D on the interfacial heat flux, we present on the Figures 4.51a-c the obtained results at different instants of the transient period for different values of the parameter D.

On these Figures, one notes that the values of the interfacial heat flux in the heated section decrease according to the parameter D. This is due to the fact that for low values of D, the thermal resistance and the thermal capacity of the pipe wall are weaker. Consequently, the applied heat flux at the outer surface is easily transferred to the fluid. Upstream and downstream of the heated section, the diffusion of the heat increases with the increase of D.

Let's note that at the instant $t = 5$, Figure 4.51a, the heat transfer is globally dominated by conduction.
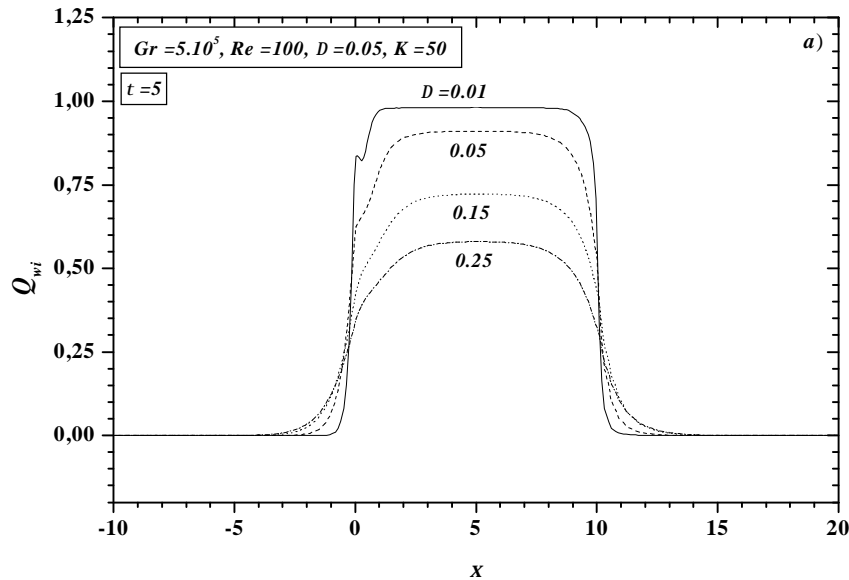
Figure 4.51a Effect of the parameter D on the axial distribution of the interfacial heat flux at $t = 5$.

As the time goes on, Figure 4.51b, the effects of convection become more important and we attend, as seen previously, to an important redistribution of the energy provided to the system at the vicinity of the inlet of the heated section. One also notes, that with the increase of D, the corresponding maximum and minimum of the redistributed energy decreases, while

----

the heat exchange surface between the fluid and the pipe wall increases. These results are a direct consequence of the effect of the axial conduction.

At this instant *(t =25)*, the corresponding interfacial heat flux for *D* equal to *0.15* and *0.25* is negative in the heated section. Such behaviour is attributed, as we have explained it before (effect of the conductivity ratio) to the large values of the thermal capacity and the thermal resistance. Thus, at this period of the transient regime, the energy evacuated by the recirculation cell is higher than the one transmitted to the wall-fluid interface through the pipe wall. It results an exchange of heat from the fluid to the pipe wall.
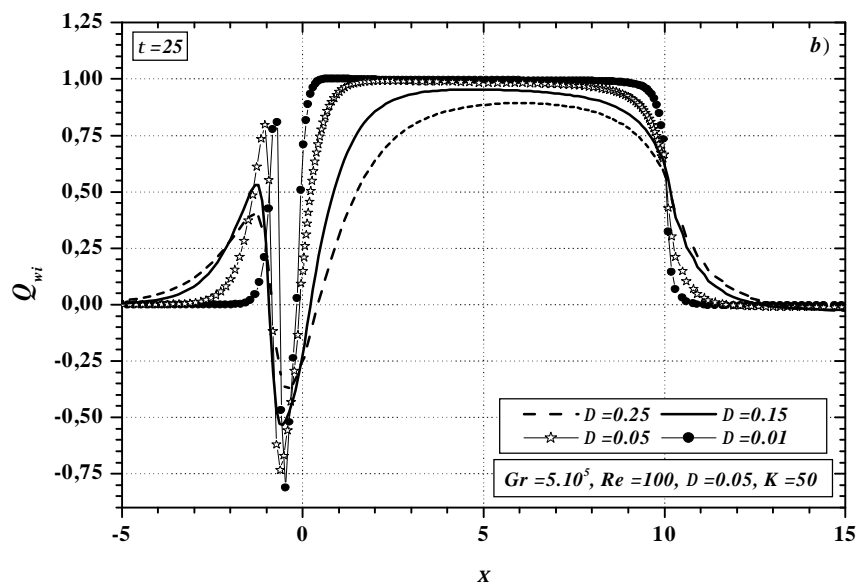
Figure 4.51b Effect of the parameter *D* on the axial distribution of the interfacial heat flux

With further increase in time, the thermal lag between the different curves increases considerably. So, in Figure 4.51c, one notes that with the decrease of the values of the parameter*D*, the redistribution of the applied heat flux becomes closer to the inlet of the heated section. This behaviour continues until the steady state regime, not represented here, because of a too long upstream section for the cases *D=0.15* and *0.25*.

Finally, one note that the time needed to reach the steady state increases with the values of the parameter *D.*

Chapter 4   *Numerical results*
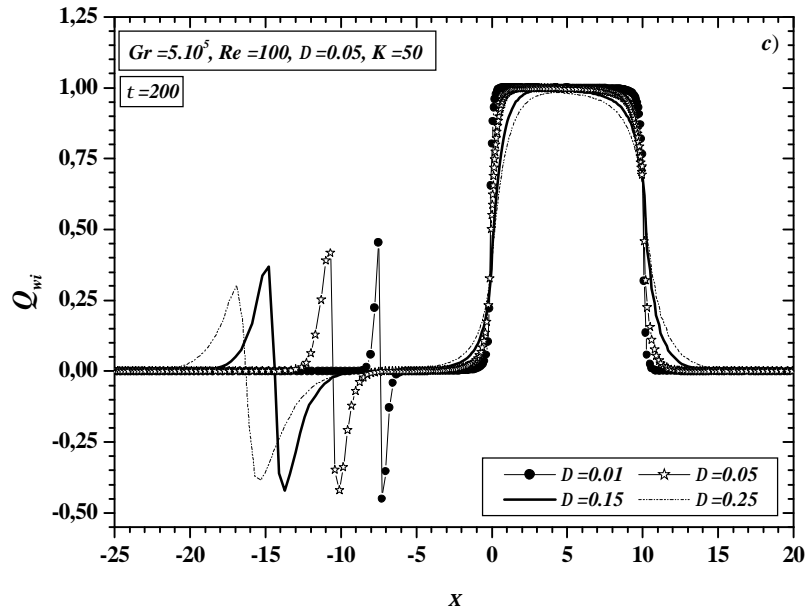
Figure 4.51c Effect of the parameter D on the axial distribution of the interfacial heat flux

For two extreme values of the pipe wall thickness-to-diameter ratio D and for the same instants that those corresponding to the case of the interfacial heat flux, we present in Figures 4.52a-b, the axial evolution of the friction coefficient ratio.

Through these two Figures, one notes that at $t=5$ (Figure 4.52a), the friction coefficient ratio in the heated section corresponding to $D=0.01$ is more distorted than the one corresponding to $D=0.25$. This is due to the fact that the quantity of energy transferred to the wall-fluid interface for $D=0.01$ is more important than the one relative to $D=0.25$ (Figure 4.51a). Consequently, the effect of the natural convection is more important. Outside of the heated section, the two curves corresponding to $D=0.01$ and $D=0.25$ are superposed.

With elapsing time, the distortion relative to $D=0.25$ becomes more pronounced that the one of $D=0.01$ due to the effects of the thermal inertia of the system and the axial wall conduction. Consequently, at the instant $t=25$, one notes that in the vicinity of the inlet and the exit of the heated section, the distortion of the friction coefficient for $D=0.25$ is larger than the one corresponding to $D=0.01$.

This behaviour continues until the steady state with more and more important distortions as the values of D increase, in particular in the upstream section, as one can see it in Figure 4.52b.

Far from the exit of the heated section, the different curves join themselves, indicating that the system tends toward an established regime characterized by a ratio of the friction coefficient equal to 1 corresponding to the case of the forced convection.

In Figures 4.53a and 4.53b, one presents the radial distribution of temperatures at the inlet of the heated section for two values of the parameter D and, for different instants of the transient period representing the development and the disappearance of the maximum of temperature profiles at this axial position.

On these Figures, one notices that the development of the maximum corresponding to $D=0.01$ is more pronounced. Thus, at $t=21$, the maximum value reached by the radial temperature is greater than 0.26 for $D=0.01$, whereas for $D=0.25$ it is of the order of 0.18. One also notes that these maxima remain longer for $D=0.25$ than for $D=0.01$. These results represent a direct consequence of the effect of the thermal capacity and the axial wall conduction.
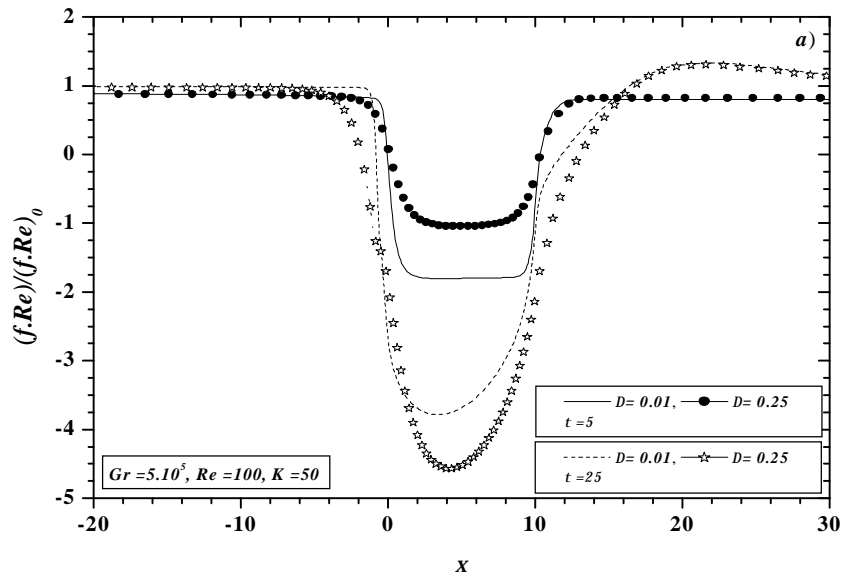
Face 4.52a Effect of the parameter Δ on the axial distribution of the friction coefficient ratio at $t=5$ and $t=25$.

Chapter 4   *Numerical results*
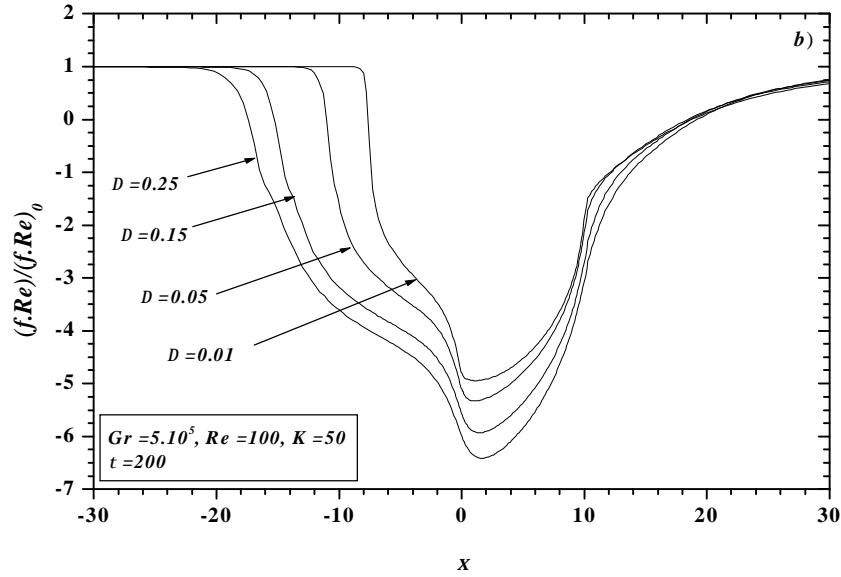
Figure 4.52b Effect of the parameter Δ on the axial distribution of the friction coefficient ratio at *t=200.*
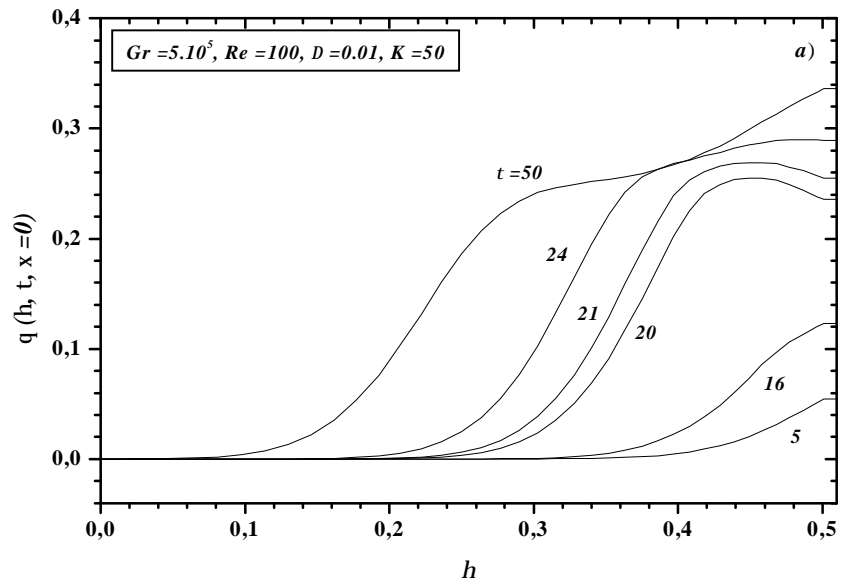
Figure 4.53a Radial distribution of temperature profiles at *x=0* for different instants of the transient period *D=0.01*.

Chapter 4   *Numerical results*
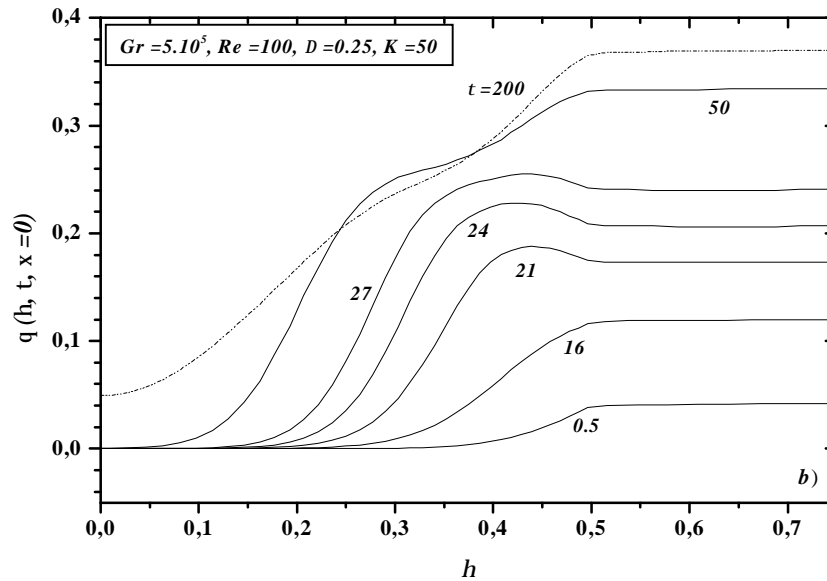
Figure 4.53b Radial distribution of temperature profiles at *x=0* for different instants of the transient period *D=0.25*.

In order to improve our understanding of the effect of the dimensionless pipe wall thickness on the heat transfer characteristics in the unsteady mixed convection, we present in Figure 4.54, the transient evolution of temperatures difference at the wall-fluid interface *(Dq$_{wall\text{-}fluid}$),* for the analysed preceding values of the parameter *D* at the same axial position *x=0.*

On this Figure, one notes that the maximum and the minimum of the temperatures difference at the wall-fluid interface become more pronounced with the decrease of the *D*. One also notes, that the period of time during which the heat transfer is from the fluid to the pipe wall, increase with the increase of the pipe wall thickness.

Let's recall that these maxima and minima correspond respectively to a heat transfer from the pipe wall to the fluid and, from the fluid to the pipe wall.

Finally, one notes that during the transient period where the effect of the natural convection effect is negligible *(t£ 15)*, the temperatures difference *(Dq$_{wall\text{-}fluid}$)* corresponding to *D=0.01* present the weakest values.

From this it can be concluded that the presence of the pipe wall has a considerable influence on the characteristics of the heat transfer during the transient period and, therefore,

the effects of the pipe wall cannot be disregarded in the case of the transient conjugated mixed convection heat transfer.
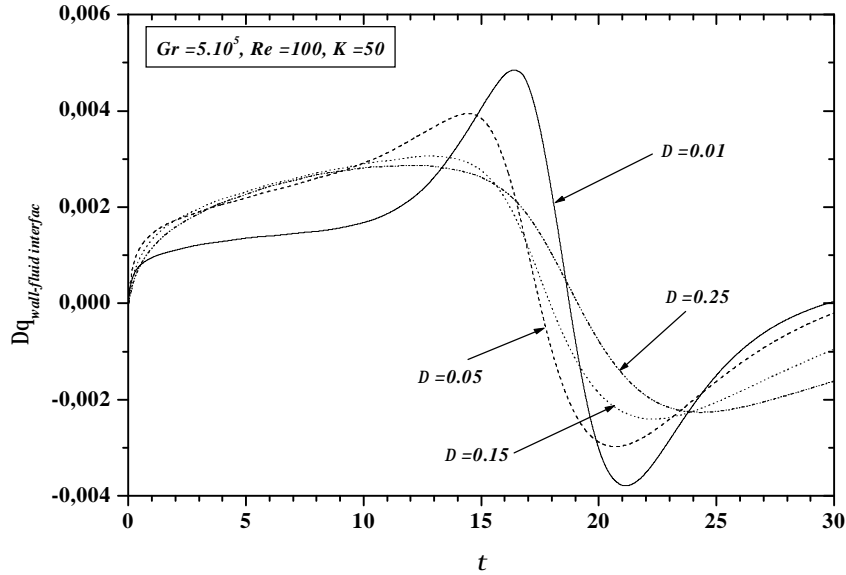
Figure 4.54 Transient evolution of the difference of temperature at the wall-fluid interface $Dq_{wall\text{-}fluid}$ at $x=0$.

4.3.9 Influence of Grashof and Reynolds numbers for the same Richardson number

The transient axial evolution of Q_{wi} for two values of the Reynolds and Grashof numbers, respectively *(10, 100)* and *$(5.10^3, 5.10^5)$* is shown in Figures 4.55a-c. For these two values of Reynolds and Grashof numbers, the Richardson number has the same value *Ri=50*. In the beginning of the transient period the values of the interfacial heat flux for *(Re, Gr)=(10, 5.10^3)* are greater than these relative to *(Re, Gr)=(100, 5.10^5)*, see Figure 4.55a. With elapsing time, Archimedes forces take the over on the viscous forces, in particular for the case *(Re, Gr)=(100, 5.10^5)*. This leads to the appearance of a recirculation cell, more intense for the case *(Re, Gr)=(100, 5.10^5)*, see Figures 4.56a-b. This result in negative values of Q_{wi} in the vicinity of the inlet of the heated section, see Figure 4.55b. For the case *(Re, Gr)=(10, 5.10^3)*, one notices that the transient distribution of Q_{wi} is similar to the one relative to the case of the pure forced convection with axial wall conduction effect. This is due to the fact that in this case the recirculation cell is very weak, therefore, it remain confined in the heated section (Figure 4.56a).

Chapter 4   *Numerical results*

This behaviour continues for the two cases until the steady state, see Figure 4.55c. At this final time, one notes the absence of any redistribution of the interfacial heat flux in the upstream section for the case *(Re, Gr)=(10, 5.10³)*, contrary to the case *(Re, Gr)=(100, 5.10⁵)*.
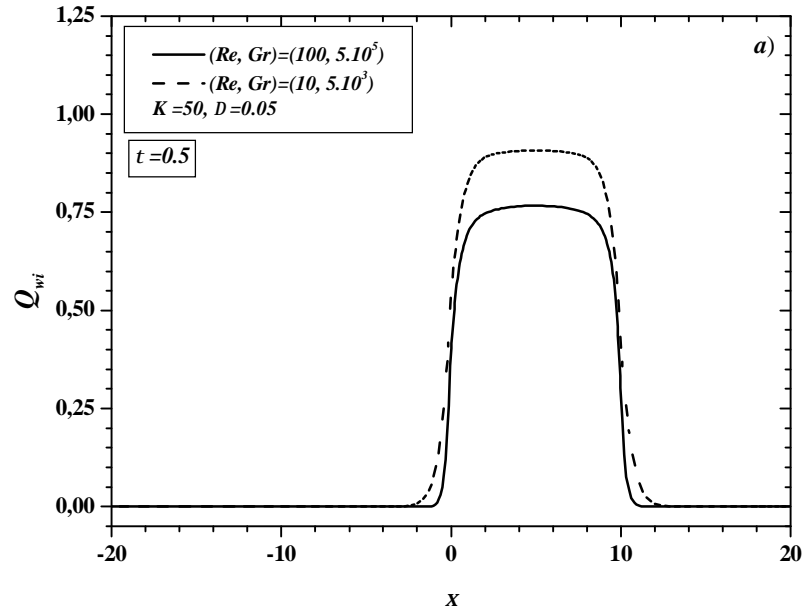
Face 4.55a Axial distribution of the interfacial heat flux at $t=0.5$
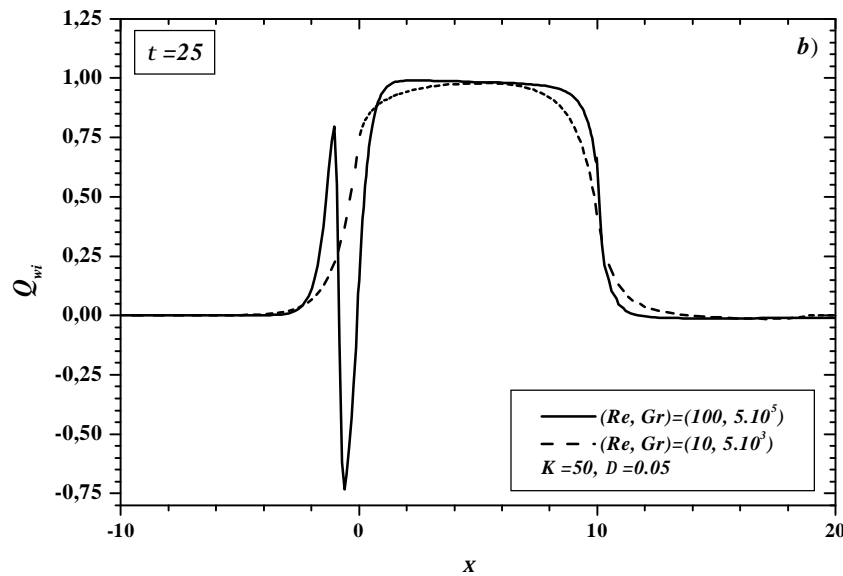
Figure 4.55b Axial distribution of the interfacial heat flux at $t=25$.
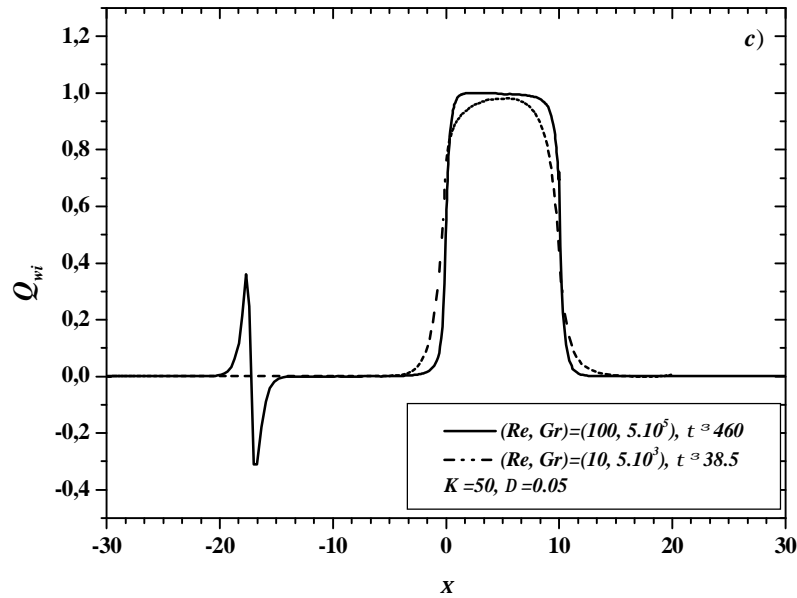
Figure 4.55c Axial distribution of the interfacial heat flux at the steady state.
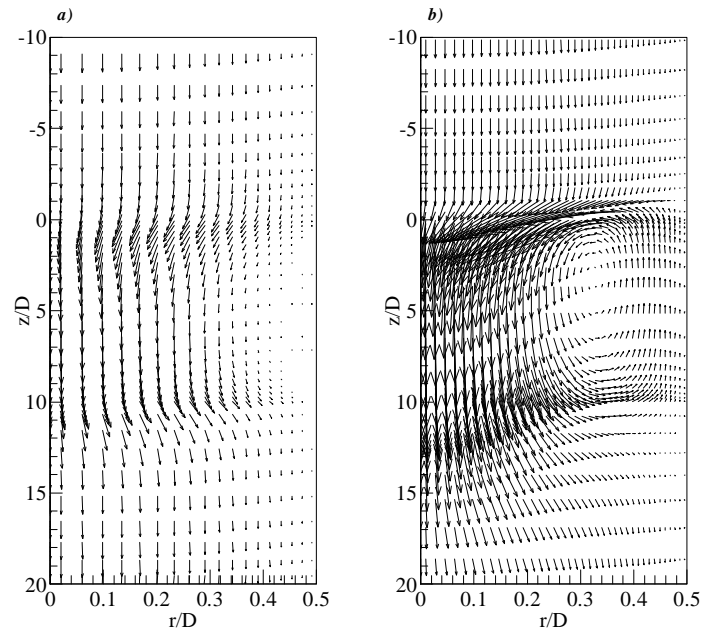
Figures 4.56a-b Vector velocities at $t = 25$: a)$(Re, Gr)=(10, 5.10^3)$, b)$(Re, Gr)=(100, 5.10^5)$

The corresponding transient axial evolution of the friction coefficient ratio is illustrated in Figures 4.57a-b. One notes a weak distortion of the friction coefficient ratio relative to the case $(Re, Gr)=(10, 5.10^3)$. This distortion is limited to the heated section

Chapter 4   *Numerical results*

(0£x£10), contrary to the case *(Re, Gr)=(100, 5.10⁵)* where the distortion spreads upstream and downstream of the heated section. This justifies the confinement of the recirculation cell at the interior of the heated section for the case *(Re, Gr)=(10, 5.10³*, and consequently, there were no redistribution of the interfacial heat flux in the upstream section.
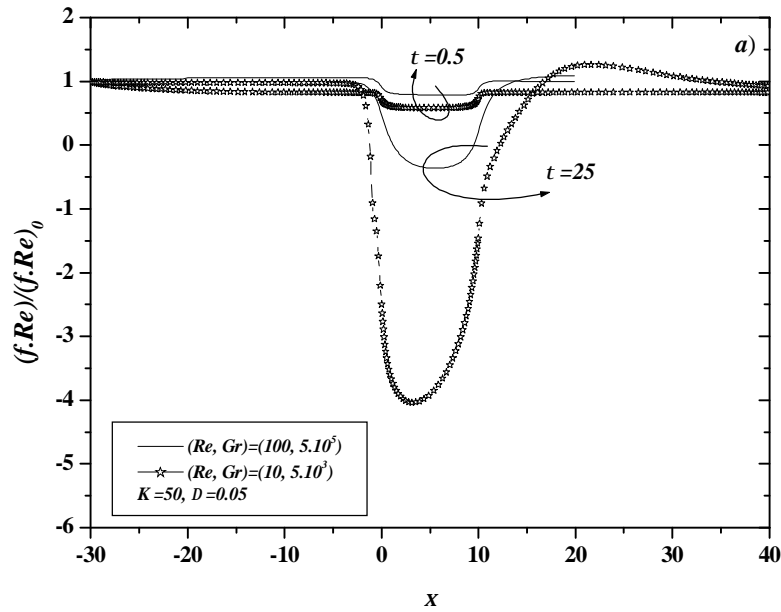
Face 4.57a Axial distribution of the friction coefficient ratio at *t =0.5* and *25*.
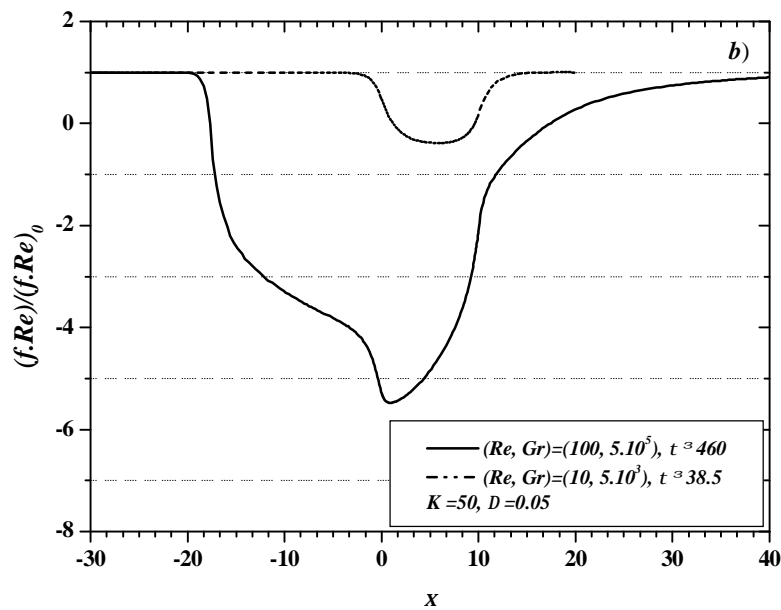
Figure 4.57b Axial distribution of the friction coefficient ratio at the steady state.

The radial distribution of temperatures in the heated section corresponding to these two cases is presented in Figures 4.58 and 4.59. One observe that the radial distribution of temperatures, relative to the case *(Re, Gr)=(10, 5.10^3)* presents no distortion and, that this last is greatly similar to the one of pure forced convection. On the other hand, the one relative to the case *(Re, Gr)=(100, 5.10^5)* present an important distortion along the heated section.

Furthermore, one notices in Figure 4.58, that the temperature at *x=0* is greater to the one at *x=5* and *10* on nearly the half of the cross-section, due to a strong reversed flow at this region. In Figure 4.59, one notes the inverse.

Let's note that the time needed for the system to reach the steady state for the case *(Re, Gr)=(100, 5.10^5)* is more important than the corresponding one for the case *(Re, Gr)=(10, 5.10^3)*.

From this comparison it can be concluded that the characteristics of the heat transfer by mixed convection are characterized in addition to the number of Richardson *(Ri=Gr/Re^2)* by the values of the Reynolds (*Re*) and Grashof (*Gr*) numbers.
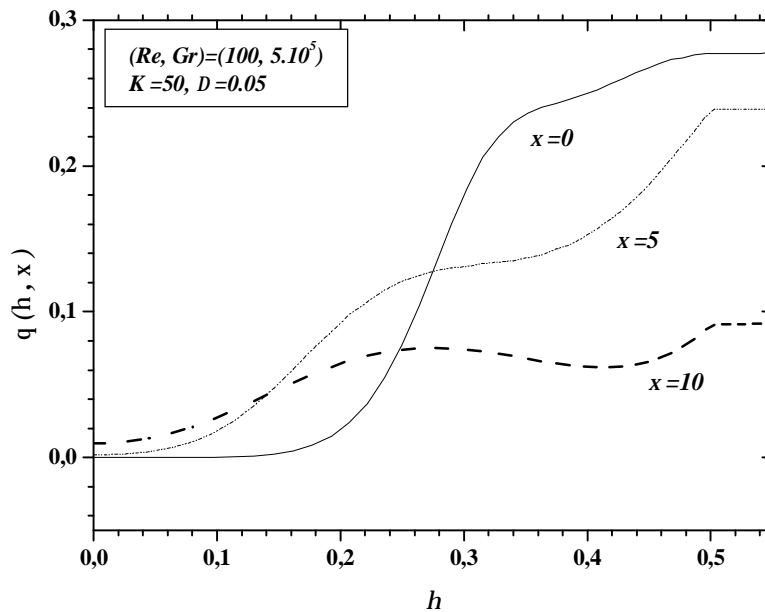
Figure 4.58 Radial distribution of temperature profiles in the heated section at *t* =25 *(Re, Gr)=(100, 5.10^5)*

Chapter 4   *Numerical results*
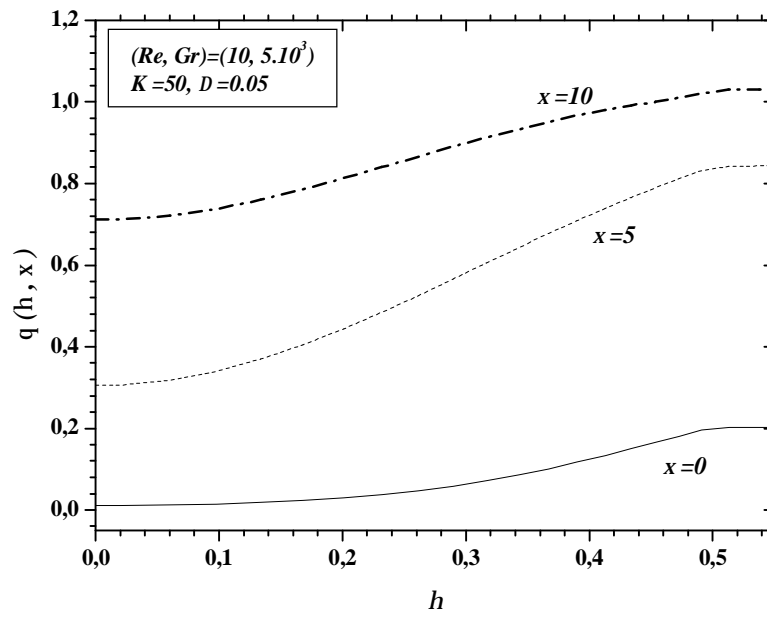
Figure 4.59 Radial distribution of temperature profiles in the heated section at $t = 25$ *(Re, Gr)=(10, 5.10³)*

Chapter 4   *Numerical results*

----

5 General conclusion and perspective

5.1 Contribution of the present work

In the present work, a numerical study has been performed to investigate the unsteady conjugated downward laminar mixed convection in circular pipe submitted partially to a uniform and constant wall heat flux. The solution takes wall conduction and wall heat capacity in to account.

The various investigated parameters were the Reynolds and Grashof numbers, the thermal conductivity and diffusivity ratios between the pipe wall and the fluid, respectively K and A, and the dimensionless wall thickness D.

For the typical studied cases, the reversed flow is limited to the heated section during the early transient while, with elapsing time, such recirculation zone becomes more important and, is spreading upstream of the heated section.

This recirculation cell spreads rapidly towards the upstream section for $(Gr, Re) = (5.10^3, 1)$, while for $(Gr, Re) = (5.10^5, 100)$ it remains confined longer in the heated section, resulting in a more pronounced minimum and maximum of Q_{wi} in the inlet of the heated section.

The presence of the reversed flow region has drastically perturbed the internal flow as well as the thermal field, resulting in negative values of the friction coefficient and a significant redistributed portion of the applied heat flux in the upstream section where no energy is directly applied.

Moreover, the radial temperature profile at $x=0$ increases and presents a maximum at the vicinity of the wall-fluid interface for all values of K, over a specific period of the transient for $(Gr, Re) = (5.10^5, 100)$ due to the fact that the cell remains confined longer in the heated section before spreading towards the adiabatic section. Furthermore, this maximum of the radial temperature profile at the vicinity of the wall-fluid interface has also been observed at every axial position of the upstream section reached by the reciculation cell.

Results have also shown that the upstream redistribution of the applied heat flux and consequently the upstream widening of the cell slowdown with the decrease of A and the dimensionless wall thickness D.

It is also found that the transient redistribution of the applied heat flux in the adiabatic upstream section slowdown with the increase of K for the case when the axial conduction is

significant in the fluid (*Pe=5*) and in the pipe wall, whereas when the axial conduction in the fluid is neglected (*Pe=500*), the transient evolution of this redistribution is reversed.

For the two values of *Gr* and *Re* numbers, the time required to the heat transfer to reach the steady state increases with the decrease of K, contrary to the of forced convection case [60].

With the increases of the Grashof number, the upstream redistribution of the applied heat flux is more and more localised far from the inlet of the heated section.

5. 3 Perspectives of this work

Although the results presented in this work form a coherent whole, other aspects could be the subjects of ulterior research, of which these:

The numerical code could be generalized by adding the required elements to simulate the turbulent flows. Indeed, the present results are only valid for a very restricted rang of *Re* and *Gr* corresponding to laminar flow regime. This last extension would permit to widen the application fields of the generated results.

It would be interesting to examine the effects of the viscous dissipation. Indeed, Barletta [72] has examined this effect on the steady fully developed mixed convection in a parallel flat vertical channel. He found that the effect of viscous dissipation is important especially in the case of upward flow. Moreover, for asymmetric heating, it has been shown that viscous dissipation enhances the effect of flow reversal in the case of downward flow while it lowers this effect in the case of upward flow.

The extension of this work to the case of concentric annular duct encountered in numerous heat transfer and fluid flow devices involving two fluids. One fluid flows through the inner tube while the other flows through the annular passage between the two tubes. For example, heat exchangers designed for chemical processes require the consideration of mixed convection in annular flow.

The extension of the present work to the time-dependant [50], or the time-periodic [51, 73] boundary conditions (wall temperature or wall heat flux).

ملــــــخص :

في هذه الأطروحة نتناول دراسة التبادل الحراري الانتقالي بواسطــة الحمل المختلط (حمل قسري + حمل طبيعي) بين جريان رقا ئقي و ماسورة ذات شكل أسطواني وذات سمك غير مهمل في وضع شاقولي. المأسورة خاضعة على طول L_h، يساوي 10 مرات القطر الهيدروليكي، لكثافة تسخين منتظم و ثابث. يضاف لهذا الطول المسخن(L_h)، أجزاء كاتمة L_d و L_u أمام وخلف الطول المسخن، على الترتيب. السائل يأتي من الأعلى، أي من بداية الجزء الكاتم L_u و ينزل إلى الأسفل، مارا بالجزء المسخن L_h و الجزء الكاتم L_d، ليخرج من نهاية هذا الأخير. فى مثل هذه الظروف نقول أننا في حالة حمل مختلط معاكس .

حل جملة معادلات Navier-Stocks في اتجاه نشف القطر r ومحور المأسورة z مع الشروط الحدية و الابتدائية يتم بطريقة عددية نستعمل فيها طريقة الأحجام المنتهية Patankar. نستعمل طريقة SIMPLE لتحقيق الترابط بين الضغط ــ السرعة.

تجري التجارب العددية من أجل قيمة لعدد براند (Pr) يساوي 5 و من أجل قيمتين لعدد رينولدز (Re) وغراتشوف (Gr) على الترتيب (1، 100) و($Gr = 5.10^3$ و $Gr = 5.10^5$).

نقوم بدراسة تأثير الخصائص الفيزيائية (الناقلية الحرارية، معامل الانتشار الحراري) و الهندسية (سمك المأسورة) على المقادير الحرارية (كمية الحرارة المنتقلة إلى الجدار الداخلي للمأسورة و توزيع درجة الحرارة بدلالة قطر المأسورة) و المقادير الديناميكية (معامل الاحتكاك و حقل السرعة) و ذلك بدلالة الزمن.

من خلال هذه الدراسة لاحظنا بعد مرور فترة زمنية معينة، يكون فيها التبادل الحراري مضمون إلى حد كبير بواسطة التواصل الحراري، ظهور كمية من الحرارة الموفرة للمنطقة المركزية في جوار بداية هذه الأخيرة (أي عند z=0). مع مرور الزمن يتزايد تأثير التبادل الحراري بواسطة الحمل المختلط و يؤدي هذا إلى انتقال هذه الكمية من الحرارة إلى المنطقة الكاتمة L_h. تتعلق قيمة هذه الحرارة الموزعة من المنطقة الساخنة بالخصائص الفيزيائية و الهندسية، فتكون قيمتها أكبر كلما كان حاصل قسمة الناقلية الحرارية لجدار المأسورة على الناقلية الحرارية للسائل أكبر و كذلك سمك الماسورة أكبر كما أن بعد هذه الأخيرة عن مدخل المنطقة الساخنة يتناقص مع تناقص عدد غراتشوف.

عندما يكون التوصل الحراري المحوري معتبر في السائل و في جدار المأسورة، لاحظنا كذلك خلال المرحلة الانتقالية، أن سرعة انتقال هذه الكمية من الحرارة داخل المنطقة الكاتمة يتناقص بزيادة حاصل قسمة الناقلية الحرارية لجدار المأسورة على الناقلية الحرارية للسائل. كما أن هده الأخيرة تزداد مع تزايد حاصل قسمة معامل الانتشار الحراري لجدار الماسورة على معامل الانتشار الحراري للسائل. عند الوضع النهائي (المستقر) تتطابق و تتساوى جميع القيم المقابلة لمختلف معاملات الانتشار الحراري.

في الحالة التي يكون التوصل الحراري المحوري معتبرا فقط في جدار المأسور($Gr = 5.10^5$, Re = 100) ، لاحظنا أن انتقال هذه الكمية من الحرارة داخل المنطقة الكاتمة (L_d)، تتسارع مع نقصان حاصل قسمة الناقلية الحرارية للجدار على الناقلية الحرارية للسائل. في كلتا الحالتين، لاحظنا أن معامل الاحتكاك يأخذ قيم سالبة صغيرة محصورة فقط داخل المنطقة المسخنة. مع مرور الزمن، يأخذ هذا الأخير قيما سالبة معتبرة في المنطقة المسخنة، و كذلك في جزء مهم من المنطقة الكاتمة L_u. في النظام المستقر يؤول هذا الأخير إلى قيمة مطابقة لتلك المقابلة لحالة سريان قسري بعيدا عن مدخل و مخرج المنطقة المسخنة.

كلمات المفاتيح: تسخين ثابت، حمل مختلط، نظام انتقالي، ما سورة أسطوانية، نظام رقائقي

RESUME

Dans le cadre de ce travail, on présente les résultats d'une simulation numérique de la convection mixte conjuguée transitoire dans un tube vertical de géométrie cylindrique. L'épaisseur de la paroi du tube est égale à (*D*). L'écoulement est laminaire et axisymétrique. Un flux de chaleur uniforme (*Q*) est appliqué à la surface externe du tube, sur une section centrale, d'une longueur égale à 10 fois le diamètre hydraulique. Cette section est comprise entre deux sections adiabatiques, respectivement L_u et L_d. De plus, le fluide pénètre au haut du tube pour se diriger vers le bas; par conséquent on est en présence d'un écoulement de convection mixte opposé. Les équations gouvernantes sont résolues numériquement en utilisant la méthode classique des volumes finis développée par Patankar. Le couplage pression-vitesse est assuré en utilisant l'algorithme SIMPLE.

Deux nombres de Grashof ont été choisis, 5.10^3 et 5.10^5. Deux vitesses d'écoulement ont été retenues, conduisant à des nombres de Reynolds de *1* et *100*, qualifiés de bas et de haut *Re*. Les rapports Gr/Re^2 correspondants sont de *5000* et *50*, respectivement. On étudie l'influence des propriétés physiques et géométriques sur l'évolution transitoire des grandeurs thermiques (flux de chaleur à l'interface paroi-fluide et température) et dynamiques(coefficient de frottement et vecteurs vitesses).

Pendant les premières périodes du régime transitoire où le transfert de chaleur est globalement dominé par conduction, nous avons constaté une certaine quantité d'énergie au voisinage immédiat de l'entrée de la section chauffée *(x=0)*. Plus tard, les mouvements convectifs s'intensifient. Il en résulte une augmentation de la valeur de cette quantité d'énergie et une redistribution de cette dernière dans la section de préchauffage. La valeur et la position axiale de cette redistribution dépend du rapport des conductivités et des diffusivités thermiques de la paroi à celle du fluide ainsi que de l'épaisseur de la paroi.

Nous avons constaté aussi que la redistribution du flux de chaleur imposé dans la section de préchauffage ralentit avec l'augmentation du rapport des conductivités et la diminution du rapport des diffusivités dans le cas où la conduction axiale est significative dans la paroi et dans le fluide *(Pe=5)*. Dans le cas où la conduction axiale dans le fluide, est négligeable, nous avons constaté l'effet inverse. Pour les deux cas étudiés, nous avons constaté que le coefficient de frottement prend de faibles valeurs négatives dans la section chauffée. Avec le temps, ces valeurs augmentent et s'étendent vers la section adiabatique de préchauffage. Loin de l'entrée et de la sortie de la section chauffée, la valeur de ce dernier tend vers celle d'un écoulement isotherme pleinement développé.

Mots clés : flux de chaleur, convection mixte, régime transitoire, conduite cylindrique, régime laminaire

SUMMARY OF THE THESIS

The proposed survey in this thesis appears in the setting of the conjugated laminar and transient mixed convection in a thick vertical conduct. The external surface of the conduct is submitted to a constant and uniform heat flux, applied on a central section of length equal to ten times the hydraulic diameter. Two adiabatic sections have been added upstream and downstream the central section. Besides, the fluid penetrates to the top of the conduct to head downwards, therefore one is in presence of opposed mixed convection flow (unfavourable).

The objective of this work consists in finalizing a two dimensional numerical code to study the problems of forced, free and mixed convection in the transient regime in thick cylindrical conducts. The originality of this work resides in the consideration of the transient phenomena and the wall-fluid coupling. The numerous analyses and illustrations presented in this thesis put in evidence some original and interesting results that contribute in general to the improvement of the knowledge in the domain of the heat transfers, and in particular of the heat transfers by mixed convection.

In the beginning of the transient, we noted that the flow corresponds to the case of 'pure forced convection'. Consequently, the interfacial heat present no distribution towards the upstream adiabatic section due to the weak intensity of the recirculation cell, which still enclosed in the heated section. With elapsing time, the effects of the natural convection close to the pipe wall become more pronounced and act on the descendant main flow. This leads to increase the intensity of the recirculation cell, driving to an evacuation of a quantity of energy toward the upstream adiabatic section. The analysis of the effects of the physical and geometrical properties have shown that the redistribution of the interfacial heat flux in the upstream adiabatic section accelerates with the increase of the wall-to-fluid thermal conductivity and the thermal diffusivity ratios, and also with the increase of the dimensionless thickness of the pipe wall. Otherwise, we noted for some cases that the radial distribution of the temperatures present, during a weak period of the transient, a local maximum close to the pipe wall. This local maximum appears to the neighborhood of the entry of the heated section and also to every axial position of the upstream section reached by the recirculation cell.

Key words: heat flux, mixed convection, transient laminar regime, cylindrical duct, opposed-buoyancy

TABLE OF CONTENTS

Contents table

Nomenclature

Symbol	**Definition**

A — wall-to-fluid thermal diffusivity ratio $(=a_w/a_f)$

D — tube diameter $(=2R_i)$, *m*

F — friction coefficient, *$Kg.m^{-1}.s^{-2}$*

g — acceleration due to gravity, *$m.s^{-2}$*

Gr_Q — Grashof number $(=gbQD^4/n^2k_f)$

K — wall-to-fluid thermal conductivity ratio $(= k_w/k_f)$

L_u — length of the upstream section, *m*

L_h — length of the heated section, *m*

L_d — length of the downstream section, *m*

L_i^* — dimensionless length $(=L_i/D)$, *i=u, h, d*

p — pressure, *Pa*

P — dimensionnelless pressure $(=(p-r_0gz)/r_0V^2)$

Pe — Peclet number $(=Re.Pr)$

Pr — Prandtl number $(=n/a_f)$

Q — heat flux at the outer surface of the pipe, *$W.m^{-2}$*

Q_{wi} — normalized heat flux $(=(Q_{inner}/Q).(R_i/R_e))$

Q_{inner} — heat flux at the wall-fluid interface, *$W.m^{-2}$*

R_i — internal radius of the pipe, *m*

R_e — external radius of the pipe, *m*

R_e — Reynolds number *$(=V.D/v)$*

r — relate to the radial coordinate, *m*

T	temperature, K
T_0	initial or inlet temperature, K
u	axial velocity, $m.s^{-1}$
v	radial velocity, $m.s^{-1}$
u^*	dimensionless axial velocity $(=u/V)$
v^*	dimensionless radial velocity $(=v/V)$
V	average axial velocity at the entrance of the duct, $m.s^{-1}$
Z	relate to the axial coordinate, m

Greek symbols

t	dimensionless time $(=t.V/D)$
h	dimensionless radial coordinate $(=r/D)$
x	dimensionless axial coordinate $(=z/D)$
n	cinematic viscosity, $m^2.s^{-1}$
b	thermal volumetric expansion coefficient, K^{-1}
D	pipe thickness-to-diameter ratio $(= (R_e-R_i)/D)$
q	dimensionless temperature $(=T-T_0/QD/k_f)$
r	density, $kg.m^{-3}$
Dq	dimensionless temperature difference at the wall-fluide interface

Subscripts

b	bulk quantity
f	fluid
d	downstream
h	heated
u	upstream
w	wall
wi	wall-fluid interface
0	evaluated at the inlet temperature

Exponents

$*$	dimensionless value
t	designate the instant t
$t+Dt$	designate the instant $t+Dt$

List of figures

VIII

IX

List of tables

ACKNOWLEDGMENTS